nature portfolio

Peer Review File

Transmembrane voltage-gated nanopores controlled by electrically tunable in-pore chemistry

Corresponding Author: Professor Makusu Tsutsui

This file contains all reviewer reports in order by version, followed by all author rebuttals in order by version.

Version 0:

Reviewer comments:

Reviewer #1

(Remarks to the Author)
The paper reports how voltage-gated solid-state nanopores were conducted by electrically tunable chemical reactions, where the metal hydroxides repetitively precipitated and dissolute in a pore through manipulating the cation flow by transmembrane voltage in the asymmetric electrolyte solution. Under negative voltages, precipitates grow to reduce ionic current by occluding the nanopore, while inverting the voltage polarity dissolves the hydroxides reopening the pore to ionic flux. They achieve this resistive state switching by adopting low solubility metal hydroxides and the concentration polarization property of the asymmetric electrolyte solution. Overall, this concept is similar to those reported by Siwy (Nano Lett. 2006, 6, 473-477; Nat. Nanotech. 2008, 3, 51-57;), Michael (J. Phys. Condens. Matter. 2010, 22, 454127;), Nader (ACS Nano 2011, 5, 3191-319;), and Patrick (Cryst. Growth Des. 2017, 17, 6565-6571). Highly relevant state switching behaviors due to phase transition have been reported in other systems not recognized, for example reported by Author himself (ACS Applied Materials & Interfaces 2020, 52175); by Golovchenco (Phys. Rev. Lett. 2014, 024506.); among others. A correlation to the exciting concept of nanopore memristor is warranted by showing the potentiation and depressions, while the stability is a concern because of the unstable structure of the precipitated nanopore. Furthermore, the single-molecule sensing using a precipitated nanopore didn't show significant advantages, compared to the single-molecule sensing using a biochannel of protein. Overall, in my opinion, the manuscript can become acceptable if the authors can clearly state the novelty of this work over others reported previously.

Reviewer #2

(Remarks to the Author)
In this manuscript, M. Tsutsui et al. report on nanopores that allow to tune chemical reactions by means of electrical manipulation of transmembrane ion transport. Depending on the salty solutions and the pH-value across the membrane, the authors could control and block the ionic flux through the nanopores. This is attributed to shrinking of the effective pore size by formation of metal hydroxides. I think the manuscripts provides meaningful results that may be interesting for a wide readership. In general, the manuscript is well written (but polishing of the language is recommended) and well structured. Experimental results are discussed in detail. The references are well balanced. It will be necessary to improve the figure quality as some graphics are difficult to read. In addition, I would like to highlight the following points, which the authors may address in a major revision:
- The terms cis and trans may not be well known for a large readership. It may be useful to add these terms in figure 1a.
- The inset in Figure 2b is really difficult to read. Instead (or in addition) to different colors I recommend using different forms for indicating the different salts. Moreover, cis and trans may be also added in the insets.
- It is not clear to me how the core diameter is estimated in Figure 2d. Why is it given in arb. units while on the other hand, the authors discuss that the (shrinked?) core size is larger than the Debye length (which I do not put into question)
- If the salt is similar on both sides (Figure 2b) there is no change of the pore conductivity. I think this is important to understand the overall behavior, but the manuscript does not discuss this effect in detail. It could be assumed that even a small difference of the geometry, surface, salt concentration etc. could lead to a change of the conductivity upon further cycling (at least for $MnCl_2$). How does the experimental observation fit to the author's theoretical explanation? Did the author see any effect of having the same salt across the membrane but with a concentration gradient?
- On page 4, l. 94, the authors suggest that ion-ion interactions may not play (a dominant?) role because also low concentrations were tested. However, as the pores shrink, the effective concentration in the core could indeed lead to ion-ion interactions. I think this cannot be simply excluded without further evidence. Moreover, the Debye theory is not applicable for

high concentrations.
- Also on page 4, the authors report the formation of a “white substance” that is considered to be the metal hydroxide. I strongly recommend to verify this by additional spectroscopic techniques such as ex situ XPS. This would contribute to a better understanding of the proposed mechanism.
- In Figure 6h, the white and grey lines can hardly be seen. It is also not clear to me what the blue curve is.

Reviewer #3

(Remarks to the Author)
In this manuscript, the authors have made voltage gated solid-state nanopores that act as nanofluidic diodes which are electrically tunable with much higher rectification ratios than that have been reported before for such devices. The electrical tunability comes from modulating ion flow by reversible chemical reactions that form precipitation and dissolution of metal hydroxides at opposite biases. Local heat measurements show the change in temperature during the reaction and changing the voltage scan rates show reaction mediated memory effects. The authors also show single molecule sensing of DNA using a robust aluminum hydroxide precipitated nanopore.

While the experiments are innovative and yield promising results, many sections of the manuscript lack clarity and need further elaboration and detail to adequately support the conclusions. Also, the overall text readability and figure labels can be improved and here are some comments.

Novelty: The authors appear to be not aware of the first study that reported nanopore precipitation [“Nanoprecipitation-assisted ion current oscillations”, Nature Nanotechnology, 3:51 (2008)], which introduced many of the phenomena described in the present manuscript. The authors should properly describe that work in the introduction and describe their finding in the context of that previous work.

Clarity: The first question that a reader will have after looking at Figure 1b and 2c is whether the blockades seen at negative voltages are reversible. It is, in a way, implied as the I-V curves are measured using a voltage scan. But the authors should describe, well upfront, how the current changes as a function of time, showing multiple voltage scans and the corresponding changes in the current. Showing that the nanoprecipitation phenomena are (nearly) 100% reversible is required for the study to be of practical interest.

Presentation: Figures 1 and 4 look like proposal material. While visually impressive, they might not be the best choice to communicate a scientific result.

Other major points:

1) For figure 2a-b, the authors mention that the conductance at negative voltages can be explained by the distinct mobilities of the three cations, as shown by the linear relationship under homogeneous salt solutions. However, the order for Mg (pink) and Na (black) is opposite at negative bias between 2a and 2b as compared to the other ions. The inset of Fig. 2b showing the slope is also unclear as the ions are not labeled, with there being 3 points as compared to 4 ions shown in (a).

2) Another issue in Figures 2a and 2b is the I-V curve for 1.37M NaCl. As for this case, the conditions are same between 2a and 2b, the black line should be the same across the two figures. However, the slopes of the two lines seem different, the black line ranging from roughly -4.5 to 4.5 in (a) and between -8 to 7 in (b). What is the reason for this difference and if there are any conditions different in these two plots for NaCl, please specify.

3) The rectification ratio defined in Page 3, Line 68 should have an absolute value around the division for accuracy, as all rectification numbers reported are positive. The ionic currents shown in nA in the inset of Figure 2c and used for calculating rectification are quite small. How reproducible are these numbers, as they are used throughout the paper? In the methods section (page 11, line 275), the authors mention carrying out each measurement three times to get the average ionic current. Are these three independent measurements? If so, the error bars can be plotted for the rectification values shown in Fig. 2d to provide robust statistical significance to the derived conclusions.

4) Also in Page 3, Line 74, the authors mention that the strong rectification behaviors were dependent on the voltage scan speed (Figures S3-S6). Firstly, the figures S3-S6 are all reported at the same 65 mV/s scan speed. Page 4, Line 78 also cites Figure S3 with an order of magnitude lower scan speed, but that figure is labeled to be at 65 mV/s and does not contain the MnCl2 data as described in text.

But other figures in the main text show the dependence of the I-V curve on the Vb scan speed. What is the reason behind this difference? Are the measurements done at steady state conditions? Fig. 2d shows a big change in the rectification for CaCl2 at lower scan speed, which needs error bars from the replicate measurements for statistical accuracy.

5) For the heat dissipation measurements shown in Fig. 3d-f, the voltage scan speed is 1 mV/s. What are the rectification values for the pore at that scan speed? Is it representative of the measurement at 65 mV/ns? It is hard to gauge from the I-V curve shown. Also, it is not clear in Fig. 3e if there is a difference between the positive and negative Vb scans as all points seem the same color and not clearly distinct as Fig. 3d. Can the authors describe how the reaction enthalpy is calculated for Fig 3d at these experimental conditions?

6) For the memory effect results in Figure 4, have the authors calculated rectification ratio from the I-V curves for the scans shown? Are the rectification values cycled back upon changing the voltage sweep rate and does the clogging and de-clogging cycles affect the rectification properties of the diode?

7) The trivalent Al3+ ions are shown to form robust precipitates in Fig. 6. However, the current shown in Fig. 6c at negative bias seems to be an order of magnitude higher than the other ions in Fig 2c inset. What is the reason behind this change of magnitude? Also, during subsequent scans shown in Fig. S9, the current at negative bias increases after the 8th sweep. What is the reason behind the increase, as described the current decreases at positive bias confirming the presence of the robust precipitation layer?

8) For Fig. 6h, are they two separate measurements at the same timepoints? The grey and white curves are not clear in the figure. How do the authors infer the two peaks in the same blockade to arise from folded and non-folded DNA conformations? As the sample only has a small amount of linear DNA, it is not clear how 40% of the blockades are double peaked as described.

9) For table S1 and all pH recordings measured, is the pH recorded before or after the experiment? As there are ion translocation events and the reported pH induced rectification in Fig 3, it is important to know how much the pH varies over the course of the experiment.

Text and label suggestions:

The authors should label the cis and trans chambers in the figures for easier understanding of directionality in the figures.
Page 3, Line 58-61: Should cite Figure 2a.
Page 4, Line 95: cis or trans?
Page 22, Line 459: cations serves -> cations that serve
Figure 4b label: 38rd -> 38th

Reviewer #4

(Remarks to the Author)
I co-reviewed this manuscript with one of the reviewers who provided the listed reports. This is part of the Nature Communications initiative to facilitate training in peer review and to provide appropriate recognition for Early Career Researchers who co-review manuscripts.

Version 1:

Reviewer comments:

Reviewer #1

(Remarks to the Author)
I think the revised manuscript can be accepted for publication without further revision.

Reviewer #2

(Remarks to the Author)
I thank the authors for their detailed answer of my comment. I think most of my comments were considered in the revised manuscript. However, I still think that the numbers and labels for the figures can be slightly larger for readability. Regarding my questions concerning the case where the salt is similar on both sides: the authors commented on this issue in the response letter, but I do not see any comment regarding this issue in the manuscript.

I recommend publication of the manuscript after minor revision, which do not require reviewer approval. These minor revision include: improvement of the figure readability, a short comment on the situation where the salt is similar on both sides.

Reviewer #3

(Remarks to the Author)
The authors have implemented a number of changes to the manuscript that clarified the majority of points from the previous round of review.

One remaining concern is that the rectification measurements have not been conducted in a steady state and thus are not reproducible among repeat experiments. This can be seen in the last panels of the updated Figures S2-S7 and can also appreciated from the error bars in Fig 2d. These details are now clearly described in the text along with their reasoning for why these measurements are not fully reversible. Such stochasticity, however, somewhat limits practical utility of the described phenomena.

The authors have added error bars to Fig 2d for the rectification measurements, described as standard deviation. The

caption does not specify which measurements are included for this calculation. The range of rectification values in Fig S3e and S6e seems to be bigger. Have the authors included only a part of the curve for taking the average and the standard deviation calculations?

The choice of colors in many figures is not color blind friendly, in particular, the “orange” and the “green” dots in new figure 5f. Please revise the colors throughout the manuscript.

Reviewer #4

(Remarks to the Author)
I co-reviewed this manuscript with one of the reviewers who provided the listed reports. This is part of the Nature Communications initiative to facilitate training in peer review and to provide appropriate recognition for Early Career Researchers who co-review manuscripts.

Electrically tunable reaction-driven voltage-gated nanopores

Makusu Tsutsui, Wei-Lun Hsu, Chien Hsu, Denis Garoli, Shukun Weng, Hirofumi Daiguji, and Tomoji Kawai

We would like to express many thanks to the referees for taking his or her precious time on reviewing our manuscript and providing many constructive comments, which we find valuable and helpful to improve our manuscript. We have studied the comments carefully and made the following revision.

List of changes

1. The introduction and discussion sections were revised to state the novelty of the present work over the previous literature.

   Main text (p2 line 28 – 43)

   (Revised) Stochastic collisions of two or more substances provide opportunities for transforming their atomic components. Principles of chemistry govern these processes, facilitating the creation of diverse compounds with desirable properties, where factors such as pH, temperature, and pressure shape the energy landscape of reaction pathways at equilibrium. In contrast to the conventional diffusion-based chemical systems, meanwhile, nanoreactors have emerged as efficient platforms capable of controlling reaction kinetics within a nanoconfined space through mass flow control.[1-3] In particular, solid-state nanopore technology has proven useful for *operando* observations of the chemical synthesis of an individual nanoparticle at real time (Au nanorod, nanoparticles).[4,5] Motion control of the *in situ* formed nanoprecipitates was also demonstrated with high length-to-diameter aspect ratio conical nanochannels,[6,7] which allowed novel nanofluidic diodes via the transmembrane voltage-dependent clogging of the nanoscale conduits.[6-10] Inspired by the pioneering work, we herein report tunable chemical reactions by electrical manipulation of ion transport in a small hole for advanced fluidic devices. This method employs an ultrathin dielectric membrane hosting a nanopore connecting two distinct ionic reactant solutions for precise manipulations of the ion electromigration to enable reversible precipitation/dissolution reactions of a metal compound layer (Figure 1a).

Main text (p10 line 252 – p11 line 266)

(Added) From a viewpoint of resistive pulse sensing, it has long been a dream for solid-state nanopore technologies to enable the formation of well-defined pore structures. Structures of biological nanopores are demonstrated as tailorable at a molecular level via the engineering of point mutations in transmembrane proteins.[57] As for the solid-state nanopores, on the other hand, electron beam milling has been demonstrated as capable of controlling the size and shape of a hole with single-nanometer resolution in a dielectric membrane. However, the fabrication can be carried out only in high vacuum,[58] thus making it difficult to ensure the structure remains the same during the ionic current measurements. There is also a dielectric breakdown approach[59] that can form single-digit nanopores *in situ* by a simple voltage control. Nevertheless, the controllability of the number and size of pores is still considered a critical issue.[60] In contrast, the present method can seal a relatively large pore nearly completely with a leakage current around 100 pA at 0.5 V. Leveraging the ability to open a nanopore and finely control its size by the voltage pulsing in real time, therefore, it has a potential to become a useful tool for adjusting the pore size to fit the analytes of concern right before the resistive pulse measurements.

2. A training protocol was constructed for stable nanopore memristive characteristics.

Figure 5
(Revised)

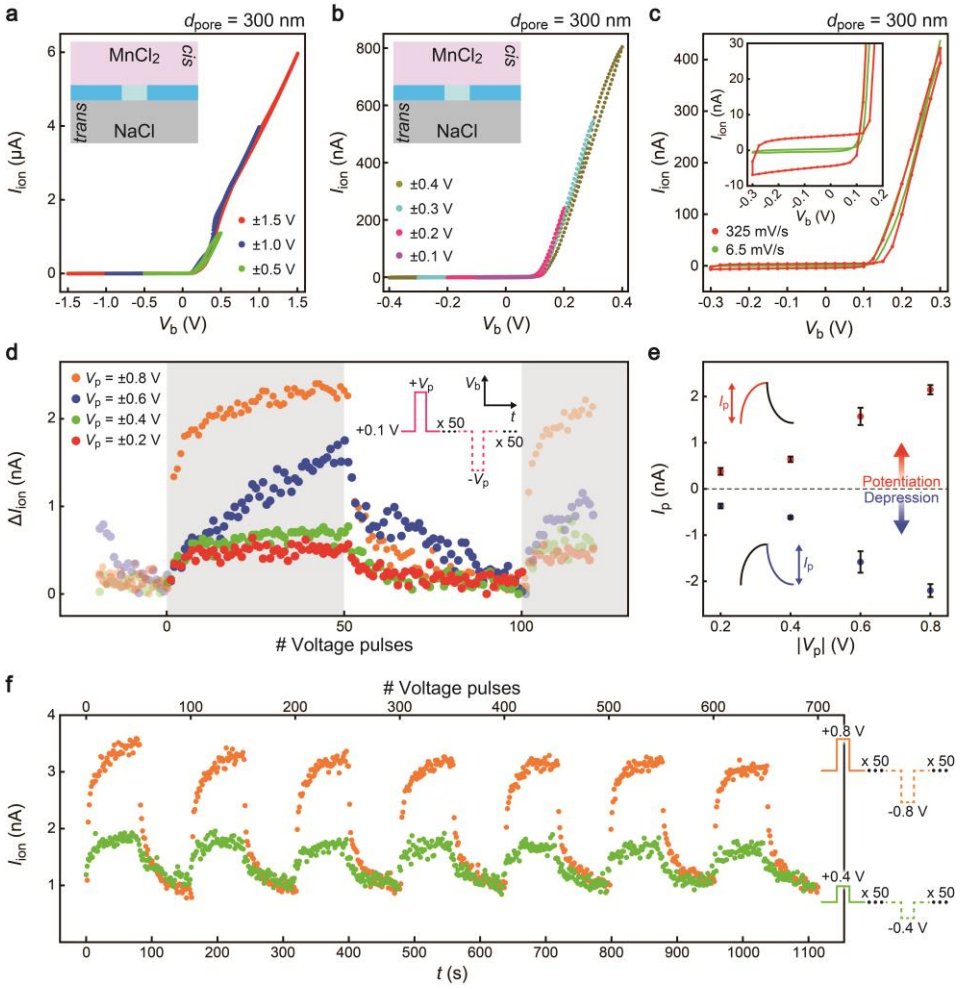

Figure 5. In-pore chemical reaction-driven nanofluidic memristor. **a-b,** I_{ion} – V_b characteristics of a 300 nm-sized nanopore with a $MnCl_2$/NaCl configuration measured under various ranges of transmembrane voltages. Note the I_{ion} remains suppressed when scanning V_b between -0.1 V and 0.1 V (b). **c,** Scan rate dependence of I_{ion} – V_b displaying pinched hysteresis loops. Inset shows a magnified view of the suppressed I_{ion} states. **d,** Memristive characteristics under the applications of 50 ms transmembrane voltage pulses of ±0.5 V amplitudes. ΔI_{ion} is the ionic current recorded at +0.1 V after each voltage pulsing (the baseline current was subtracted). The positive and negative pulses drive the potentiation (grey regions) and depression (white regions) processes of the nanopore memristor via the induced in-pore dissolution/precipitation reactions. **e,** The ionic current change I_p by the positive (red) and negative (blue) voltage pulses of amplitudes V_p. Error bars denote the standard deviations within four cycles of potentiation/depression processes. **f,** Potentiation/depression of the nanopore memristors under the voltage pulses of V_p = ±0.8 V (orange) and ±0.4 V (green). Read voltage was +0.1 V.

Figure S28

(Added)

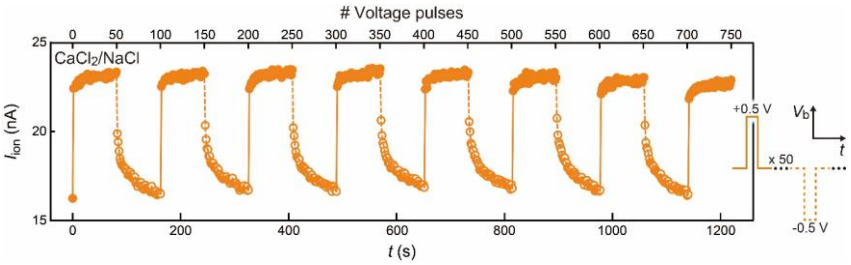

Figure S28. Stable memristive characteristics of a 300 nm-sized nanopore with a $CaCl_2$/phosphate buffered saline after training. Note the relatively high ionic current states of the $CaCl_2$ memristors ascribable to the chemical reaction equilibrium distinct to that in a $MnCl_2$/phosphate buffered saline configuration.

Figure S29

(Added)

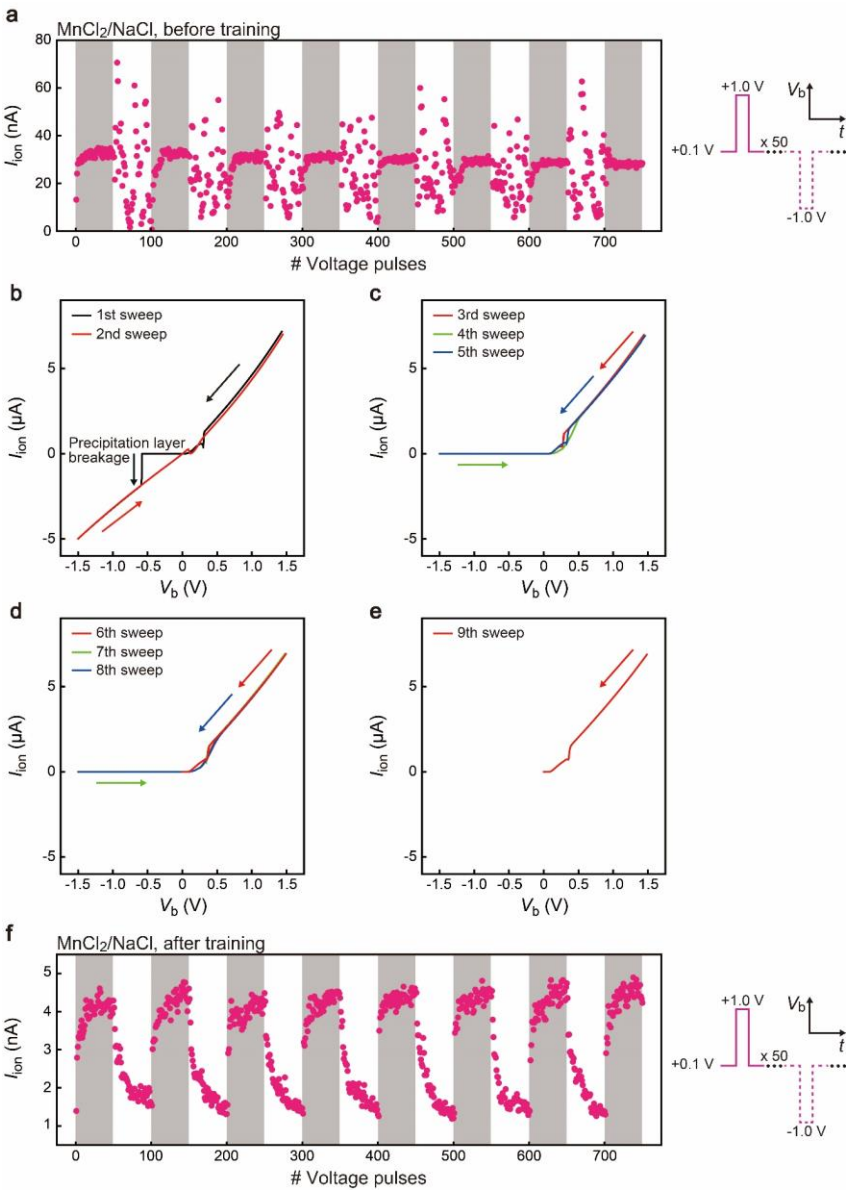

Figure S29. Training protocol for stable nanopore memristors. **a,** Memristive characteristics of a 300 nm-sized nanopore with a $MnCl_2$/phosphate buffered saline configuration without training. Applying positive and negative voltage pulses of 50 ms widths and ±0.5 V amplitudes, the ionic current tends to fluctuate upon the depression processes indicative of unstable nature of the in-pore precipitated phosphate layer under the given conditions. **b-e,** Training processes. Before driving the memristors, transmembrane voltage was scanned for 9 times between +1.5 V and -1.5 V. Initially, the precipitate layer was unstable at negative voltages (b). Repeating the voltage scanning, the I_{ion} – V_b curves become highly reversible suggesting the formation/dissolution of phosphate layers in a reproducible manner (b-d). The training ends by sweeping V_b back to 0 V (e). Subsequently, the memristors were driven by the sequence of the voltage pulses applied. **f,** An example of the memristive characteristics recorded after the training processes showing stable features in the potentiation/depression cycles.

Figure S30

(Added)

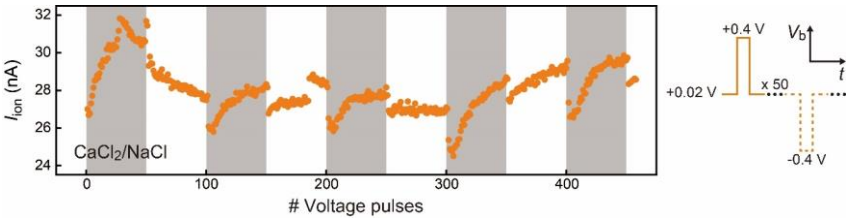

Figure S30. Unstable memristive characteristics of a 300 nm-sized nanopore with a $CaCl_2$/phosphate buffered saline without training. The ionic conductance tends to change in irregular manner against the voltage pulsing.

Main text (p7 line 173 – p8 line 183)

(Added) Similar characteristics were also found in $CaCl_2$/NaCl buffer systems, but at a relatively high conductance regime reflecting its reaction equilibrium distinct to that in the $MnCl_2$ solution (Figure S27). Here we add the importance of a training process to obtain the stable memristive characteristics. More specifically, V_b scans were implemented multiple times to reproducibly form a phosphate layer inside a nanopore that served to initialize the memristor state in prior to the subsequent potentiation/depression cycling (Figures S28 – S29). Without this pretreatment, the nanopore memristors tend to be non-controllable by the voltage pulses. Such fine control of the nanopore conductance may not be achievable with the conical nanopore approach[6-10] as it requires a formidable task of precise manipulation of the Brownian motion of a precipitated nanoparticle under the influence of the electrostatic and hydrodynamic drag forces.[43]

3. Repetitive I_{ion} – V_b characteristics measurements were performed to evaluate the stability of the extreme rectification behaviors.

Figure S2

(Added)

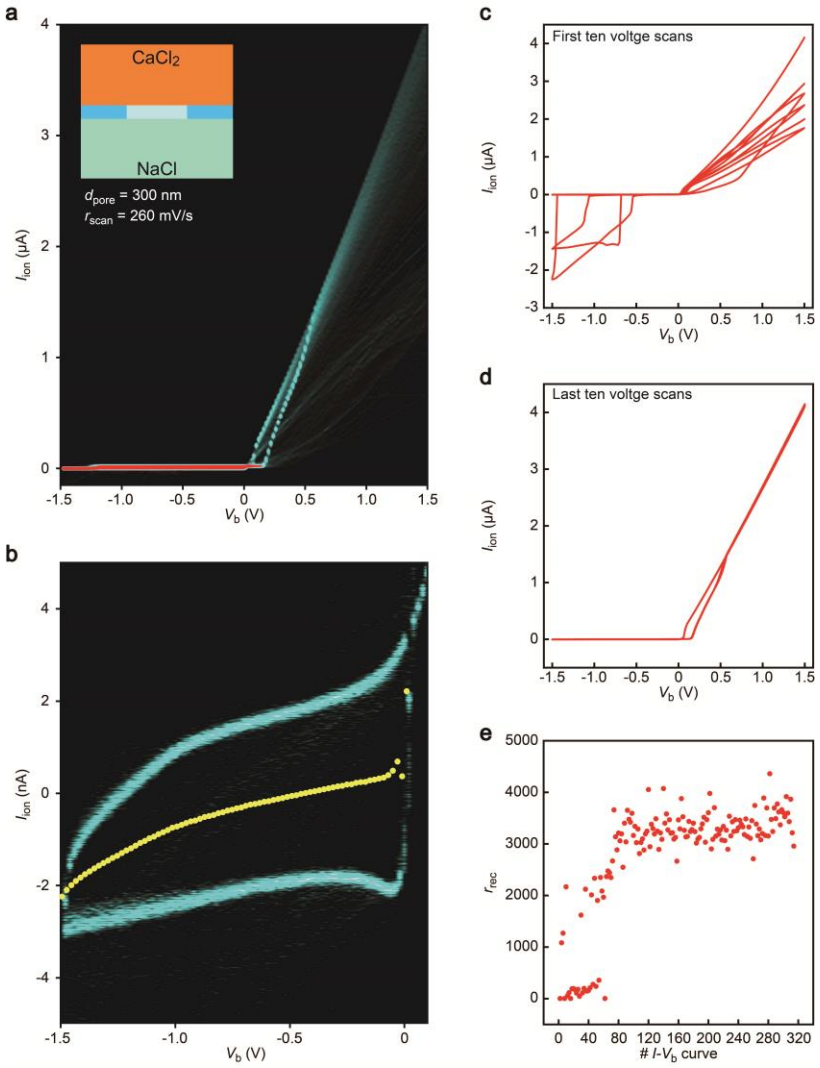

Figure S2. Reproducibility of the rectification characteristics in a 300 nm nanopore with a $CaCl_2$/phosphate buffered saline configuration under a voltage scan rate of 260 mV/s. a-b, Two dimensional histograms of 314 I_{ion} – V_b curves (a) and its close view at the negative voltage regime (b) obtained under repetitive voltage scanning from +1.5 V to -1.5 V. Yellow plots are the average of the curves acquired under the positive and negative voltage sweeps. **c,** The first ten I_{ion} – V_b curves showing relatively unstable nature of the ionic current characteristics suggestive of the fluctuating dissolution processes of the in-pore precipitated layer. **d,** In contrast, the last ten curves are highly reproducible indicating the stabilized precipitation/dissolution processes of the calcium phosphate layer formed in the nanopore. **e,** The rectification ratio r_{rec} calculated from each curve. Initially, r_{rec} tends to be low due to the inadequate time for forming nanoprecipitate seeds on the pore wall surface. After about 100 cycles of measurements, the precipitation/dissolution processes become stable giving r_{rec} around 3000.

Figure S3

(Added)

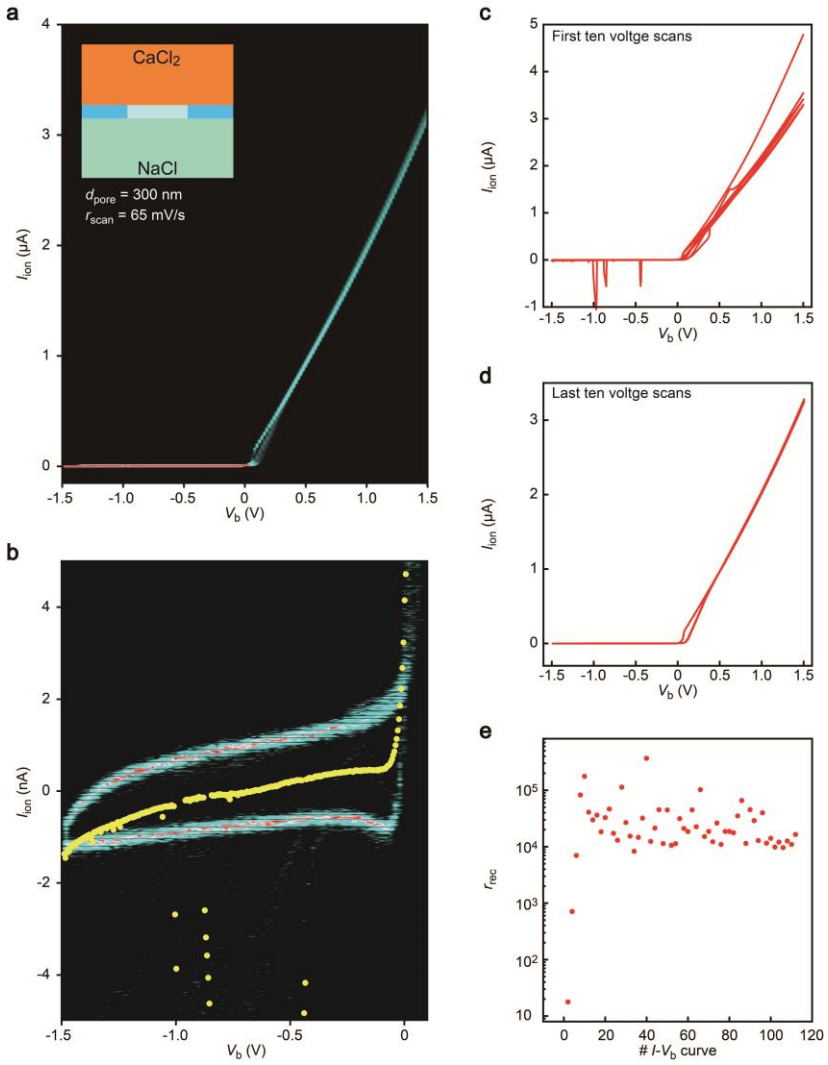

Figure S3. Reproducibility of the rectification characteristics in a 300 nm nanopore with a $CaCl_2$/phosphate buffered saline configuration under a voltage scan rate of 65 mV/s. a-b, Two dimensional histograms of 112 I_{ion} – V_b curves (a) and its close view at the negative voltage regime (b) obtained under repetitive voltage scanning from +1.5 V to -1.5 V. Yellow plots are the average of the curves acquired under the positive and negative voltage sweeps. **c,** The first ten I_{ion} – V_b curves showing relatively unstable nature of the ionic current characteristics suggestive of the fluctuating dissolution processes of the in-pore precipitated layer. **d,** In contrast, the last ten curves are highly reproducible indicating the stabilized precipitation/dissolution processes of the calcium phosphate layer formed in the nanopore. **e,** The rectification ratio r_{rec} calculated from each curve. After several cycles of measurements, r_{rec} tends to be stable at around 10^4 to 10^5.

Figure S4

(Added)

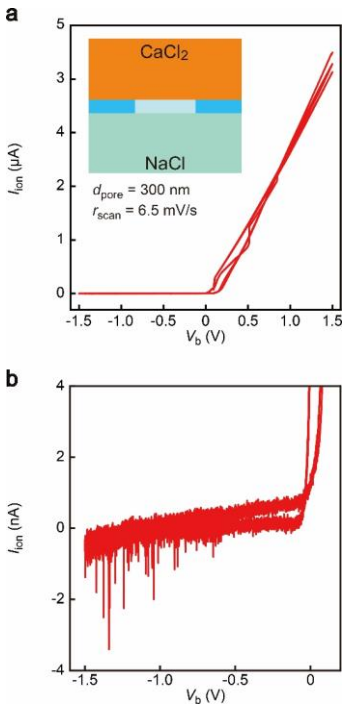

Figure S4. Reproducibility of the rectification characteristics in a 300 nm nanopore with a $CaCl_2$/phosphate buffered saline configuration under a voltage scan rate of 6.5 mV/s. a, $I_{ion} - V_b$ curves obtained under five cycles of voltage scanning from +1.5 V to -1.5 V. **b,** A close view of the suppressed ionic current at the negative V_b.

Figure S5

(Added)

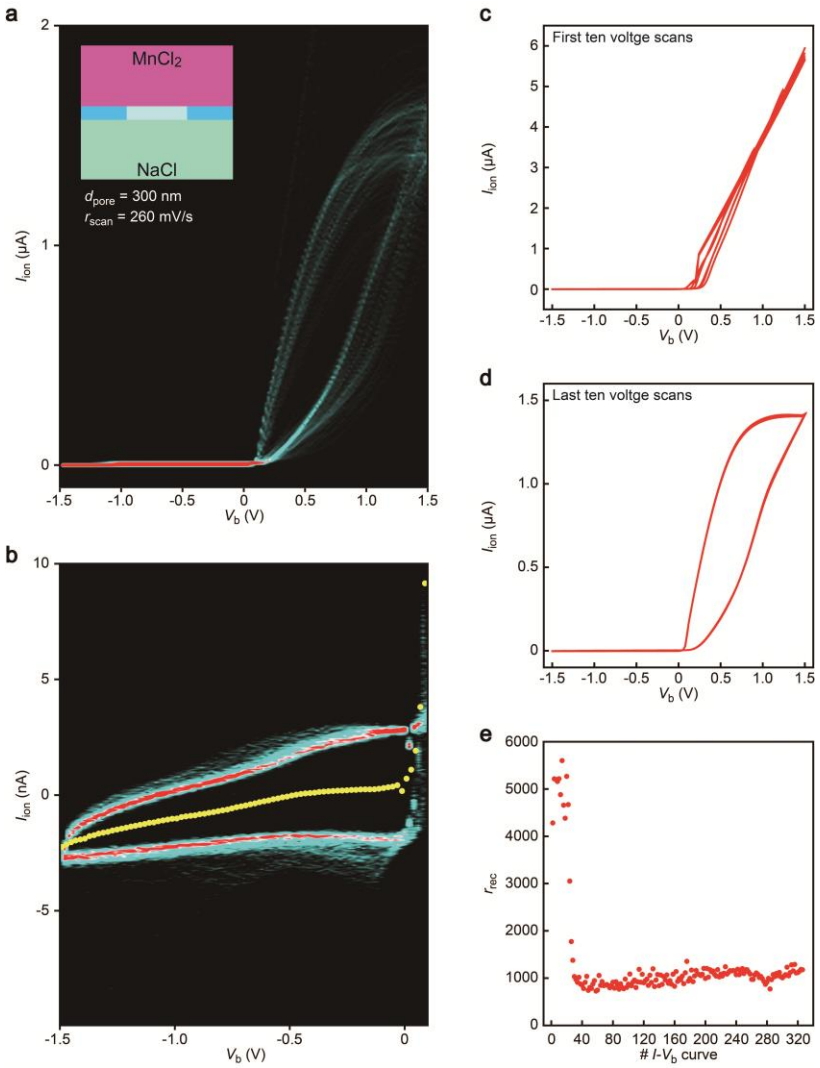

Figure S5. Reproducibility of the rectification characteristics in a 300 nm nanopore with a $MnCl_2$/phosphate buffered saline configuration under a voltage scan rate of 260 mV/s. a-b, Two dimensional histograms of 314 I_{ion} – V_b curves (a) and its close view at the negative voltage regime (b) obtained under repetitive voltage scanning from +1.5 V to -1.5 V. Yellow plots are the average of the curves acquired under the positive and negative voltage sweeps. **c,** The first ten I_{ion} – V_b curves showing relatively unstable nature of the ionic current characteristics at the positive voltages suggestive of the fluctuating dissolution processes of the in-pore precipitated layer. **d,** In contrast, the last ten curves are highly reproducible indicating the stabilized precipitation/dissolution processes of the calcium phosphate layer formed in the nanopore. **e,** The rectification ratio r_{rec} calculated from each curve. Initially, r_{rec} tends to be low due to the inadequate time for forming nanoprecipitate seeds on the pore wall surface. After tens of cycles of measurements, the precipitation/dissolution processes become stable giving r_{rec} around 1000.

Figure S6

(Added)

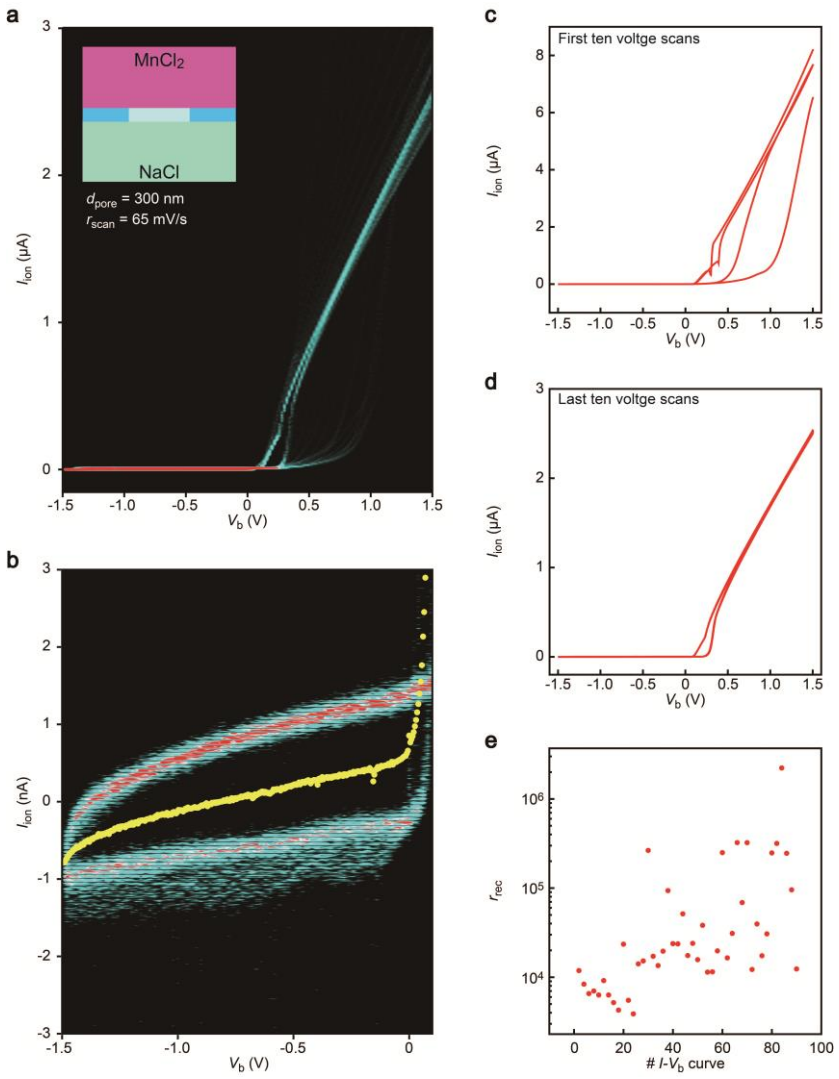

Figure S6. Reproducibility of the rectification characteristics in a 300 nm nanopore with a $MnCl_2$/phosphate buffered saline configuration under a voltage scan rate of 65 mV/s. a-b, Two dimensional histograms of 112 I_{ion} – V_b curves (a) and its close view at the negative voltage regime (b) obtained under repetitive voltage scanning from +1.5 V to -1.5 V. Yellow plots are the average of the curves acquired under the positive and negative voltage sweeps. **c,** The first ten I_{ion} – V_b curves showing relatively unstable nature of the ionic current characteristics suggestive of the fluctuating dissolution processes of the in-pore precipitated layer. **d,** In contrast, the last ten curves are highly reproducible indicating the stabilized precipitation/dissolution processes of the calcium phosphate layer formed in the nanopore. **e,** The rectification ratio r_{rec} calculated from each curve with values up to over 10^6.

Figure S7

(Added)

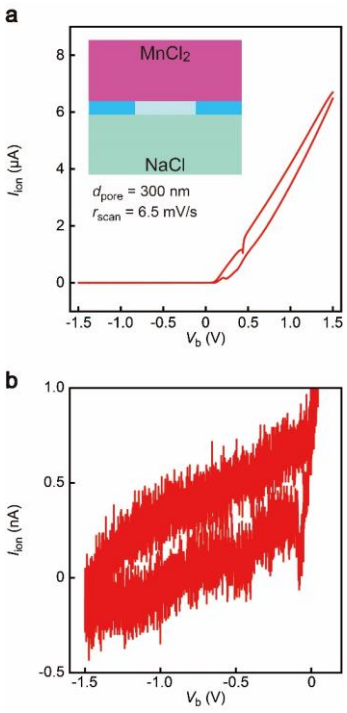

Figure S7. Reproducibility of the rectification characteristics in a 300 nm nanopore with a $MnCl_2$/phosphate buffered saline configuration under a voltage scan rate of 6.5 mV/s. **a,** $I_{ion} - V_b$ curves obtained under five cycles of voltage scanning from +1.5 V to -1.5 V. **b,** A close view of the suppressed ionic current at the negative V_b.

Figure S14

(Added)

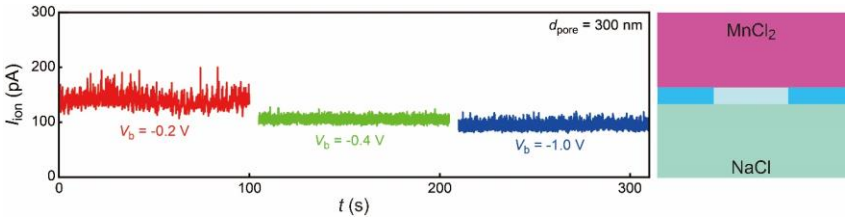

Figure S14. Ionic current flowing through a 300 nm nanopore of a $MnCl_2$/phosphate buffered saline configuration under negative transmembrane voltage recorded at 10 kHz. $I_{ion} - t$ traces of a 300 nm nanopore sealed by the phosphate compound under the negative transmembrane voltage of -0.2 V (red), -0.4 V (green), and -1.0 V (blue). The initial conditions were set as the same by applying +1.0 V to fully open the nanopore prior to the measurements at the negative voltages. The ionic current is stable at around 100 pA for over 100 seconds indicative of nearly complete sealing of the nanopore via the precipitated phosphate layer. The infinitesimal ionic current may be attributed to a single-digit nanopore formed in the precipitate layer, where particular ion-ion interactions[S6,S7] would take place to affect the ionic conductance.

4. Ionic current measurements in phosphate-free NaCl solutions and spectroscopy analyses of the white precipitates were carried out.

Figure S21

(Added)

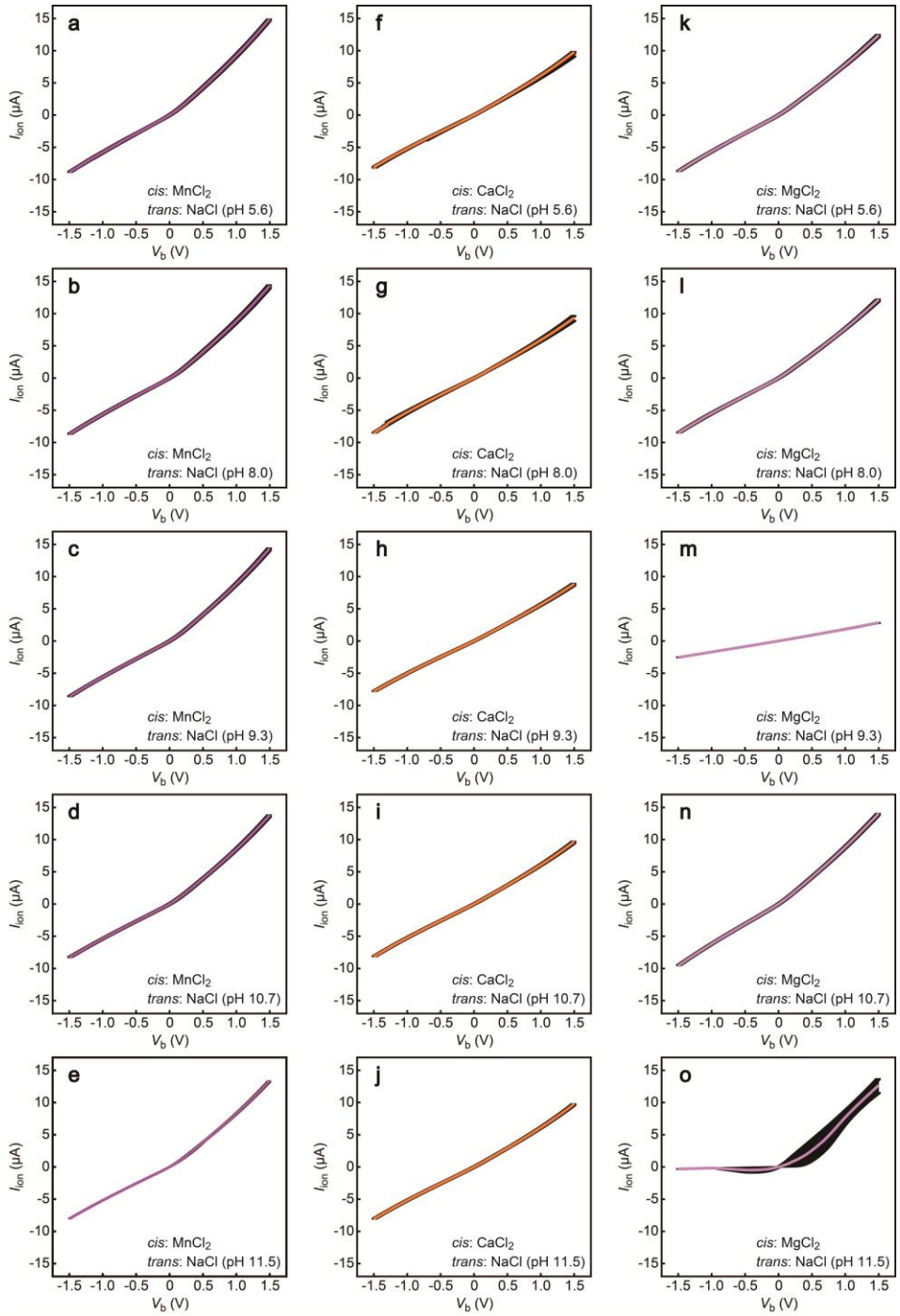

Figure S21. Ionic current characteristics in phosphate-free NaCl water (1.4 M) of various pH. a-e, I_{ion} – V_b curves recorded for a 300 nm nanopore with a $MnCl_2$/phosphate-free NaCl water configuration (r_{scan} = 65 mV/s). The pH of the NaCl water was adjusted to 5.6 (a), 8.0 (b), 9.3 (c), 10.7 (d), and 11.5 (c) using NaOH and HCl. Error bars are the standard deviations calculated from the three ionic current curves

recorded. **f-o,** The same sets of data obtained for $CaCl_2$ (f-j) and $MgCl_2$ solutions (k-o). No signs of in-pore precipitation were found at moderate pH manifesting the role of the phosphoric acid in the phosphate buffered saline on the extreme rectifications observed at pH 7.6. Meanwhile, $MgCl_2$ demonstrated a rectifying behavior (o) ascribed to precipitation/dissolution reactions of $Mg(OH)_x$ at the highly alkaline pH.

Figure S22

(Added)

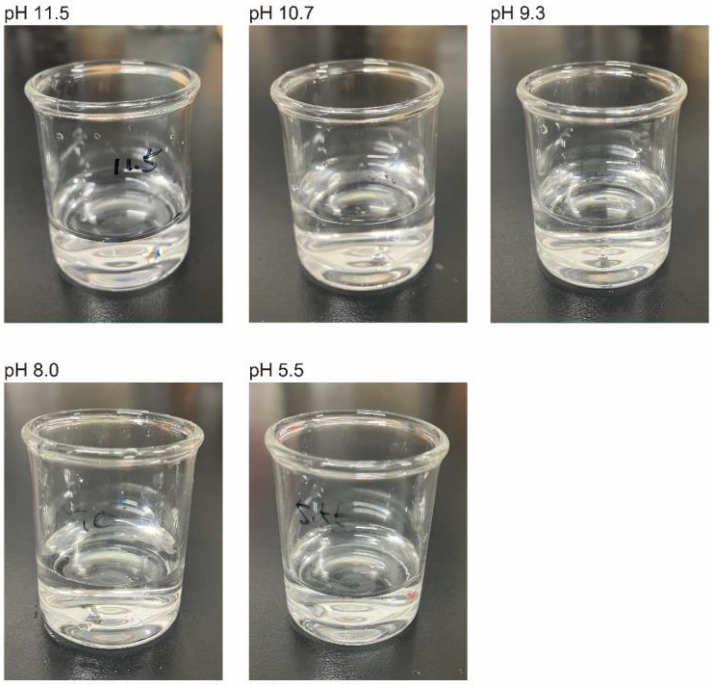

Figure S22. Reaction in phosphate-free NaCl solutions. Photographs taken after adding 100 µl of 2 M $CaCl_2$ into the 10 ml phosphate free NaCl water (1.4 M) in a beaker. No notable change in the appearance of the liquid was observed indicating the absence of any precipitation reaction. We note that this is a case only when the NaCl concentration is over 1 M. Under lower salinity conditions, precipitates were found to be generated upon mixing the $CaCl_2$ solutions with alkaline water attributed to the precipitation of calcium hydroxides.

Figure S19
(Added)

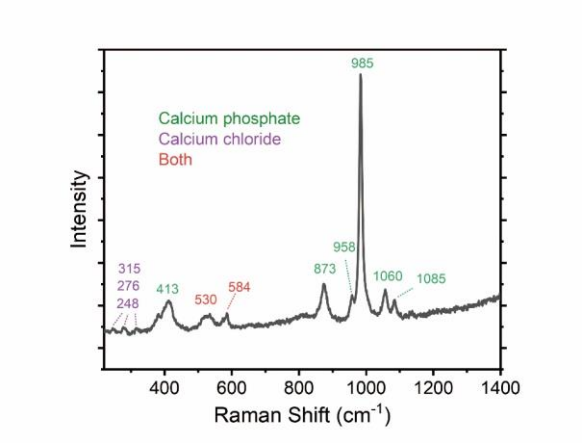

Figure S19. Raman spectrum of the white substance precipitated in the mixture solution of $CaCl_2$ water and phosphate buffered saline. Literature values of characteristic Raman peaks for $Ca(OH)_2$ are reported to be found at around 260 cm^{-1}, 260 cm^{-1}, 360 cm^{-1}, 700 cm^{-1}, and 1100 cm^{-1},[S8,S9] which are not present in the spectrum obtained for the white precipitates (red). Instead, the pronounced peaks at around 400 cm^{-1} and 1000 cm^{-1} (green) suggest that the white precipitates are comprised mostly with $CaPO_x$[S10,S11], in addition to a small amount of $CaCl_2$ (purple).

Figure S20

(Added)

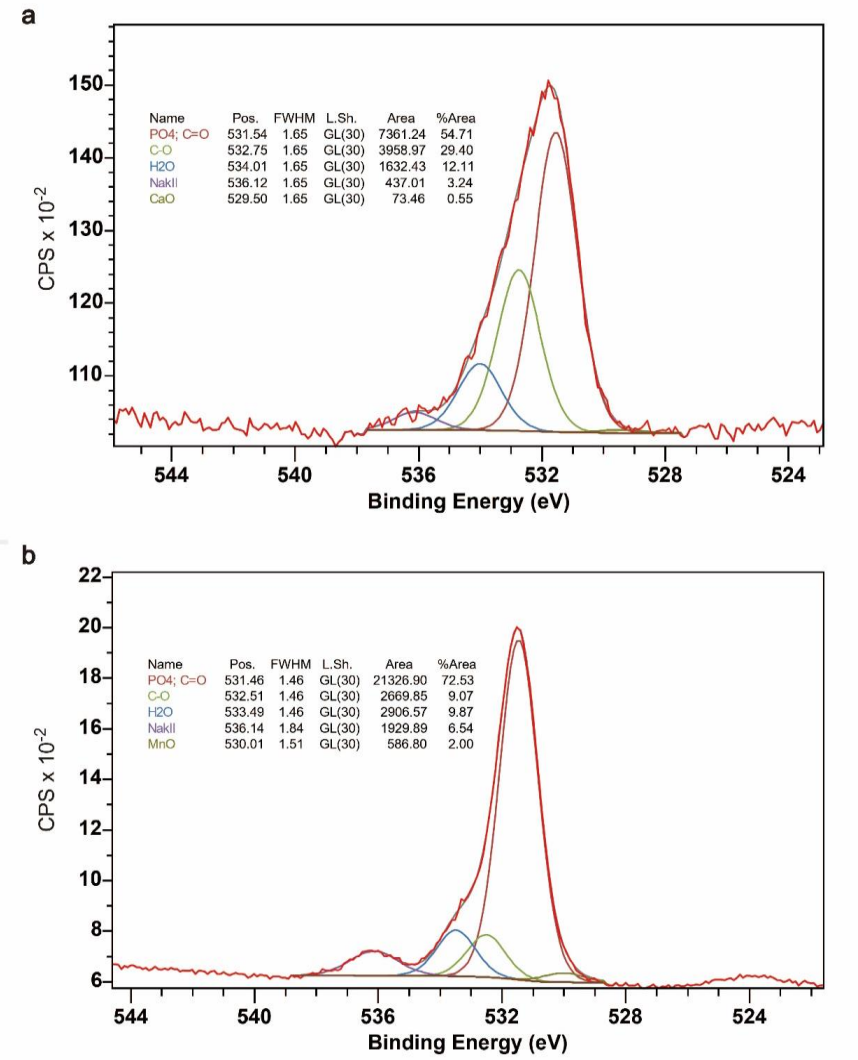

Figure S20. X-ray photoelectron spectroscopy (XPS) analysis of precipitate compounds. **a-b,** XPS spectra of white precipitated appeared in mixture solutions of 2 M $MnCl_2$ (a) and $CaCl_2$ (b) with phosphate buffered saline. The features at around 531 eV indicate that the precipitates are phosphate compounds.

Main text (p2 line 52 – p3 line 54)

(Added)

Ionic current (I_{ion}) was measured under transmembrane voltage (V_b) with a scan rate (r_{scan}) of 65 mV/s in phosphate buffered saline containing 1.37 M NaCl at pH 7.4 (hereafter, NaCl solution refers to the phosphate buffer unless otherwise denoted).

Main text (p5 line 110 – p6 line 128)

(Added)

In fact, white substance appeared upon mixing bulk solutions in a flask (Figure S18),

which is ascribable to precipitation reactions of divalent and trivalent cations with the phosphoric acid included in the electrolyte buffer to form metal phosphates, as we confirmed by x-ray photoelectron and Raman spectroscopy analyses (Figures S19-S20).[7,33]

The role of phosphoric acid was verified by replacing the phosphate-buffered saline at the *trans* with phosphate-free NaCl water of salt concentration 1.4 M. The ionic current characteristics were revealed as featureless denoting the absence of the precipitation reactions in the range of pH from 5.5 to 11.7 (Figure S21). Consistently, no precipitates were found in the mixture solutions (Figures S22). These results unambiguously indicated the in-pore formations and dissolutions of metal phosphates via the reaction between the divalent cations and phosphoric acids as the cause of the extreme ionic current rectification behaviors, where the electromigration of Ca^{2+} at negative voltages leads to the local synthesis and growth of the phosphate layer to almost completely seal the pore, and the reverse reaction in the acidic $CaCl_2$ solution dissolve the nanoprecipitate upon ceasing the Ca^{2+} supply at $V_b > 0$. As such, solution pH plays a role in the reaction equilibrium, where the rectifying behaviors were demonstrated to disappear under acidic conditions prohibiting the in-pore precipitations of the metal phosphates (Figure S24).

Main text (p6 line 146 – 150)

(Revised)

Although the synthesis of the metal phosphates in non-alkaline media is generally complicated processes for predicting whether the reactions inside the nanopore should be endothermic or exothermic,[39,40] the overall results consistently suggest the ion transport-mediated in-pore precipitation/dissolution as a primary factor of the extreme I_{ion} rectifications.

5. A reason for the relatively high capture rates of the linear DNA was explained.

Main text (p9 line 237 – 243)

(Added) Here, it is noted that the gyration radius of ColE1 DNA is estimated to be 194 nm, which is much larger than d_{pore}. Therefore, the polynucleotide chains are required to be dis-entangled before the electrophoretic translocation.[50] In this context, the supercoiled conformations of the cyclic-formed plasmids anticipate larger entropy barrier compared to that for the flexible linear DNA strands of the same length.[51] This would be a reason why the linear genome was detected

relatively frequently in the resistive pulse measurements.

6. Error bars were added to Figure 2d.

Figure 2d

(Revised)

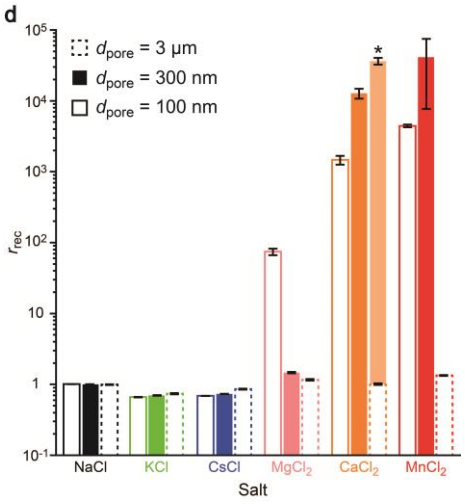

Response to the reviewers

Reviewer #1

Reviewers Comments:

The paper reports how voltage-gated solid-state nanopores were conducted by electrically tunable chemical reactions, where the metal hydroxides repetitively precipitated and dissolute in a pore through manipulating the cation flow by transmembrane voltage in the asymmetric electrolyte solution. Under negative voltages, precipitates grow to reduce ionic current by occluding the nanopore, while inverting the voltage polarity dissolves the hydroxides reopening the pore to ionic flux. They achieve this resistive state switching by adopting low solubility metal hydroxides and the concentration polarization property of the asymmetric electrolyte solution. Overall, this concept is similar to those reported by Siwy (Nano Lett. 2006, 6, 473-477; Nat. Nanotech. 2008, 3, 51-57;), Michael (J. Phys. Condens. Matter. 2010, 22, 454127;), Nader (ACS Nano 2011, 5, 3191-319;), and Patrick (Cryst. Growth Des. 2017, 17, 6565-6571). Highly relevant state switching behaviors due to phase transition have been reported in other systems not recognized, for example reported by Author himself (ACS Applied Materials & Interfaces 2020, 52175); by Golovchenco (Phys. Rev. Lett. 2014, 024506.); among others. A correlation to the exciting concept of nanopore memristor is warranted by showing the potentiation and depressions, while the stability is a concern because of the unstable structure of the precipitated nanopore. Furthermore, the single-molecule sensing using a precipitated nanopore didn't show significant advantages, compared to the single-molecule sensing using a biochannel of protein. Overall, in my opinion, the manuscript can become acceptable if the authors can clearly state the novelty of this work over others reported previously.

(Reply)

First of all, we sincerely appreciate the reviewer for the positive remark on our work, and the important suggestion to clarify the significance of the present findings over the previous research.

Regarding the pioneering experiments using conical nanochannels, the approach is indeed quite similar in the sense that they utilize the in-pore reactions to form nanoprecipitates near nanopores, which allows the observations of the intriguing phenomenon of oscillatory modes of nanoscale precipitate motions. Compared to the high depth-to-diameter aspect ratio geometries of the conical nanochannels, meanwhile, our nanopores are designed to have significantly lower aspect ratio structures to facilitate the

control of the ion transport-mediated in-pore reactions. It provides a distinct advantage of not nucleating freely moving nanoparticles as reported in the previous literature but forming a nanoprecipitate layer for sealing a nanopore and further manipulating its growth/shrinkage kinetics via the simple transmembrane voltage. This enables the real-time control of the effective pore size from the completely sealed to fully open states with precision. Importantly, we demonstrate the reversible changes in the ionic resistance by the number of applied voltage pulses. While the stability of this nanopore memristor was a concern in the previous manuscript, as pointed out by the reviewer, it is no longer an issue as we have found a protocol for stable memristive characteristics. Specifically, the precipitation/dissolution processes were implemented inside a nanopore by scanning transmembrane voltages multiple times prior to driving the nanopore memristors. This simple training offered highly stable memristive properties that allowed us to identify the distinct characteristics of the nanopore memristors driven in different types of salt solutions (please see the revised Figure 5; please also see the newly added Figures S28-S30 about the training protocol for stable memristor operations and Figures S2-S7 along with S14 for the stability of the ionic rectification behaviors). We would like to emphasize that the previous approach cannot implement a similar task as it requires precise control of the Brownian motions of the precipitated nanoparticles under the influence of the electrostatic and hydrodynamic drag forces (as reported in Commun. Mater. 2, 29 (2021), for example). Other approaches, such as the one using the osmotic flow-mediated control of the ion concentrations (ACS Appl. Mater. & Interf. 12, 52175 (2020)) only allows binary switching of the nanopore resistance. The local heating (Phys. Rev. Lett. 113, 024506 (2014)) may be useful in controlling the ionic resistance by the associated changes in the liquid viscosity, but not for the memristor applications as laser pulses can merely induce temporal enhancement in the ionic current without any memory effect.

As a resistive pulse sensor, it has long been a dream for the solid-state nanopore technology to enable the fabrication of well-defined pore structures so as to complement the relatively unstable structures of bionanopores in lipid bilayers (Nat. Biotechnol. 26, 1153 (2008)). In this context, the state-of-the-art biological nanopore technology can tailor the pore structure at a molecular level via the engineering of point mutations in transmembrane proteins (Nat. Chem. Biol., https://doi.org/10.1038/s41589-024-01734-x). On the other hand, electron beam milling has been demonstrated as capable of controlling the size and shape of a nanopore with single-nanometer resolution in a dielectric membrane. However, the fabrication can be carried out only in high vacuum (Nat. Mater. 2, 537 (2003)), thus making it difficult to ensure the structure remains the same during the ionic current measurements. There is also a dielectric breakdown approach (Nat. Protocols 15, 122 (2020)) that can form single-digit nanopores in situ by a simple voltage control.

Nevertheless, the controllability of the number and size of pores is still considered a critical issue (Sci. Rep. 8, 1234 (2018)). In contrast, the present method can seal a relatively large pore nearly completely with a leakage current around 100 pA at 0.5 V. With the ability to open a nanopore and finely control its size by the voltage pulsing in real time, it has a potential to become a useful tool for adjusting the pore size to fit the analytes of concern right before the resistive pulse measurements. Although an interesting subject to investigate, we would like to leave it as future work since it is beyond the scope of the present work.

As explained above, the present work reports a novel method for real-time control of nanopore sizes *in situ* that allows a memristor of low power consumptions and also holds promise as an electrical valve to control the molecular translocations for advanced solid-state nanopore sensing. The principle of operation is simple and can be tested with relatively large pores that can be expected to spur a lot of follow-up studies both theoretical and experimental. Overall, we believe our work holds significance to a broad readership that warrants publication in Nature Communications.

Following the comment, we have revised the main text. We have also added new results regarding the stability of the ionic current rectifications and memristive characteristics as described below.

Main text (p2 line 28 – 43)

(Revised) Stochastic collisions of two or more substances provide opportunities for transforming their atomic components. Principles of chemistry govern these processes, facilitating the creation of diverse compounds with desirable properties, where factors such as pH, temperature, and pressure shape the energy landscape of reaction pathways at equilibrium. In contrast to the conventional diffusion-based chemical systems, meanwhile, nanoreactors have emerged as efficient platforms capable of controlling reaction kinetics within a nanoconfined space through mass flow control.[1-3] In particular, solid-state nanopore technology has proven useful for *operando* observations of the chemical synthesis of an individual nanoparticle at real time (Au nanorod, nanoparticles).[4,5] Motion control of the *in situ* formed nanoprecipitates was also demonstrated with high length-to-diameter aspect ratio conical nanochannels,[6,7] which allowed novel nanofluidic diodes via the transmembrane voltage-dependent clogging of the nanoscale conduits.[6-10] Inspired by the pioneering work, we herein report tunable chemical reactions by electrical manipulation of ion transport in a small hole for advanced fluidic devices. This method employs an ultrathin dielectric membrane hosting a nanopore connecting two distinct ionic reactant solutions for precise manipulations of the ion electromigration

to enable reversible precipitation/dissolution reactions of a metal compound layer (Figure 1a).

Main text (p7 line 173 – p8 line 183)

(Added) Similar characteristics were also found in $CaCl_2$/NaCl buffer systems, but at a relatively high conductance regime reflecting its reaction equilibrium distinct to that in the $MnCl_2$ solution (Figure S27). Here we add the importance of a training process to obtain the stable memristive characteristics. More specifically, V_b scans were implemented multiple times to reproducibly form a phosphate layer inside a nanopore that served to initialize the memristor state in prior to the subsequent potentiation/depression cycling (Figures S28 – S29). Without this pretreatment, the nanopore memristors tend to be non-controllable by the voltage pulses. Such fine control of the nanopore conductance may not be achievable with the conical nanopore approach[6-10] as it requires a formidable task of precise manipulation of the Brownian motion of a precipitated nanoparticle under the influence of the electrostatic and hydrodynamic drag forces.[43]

Main text (p10 line 252 – p11 line 266)

(Added) From a viewpoint of resistive pulse sensing, it has long been a dream for solid-state nanopore technologies to enable the formation of well-defined pore structures. Structures of biological nanopores are demonstrated as tailorable at a molecular level via the engineering of point mutations in transmembrane proteins.[57] As for the solid-state nanopores, on the other hand, electron beam milling has been demonstrated as capable of controlling the size and shape of a hole with single-nanometer resolution in a dielectric membrane. However, the fabrication can be carried out only in high vacuum,[58] thus making it difficult to ensure the structure remains the same during the ionic current measurements. There is also a dielectric breakdown approach[59] that can form single-digit nanopores *in situ* by a simple voltage control. Nevertheless, the controllability of the number and size of pores is still considered a critical issue.[60] In contrast, the present method can seal a relatively large pore nearly completely with a leakage current around 100 pA at 0.5 V. Leveraging the ability to open a nanopore and finely control its size by the voltage pulsing in real time, therefore, it has a potential to become a useful tool for adjusting the pore size to fit the analytes of concern right before the resistive pulse measurements.

Figure S2

(Added)

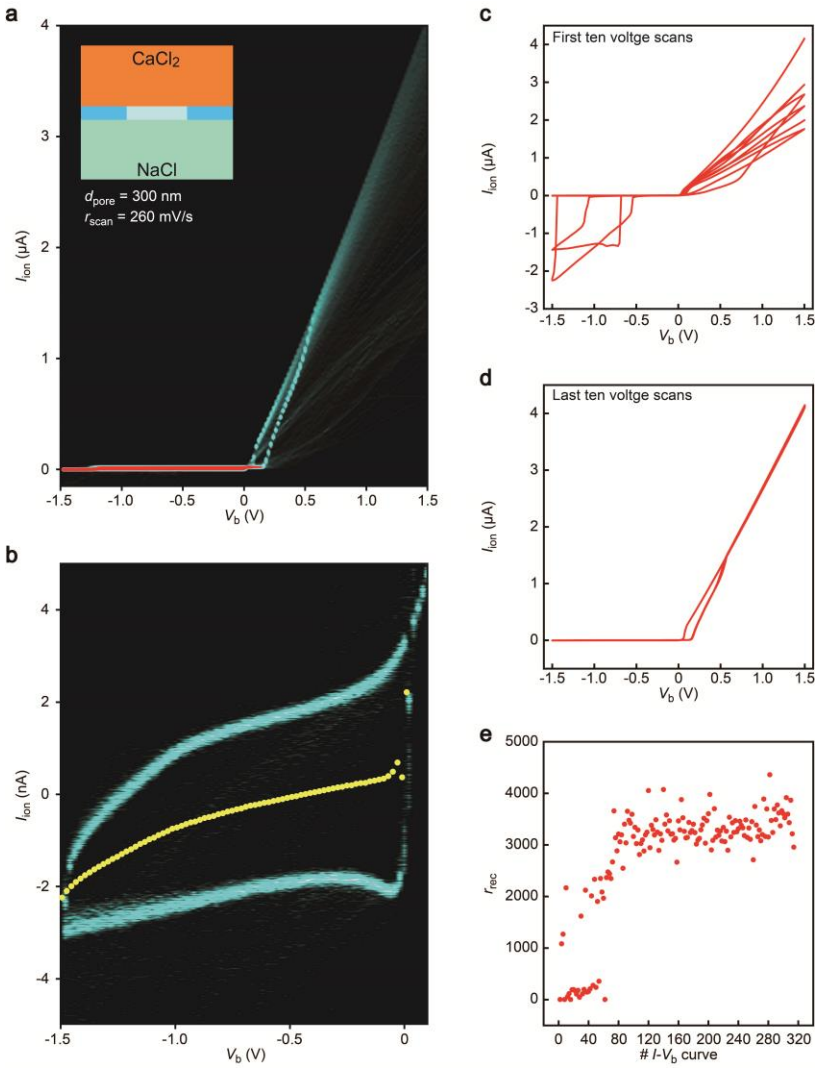

Figure S2. Reproducibility of the rectification characteristics in a 300 nm nanopore with a $CaCl_2$/phosphate buffered saline configuration under a voltage scan rate of 260 mV/s. a-b, Two dimensional histograms of 314 I_{ion} – V_b curves (a) and its close view at the negative voltage regime (b) obtained under repetitive voltage scanning from +1.5 V to -1.5 V. Yellow plots are the average of the curves acquired under the positive and negative voltage sweeps. **c,** The first ten I_{ion} – V_b curves showing relatively unstable nature of the ionic current characteristics suggestive of the fluctuating dissolution processes of the in-pore precipitated layer. **d,** In contrast, the last ten curves are highly reproducible indicating the stabilized precipitation/dissolution processes of the calcium phosphate layer formed in the nanopore. **e,** The rectification ratio r_{rec} calculated from each curve. Initially, r_{rec} tends to be low due to the inadequate time for forming nanoprecipitate seeds on the pore wall surface. After about 100 cycles of measurements, the precipitation/dissolution processes become stable giving r_{rec} around 3000.

Figure S3

(Added)

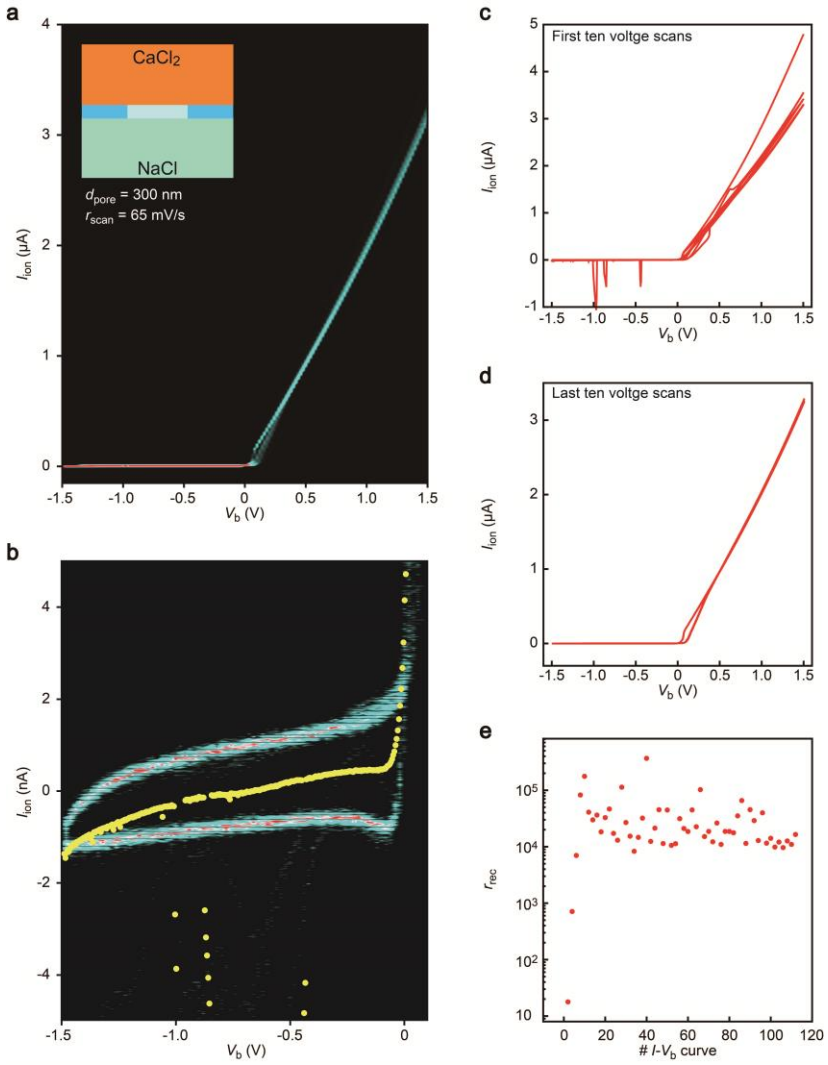

Figure S3. Reproducibility of the rectification characteristics in a 300 nm nanopore with a $CaCl_2$/phosphate buffered saline configuration under a voltage scan rate of 65 mV/s. a-b, Two dimensional histograms of 112 I_{ion} – V_b curves (a) and its close view at the negative voltage regime (b) obtained under repetitive voltage scanning from +1.5 V to -1.5 V. Yellow plots are the average of the curves acquired under the positive and negative voltage sweeps. **c,** The first ten I_{ion} – V_b curves showing relatively unstable nature of the ionic current characteristics suggestive of the fluctuating dissolution processes of the in-pore precipitated layer. **d,** In contrast, the last ten curves are highly reproducible indicating the stabilized precipitation/dissolution processes of the calcium phosphate layer formed in the nanopore. **e,** The rectification ratio r_{rec} calculated from each curve. After several cycles of measurements, r_{rec} tends to be stable at around 10^4 to 10^5.

Figure S4

(Added)

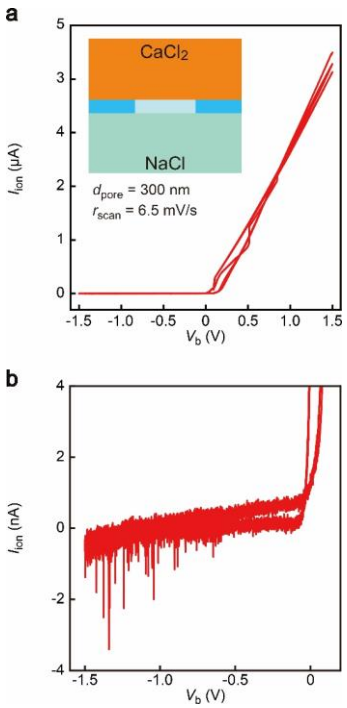

Figure S4. Reproducibility of the rectification characteristics in a 300 nm nanopore with a $CaCl_2$/phosphate buffered saline configuration under a voltage scan rate of 6.5 mV/s. a, $I_{ion} - V_b$ curves obtained under five cycles of voltage scanning from +1.5 V to -1.5 V. **b,** A close view of the suppressed ionic current at the negative V_b.

Figure S5

(Added)

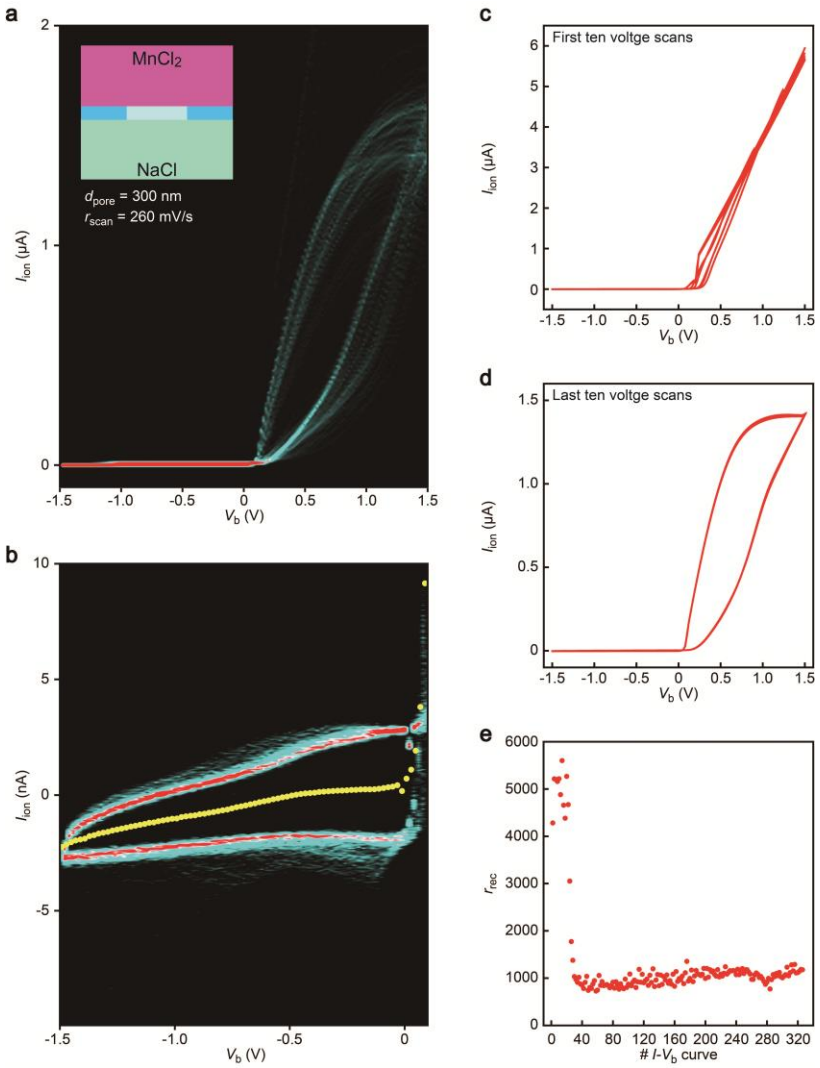

Figure S5. Reproducibility of the rectification characteristics in a 300 nm nanopore with a $MnCl_2$/phosphate buffered saline configuration under a voltage scan rate of 260 mV/s. a-b, Two dimensional histograms of 314 I_{ion} – V_b curves (a) and its close view at the negative voltage regime (b) obtained under repetitive voltage scanning from +1.5 V to -1.5 V. Yellow plots are the average of the curves acquired under the positive and negative voltage sweeps. **c,** The first ten I_{ion} – V_b curves showing relatively unstable nature of the ionic current characteristics at the positive voltages suggestive of the fluctuating dissolution processes of the in-pore precipitated layer. **d,** In contrast, the last ten curves are highly reproducible indicating the stabilized precipitation/dissolution processes of the calcium phosphate layer formed in the nanopore. **e,** The rectification ratio r_{rec} calculated from each curve. Initially, r_{rec} tends to be low due to the inadequate time for forming nanoprecipitate seeds on the pore wall surface. After tens of cycles of measurements, the precipitation/dissolution processes become stable giving r_{rec} around 1000.

Figure S6

(Added)

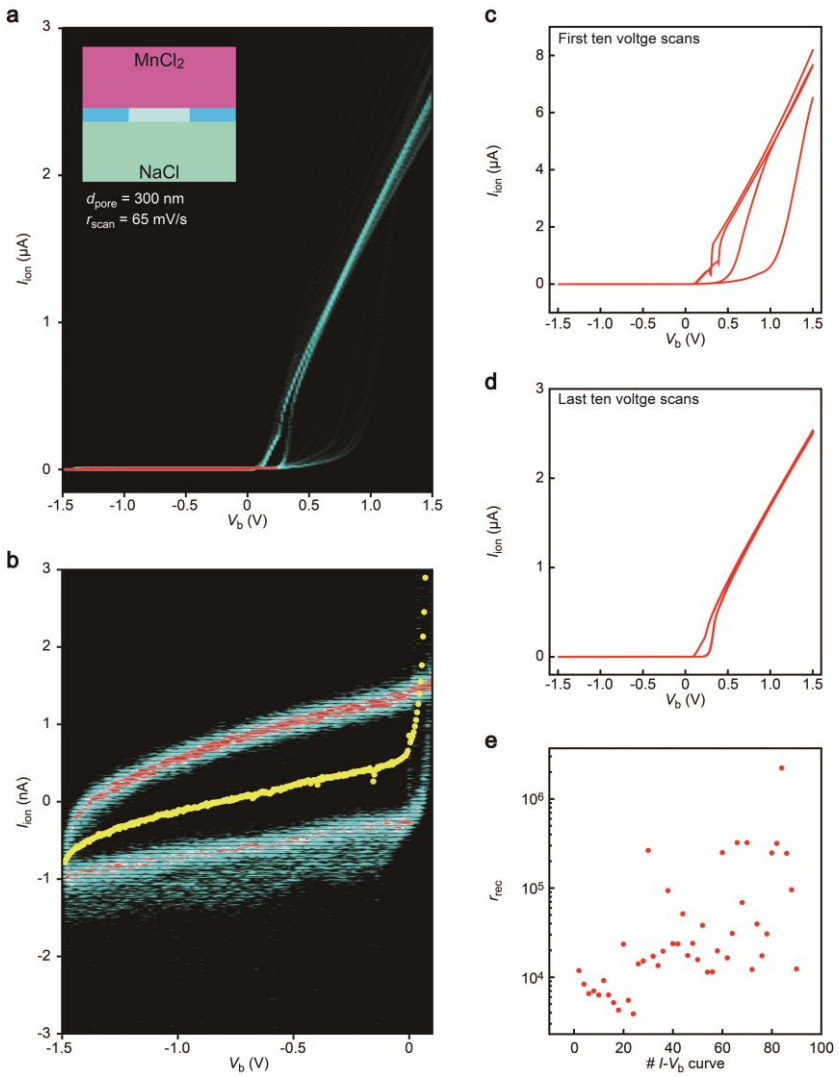

Figure S6. Reproducibility of the rectification characteristics in a 300 nm nanopore with a $MnCl_2$/phosphate buffered saline configuration under a voltage scan rate of 65 mV/s. a-b, Two dimensional histograms of 112 I_{ion} – V_b curves (a) and its close view at the negative voltage regime (b) obtained under repetitive voltage scanning from +1.5 V to -1.5 V. Yellow plots are the average of the curves acquired under the positive and negative voltage sweeps. **c,** The first ten I_{ion} – V_b curves showing relatively unstable nature of the ionic current characteristics suggestive of the fluctuating dissolution processes of the in-pore precipitated layer. **d,** In contrast, the last ten curves are highly reproducible indicating the stabilized precipitation/dissolution processes of the calcium phosphate layer formed in the nanopore. **e,** The rectification ratio r_{rec} calculated from each curve with values up to over 10^6.

Figure S7

(Added)

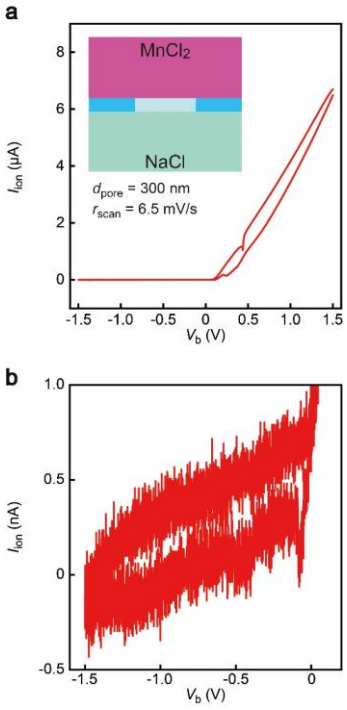

Figure S7. Reproducibility of the rectification characteristics in a 300 nm nanopore with a $MnCl_2$/phosphate buffered saline configuration under a voltage scan rate of 6.5 mV/s. **a,** $I_{ion} - V_b$ curves obtained under five cycles of voltage scanning from +1.5 V to -1.5 V. **b,** A close view of the suppressed ionic current at the negative V_b.

Figure 5
(Revised)

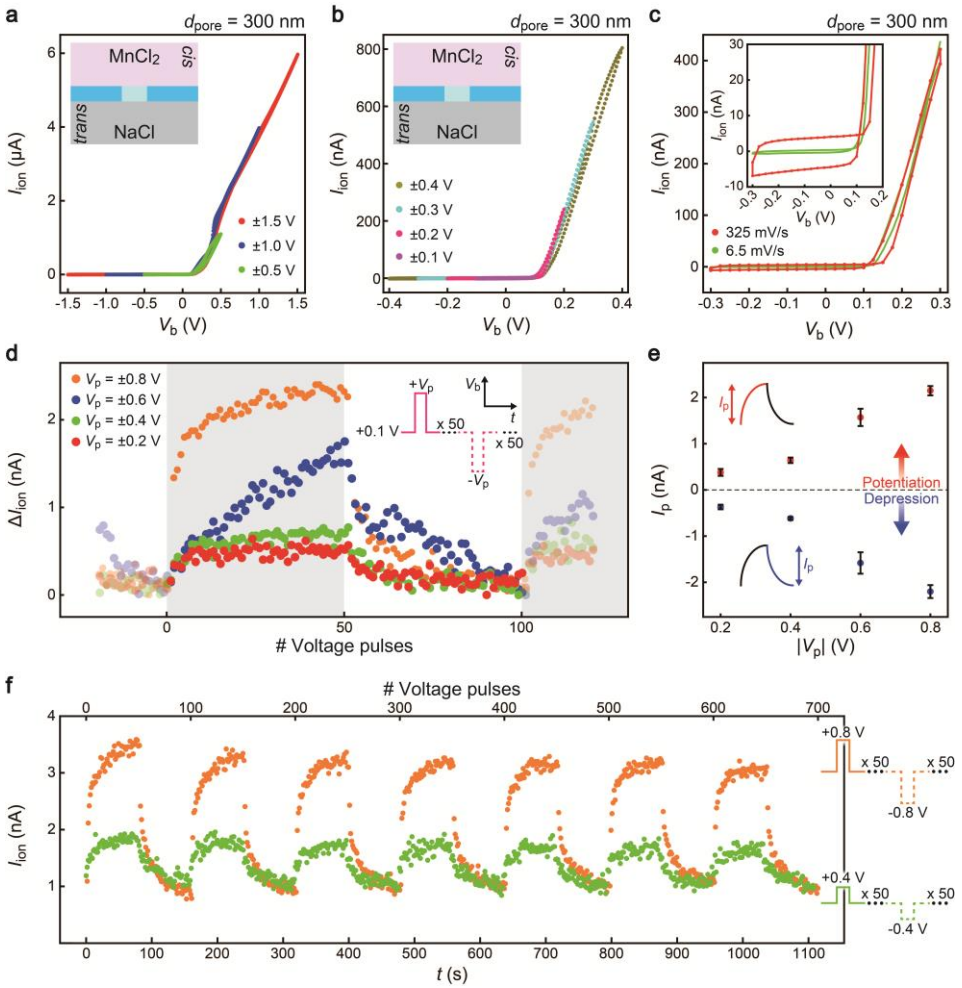

Figure 5. In-pore chemical reaction-driven nanofluidic memristor. **a-b,** I_{ion} – V_b characteristics of a 300 nm-sized nanopore with a $MnCl_2$/NaCl configuration measured under various ranges of transmembrane voltages. Note the I_{ion} remains suppressed when scanning V_b between -0.1 V and 0.1 V (b). **c,** Scan rate dependence of I_{ion} – V_b displaying pinched hysteresis loops. Inset shows a magnified view of the suppressed I_{ion} states. **d,** Memristive characteristics under the applications of 50 ms transmembrane voltage pulses of ±0.5 V amplitudes. ΔI_{ion} is the ionic current recorded at +0.1 V after each voltage pulsing (the baseline current was subtracted). The positive and negative pulses drive the potentiation (grey regions) and depression (white regions) processes of the nanopore memristor via the induced in-pore dissolution/precipitation reactions. **e,** The ionic current change I_p by the positive (red) and negative (blue) voltage pulses of amplitudes V_p. Error bars denote the standard deviations within four cycles of potentiation/depression processes. **f,** Potentiation/depression of the nanopore memristors under the voltage pulses of V_p = ±0.8 V (orange) and ±0.4 V (green). Read voltage was +0.1 V.

Figure S28

(Added)

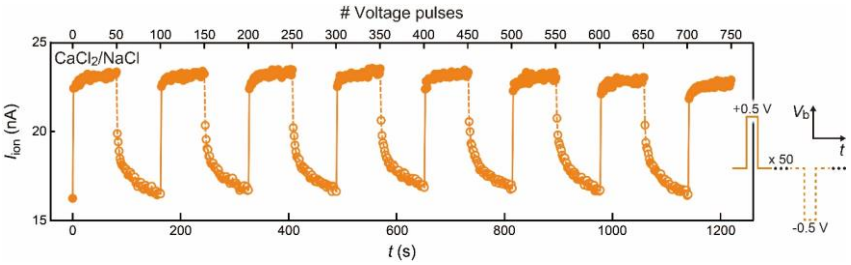

Figure S28. Stable memristive characteristics of a 300 nm-sized nanopore with a $CaCl_2$/phosphate buffered saline after training. Note the relatively high ionic current states of the $CaCl_2$ memristors ascribable to the chemical reaction equilibrium distinct to that in a $MnCl_2$/phosphate buffered saline configuration.

Figure S29

(Added)

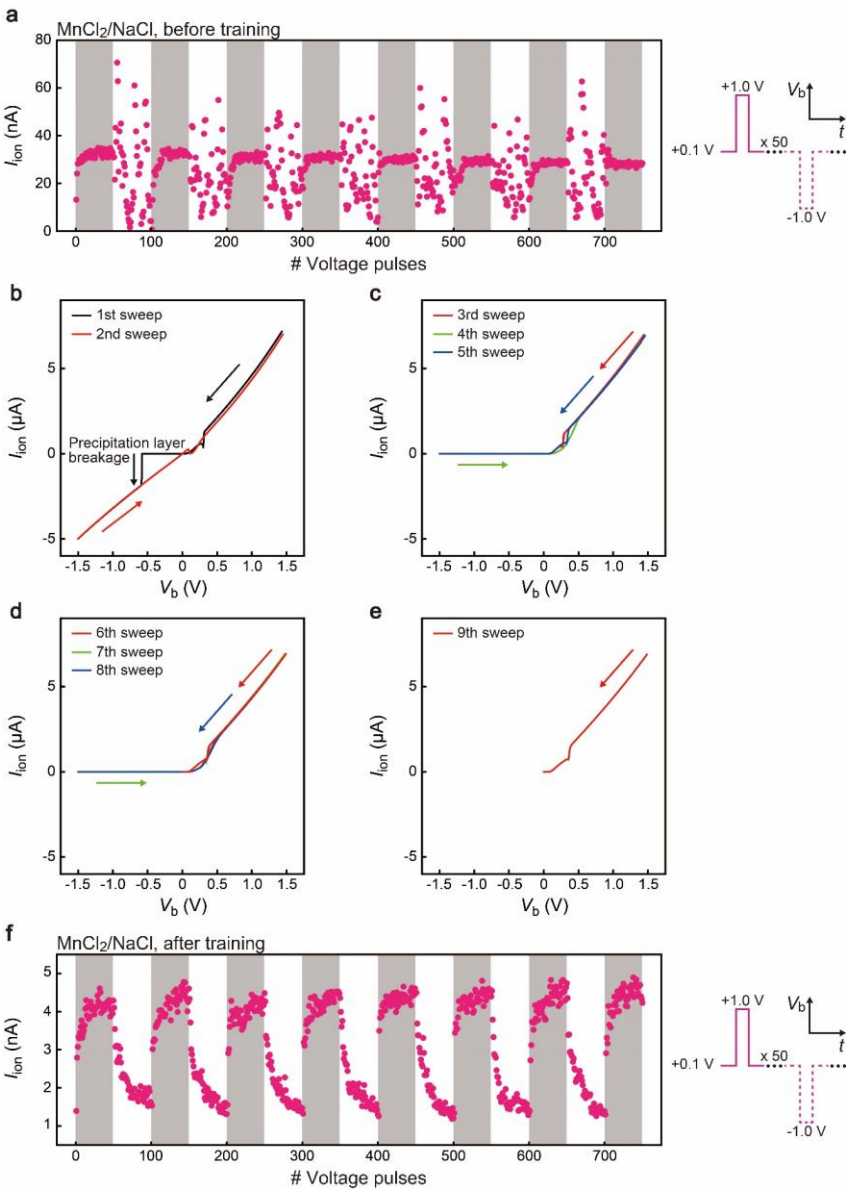

Figure S29. Training protocol for stable nanopore memristors. a, Memristive characteristics of a 300 nm-sized nanopore with a $MnCl_2$/phosphate buffered saline configuration without training. Applying positive and negative voltage pulses of 50 ms widths and ±0.5 V amplitudes, the ionic current tends to fluctuate upon the depression processes indicative of unstable nature of the in-pore precipitated phosphate layer under the given conditions. **b-e,** Training processes. Before driving the memristors, transmembrane voltage was scanned for 9 times between +1.5 V and -1.5 V. Initially, the precipitate layer was unstable at negative voltages (b). Repeating the voltage scanning, the I_{ion} – V_b curves become highly reversible suggesting the formation/dissolution of phosphate layers in a reproducible manner (b-d). The training ends by sweeping V_b back to 0 V (e). Subsequently, the memristors were driven by the sequence of the voltage pulses applied. **f,** An example of the memristive characteristics recorded after the training processes showing stable features in the potentiation/depression cycles.

Figure S30

(Added)

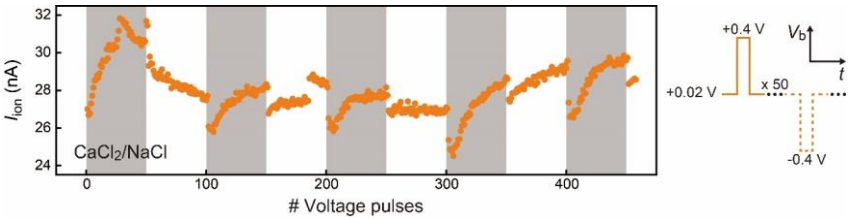

Figure S30. Unstable memristive characteristics of a 300 nm-sized nanopore with a $CaCl_2$/phosphate buffered saline without training. The ionic conductance tends to change in irregular manner against the voltage pulsing.

Response to the reviewers

Reviewer #2

In this manuscript, M. Tsutsui et al. report on nanopores that allow to tune chemical reactions by means of electrical manipulation of transmembrane ion transport. Depending on the salty solutions and the pH-value across the membrane, the authors could control and block the ionic flux through the nanopores. This is attributed to shrinking of the effective pore size by formation of metal hydroxides. I think the manuscripts provides meaningful results that may be interesting for a wide readership. In general, the manuscript is well written (but polishing of the language is recommended) and well structured. Experimental results are discussed in detail. The references are well balanced. It will be necessary to improve the figure quality as some graphics are difficult to read. In addition, I would like to highlight the following points, which the authors may address in a major revision:

(Reply)

We are grateful for the positive opinion about the present work. We have studied the comments carefully and revised the manuscript accordingly as we described in the point-by-point reply below.

- The terms cis and trans may not be well known for a large readership. It may be useful to add these terms in figure 1a.

(Reply)

Thank you very much for letting us know the lack of critical information. We have labelled *cis* and *trans* in Figure 1a.

Figure 2a

(Revised)

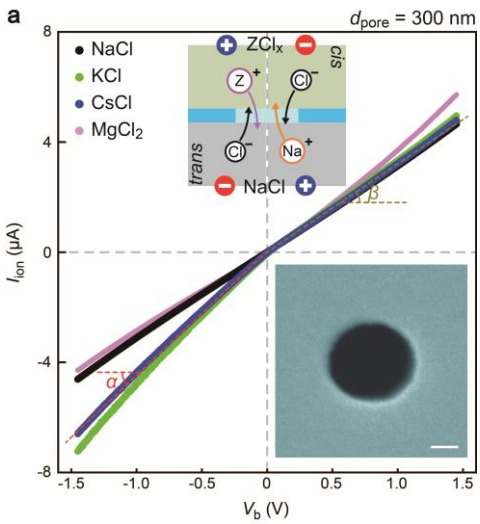

- The inset in Figure 2b is really difficult to read. Instead (or in addition) to different colors I recommend using different forms for indicating the different salts. Moreover, cis and trans may be also added in the insets.

(Reply)

Thank you for the suggestion. We have changed the form of the plots for β to square and labeled the type of salts in the inset. We have also added labels denoting *cis* and *trans* in Figures 2a, 2b, and 2c.

Figure 2a

(Revised)

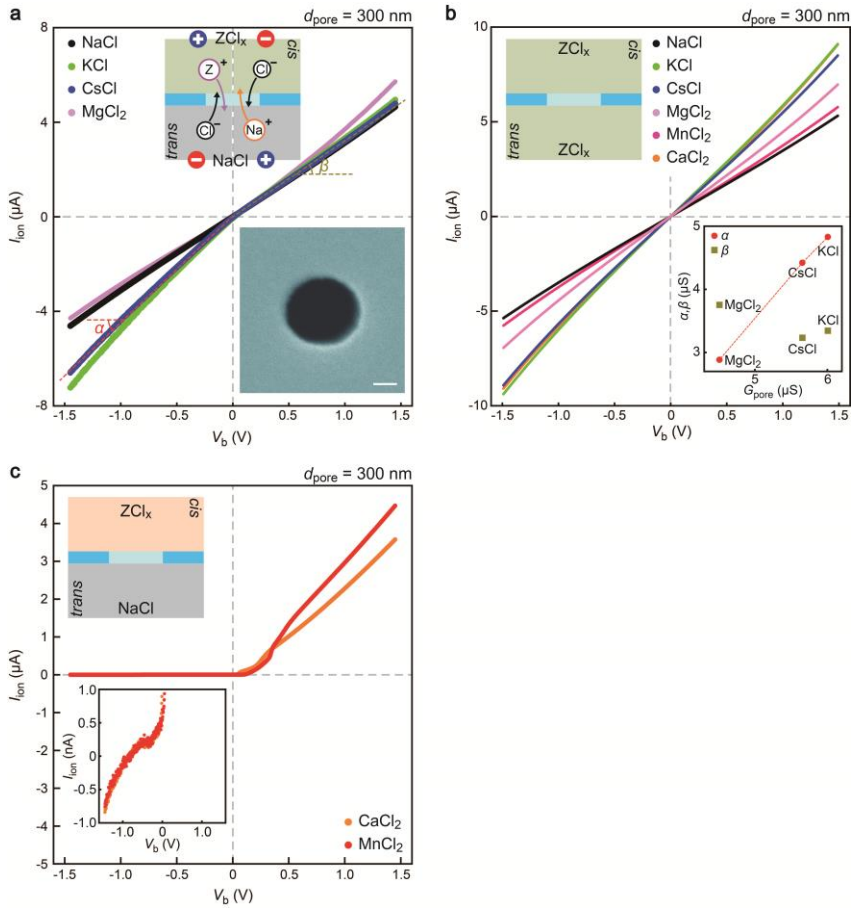

- It is not clear to me how the core diameter is estimated in Figure 2d. Why is it given in arb. units while on the other hand, the authors discuss that the (shrinked?) core size is larger than the Debye length (which I do not put into question)

(Reply)

Thank you for the comment. The rectification ratio, r_{rec}, has been calculated from the ratio of the ionic current at +1 V and -1 V. As pointed out by the reviewer, the unit is dimensionless and inappropriate to be described as arb. units. We have revised the unit of r_{rec} as shown below. In the figure, we have also added error bars denoting the variations in the rectification ratio.

Figure 2d

(Revised)

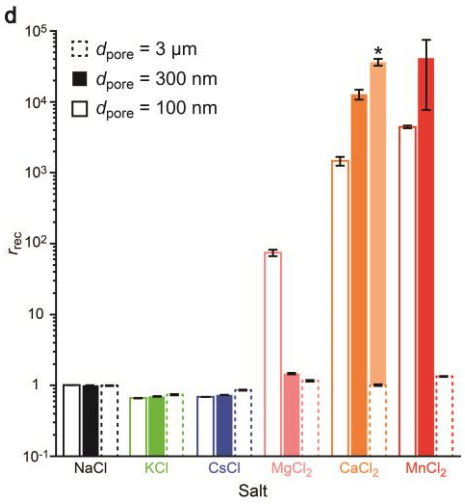

- If the salt is similar on both sides (Figure 2b) there is no change of the pore conductivity. I think this is important to understand the overall behavior, but the manuscript does not discuss this effect in detail. It could be assumed that even a small difference of the geometry, surface, salt concentration etc. could lead to a change of the conductivity upon further cycling (at least for MnCl2). How does the experimental observation fit to the author's theoretical explanation? Did the author see any effect of having the same salt across the membrane but with a concentration gradient?

(Reply)

Thank you very much for the constructive comment. As the reviewer points out, there are some factors that affect the conductance other than nanopore size. Perhaps the most well known phenomenon is the ionic current rectification in a permselective nanopore under salinity difference, where the conductance tends to be larger (smaller) when the transmembrane voltage drives the transport of high (low) concentration anions (anion-selective) or cations (cation-selective) (ACS Nano 18, 15046 (2024)).

Electroosmotic flow also gives similar effect in larger pores by diluting the local ion concentration in a voltage polarity dependent manner (ACS Nano 4, 477 (2010)). In case of the strong rectifications observed for the $MnCl_2$/NaCl and CaCl2/NaCl systems, in stark contrast, there were only small salinity difference (2 M against 1.37 M) across the membrane. Furthermore, the high ionic strength as well as the relatively large pore diameters anticipates negligible permselectivity of the ion transport. Therefore, the present results cannot be explained by these conventional mechanisms involving no changes in the nanopore geometries.

Meanwhile, there are several results supporting our theoretical explanation. First of all, mixing two specific salt solutions induce chemical reactions to generate white precipitates as we showed in Figure S10 of the previous manuscript (Figure S18 in the revised version). We observed this to happen for $MnCl_2$, $CaCl_2$, and $AlCl_3$; and for these salts, we found the strong rectification behaviors in the I_{ion} - V_b measurements. It is naturally attributed to the voltage-dependent precipitation/dissolution reactions that leads to nucleation and growth/shrinkage of nanoprecipitates inside a nanopore. More directly, the scanning electron microscopy observations confirmed the precipitated compound inside the nanopore after the precipitation reaction. On the other hand, the ionic current curves were featureless for KCl and CsCl that caused no precipitation when mixed with the NaCl solution. All these results serve to consistently prove that the extreme rectifications as well as the memristive characteristics observed occurred via the chemical reaction-mediated changes in the nanopore sizes.

As explained above, the type of cations and pH levels at the *cis* and *trans* side of the solution dictate the in-pore precipitation/dissolution reactions. Such reactions were absent for the cases of adding salt concentration difference with the same salts, where we observed only weak rectification characteristics due to the electroosmosis mechanism as we showed in Figure S8 of the previous manuscript (Figure S16 in the revised Supplementary Information).

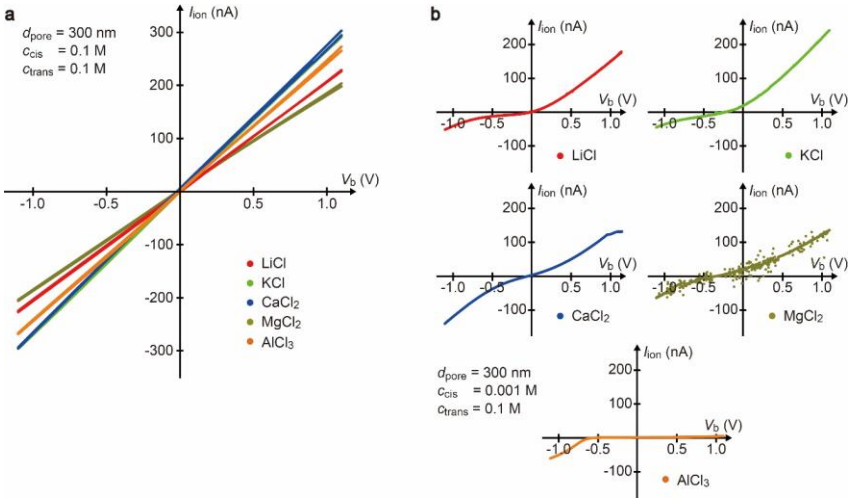

Figure S16. Ionic current characteristics of a 300 nm SiN_x nanopore under salinity gradients of various salts. **a,** In case of no salinity gradients. The ionic current showed ohmic behaviors suggesting no reaction taking place in the nanopore. **b,** The ionic current curves under 100-fold salinity gradients. Ionic current suppression was observed at positive voltages for $AlCl_3$ indicating partial pore blocking via the Al^{3+}-flow-mediated in-pore precipitation. Voltage scan rate was 65 mV/s.

- On page 4, l. 94, the authors suggest that ion-ion interactions may not play (a dominant?) role because also low concentrations were tested. However, as the pores shrink, the effective concentration in the core could indeed lead to ion-ion interactions. I think this cannot be simply excluded without further evidence. Moreover, the Debye theory is not applicable for high concentrations.

(Reply)

Thank you for raising the scrutinizing point. We first would like to emphasize that what we meant on page 4 was to describe that the strong suppression of the ionic current cannot be ascribed to the solubility limit of the salts. As for the ion-ion interactions, it appears as the non-linear dependence of the bulk solution conductivity on the salt concentrations (Figure R1) as widely known (An Introduction to Aqueous Electrolyte Solutions; John Wiley & Sons: Hoboken, NJ, 2007). Their effects are also reported to become notable in the ionic current characteristics of nanopores/nanochannels by inducing ion-ion pairing (*J. Am. Chem. Soc.* **141**, 4264-4272 (2019)), but only for the cases when their dimensions are below 8 nm, as the reviewer also points out. In contrast, the nanopores used in the present study is larger than 100 nm in diameter, where no notable influence of the ion-ion interactions on the mechanism underlying the extreme ionic current rectification is expected. On the other hand, it may be relevant for understanding the ion transport properties of the precipitate-sealed pores. As we showed in the newly added Figure S14, we found stable ionic current of around 100 pA at -0.5 V transmembrane voltage. When attributing this

current to ion flow through a single shrunk pore, its diameter is estimated to be around 1 nm assuming the conductivity of the bulk salt solutions. Nevertheless, the origin of the infinitesimal ionic current is uncertain at this time. We would like to investigate it in our future work as it is beyond the scope of the present study that focuses mainly on the mechanism of the extreme rectifications and memristive characteristics.

We made this point clear in the revised manuscript as written below.

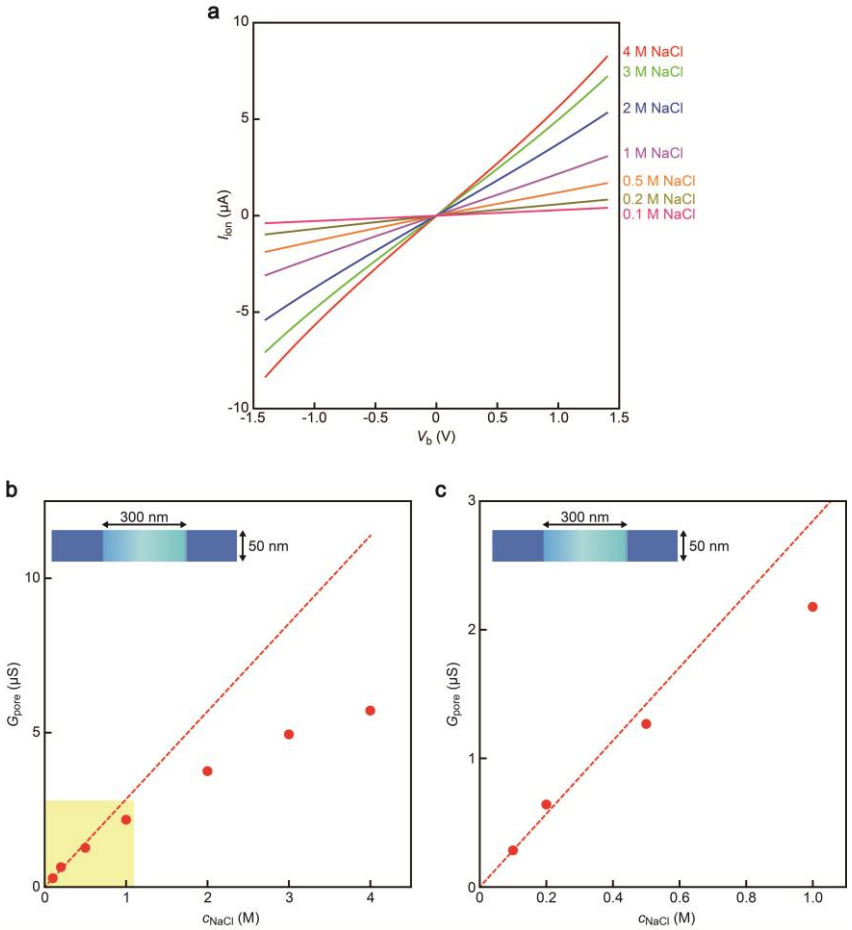

Figure R1. a, The ionic current (I_{ion}) versus transmembrane voltage (V_b) characteristics of a 300 nm-sized pore in a 50 nm-thick SiN_x membrane. The NaCl concentration of phosphate buffered saline was changed from 4 M to 0.1 M. **b,** The pore conductance (G_{pore}) estimated by linear fittings to the plots in (a). Red dashed line is a linear scaling of the conductance at the salt concentration (c_{NaCl}) of 0.1 M. **c,** A close view of the yellow region in (b). Non-linear dependence of G_{pore} on c_{NaCl} is observed at the high salt concentration conditions due to the lowered ion mobilities by the ion-ion interactions.

Main text (p4 line 98 – 102)

(Added)

Analogously, ion-ion interactions cause only minor effect on the ionic conductance as they generally become notable in single-digit nanopores.[29]

Figure S14

(Added)

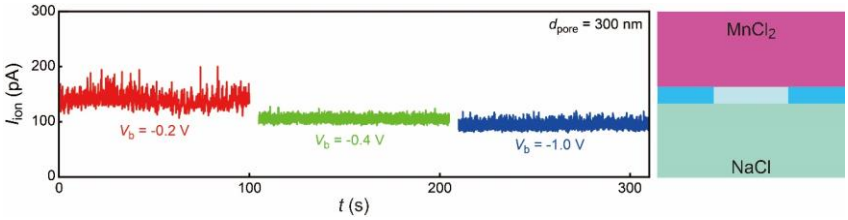

Figure S14. Ionic current flowing through a 300 nm nanopore of a $MnCl_2$/phosphate buffered saline configuration under negative transmembrane voltage recorded at 10 kHz. I_{ion} – t traces of a 300 nm nanopore sealed by the phosphate compound under the negative transmembrane voltage of -0.2 V (red), -0.4 V (green), and -1.0 V (blue). The initial conditions were set as the same by applying +1.0 V to fully open the nanopore prior to the measurements at the negative voltages. The ionic current is stable at around 100 pA for over 100 seconds indicative of nearly complete sealing of the nanopore via the precipitated phosphate layer. The infinitesimal ionic current may be attributed to a single-digit nanopore formed in the precipitate layer, where particular ion-ion interactions[S6,S7] would take place to affect the ionic conductance.

Reference:

S6. Ma, J., Li, K., Li, Z., Qiu, Y., Si, W., Ge, Y., Sha, J., Liu, L., Xie, X., Yi, H., Ni, Z., Li, D. & Chen, Y. Drastically reduced ion mobility in a nanopore due to enhanced pairing and collisions between dehydrated ions. J. Am. Chem. Soc. **141**, 4264-4272 (2019).

S7. Robin, P., Emmerich, T., Ismail, A., Nigues, A., You, Y., Nam, G. -H., Keerthi, A., Siria, A., Geim, A. K., Radha, B. & Bocquet, L. Long-term memory and synapse-like dynamics in two-dimensional nanofluidic channels. Science **379**, 161-167 (2023).

- Also on page 4, the authors report the formation of a "white substance" that is considered to be the metal hydroxide. I strongly recommend to verify this by additional spectroscopic techniques such as ex situ XPS. This would contribute to a better understanding of the proposed mechanism.

(Reply)

We greatly appreciate the reviewer for pointing out the lack of evidence regarding the white precipitates. In fact, we realized that we should verify the influence of phosphoric acid in the phosphate buffered saline used. For this, we performed the ionic current measurements by adding phosphate-free NaCl solutions of various pH from 5.5 to 11.5 (please see newly added Figures S21 and S22). In these cases, we did not find the extreme rectification characteristics suggestive of the ion transport-mediated in-pore

precipitation/dissolution reactions. Accordingly, we did not find the white precipitates when mixing the phosphate-free salt water with the $CaCl_2$ and $MnCl_2$ solutions. More directly, XPS and Raman spectroscopy analyses indicated that the white precipitates are phosphate compounds (please see newly added Figures S19 and S20). These observations unambiguously confirmed the important role of phosphoric acid in the electrolyte buffer that reacted with the divalent and trivalent cations inside the nanopore under the ion transport control via the transmembrane voltage. Meanwhile, we would like to emphasize that this does not affect the interpretation of the extreme rectification and memristive characteristics observed.

The above results were added to the main text and Supplementary Information as follows.

Figure S21

(Added)

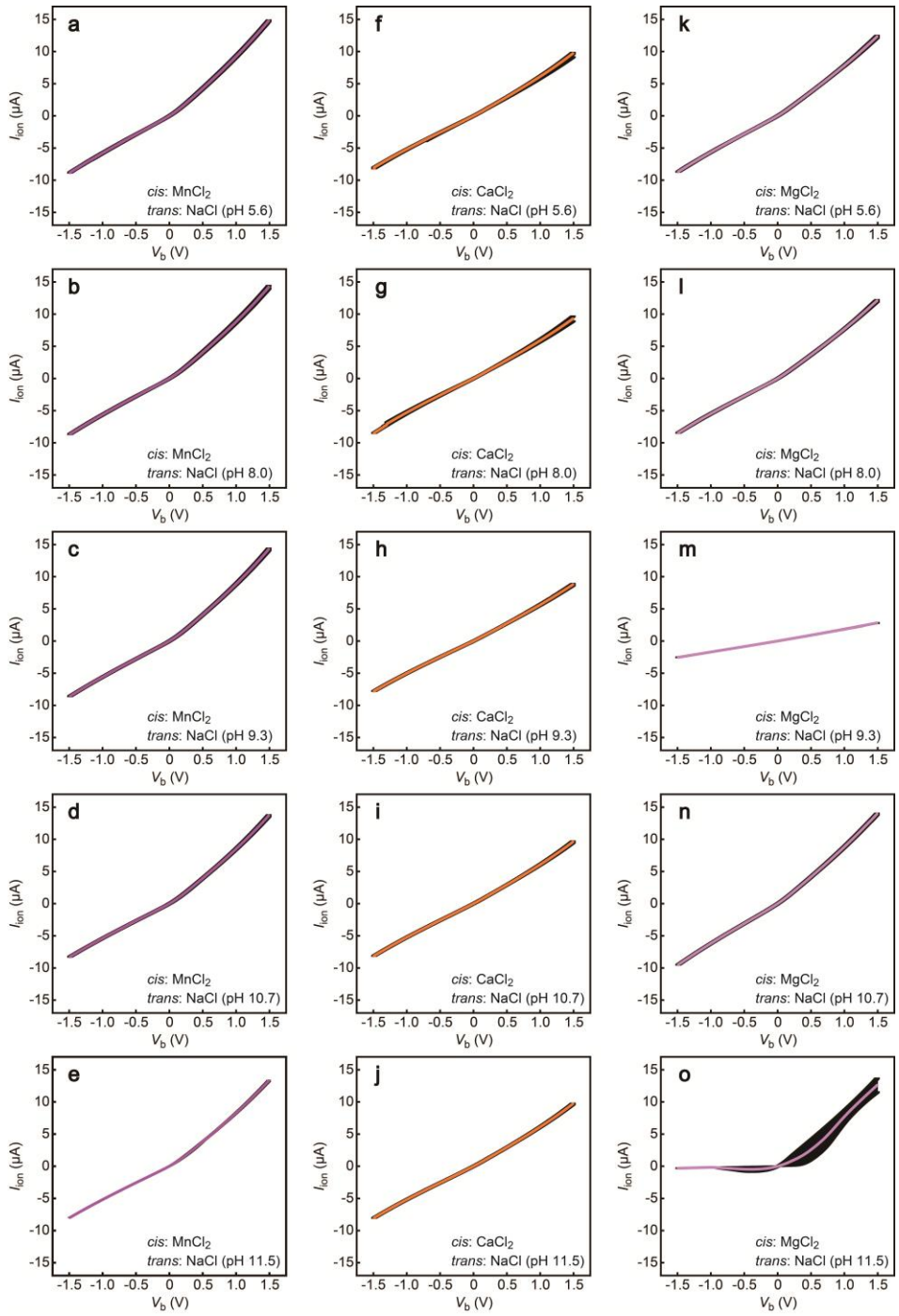

Figure S21. Ionic current characteristics in phosphate-free NaCl water (1.4 M) of various pH. a-e, I_{ion} – V_b curves recorded for a 300 nm nanopore with a $MnCl_2$/phosphate-free NaCl water configuration (r_{scan} = 65 mV/s). The pH of the NaCl water was adjusted to 5.6 (a), 8.0 (b), 9.3 (c), 10.7 (d), and 11.5 (c) using NaOH and HCl. Error bars are the standard deviations calculated from the three ionic current curves recorded. **f-o,** The same sets of data obtained for $CaCl_2$ (f-j) and $MgCl_2$ solutions (k-o). No signs of in-pore precipitation were found at moderate pH manifesting the role of the phosphoric acid in the phosphate buffered saline on the extreme rectifications observed at pH 7.6. Meanwhile, $MgCl_2$

demonstrated a rectifying behavior (o) ascribed to precipitation/dissolution reactions of $Mg(OH)_x$ at the highly alkaline pH.

Figure S22

(Added)

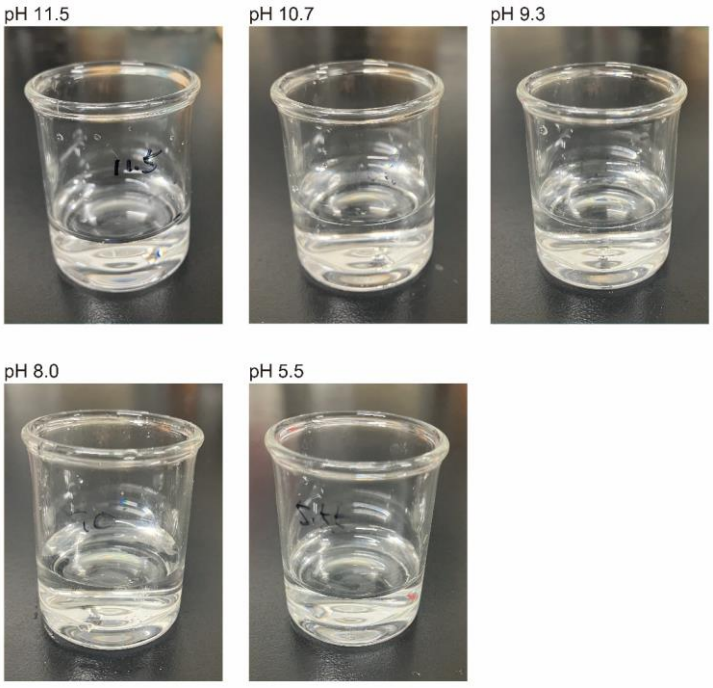

Figure S22. Reaction in phosphate-free NaCl solutions. Photographs taken after adding 100 µl of 2 M $CaCl_2$ into the 10 ml phosphate free NaCl water (1.4 M) in a beaker. No notable change in the appearance of the liquid was observed indicating the absence of any precipitation reaction. We note that this is a case only when the NaCl concentration is over 1 M. Under lower salinity conditions, precipitates were found to be generated upon mixing the $CaCl_2$ solutions with alkaline water attributed to the precipitation of calcium hydroxides.

Figure S19

(Added)

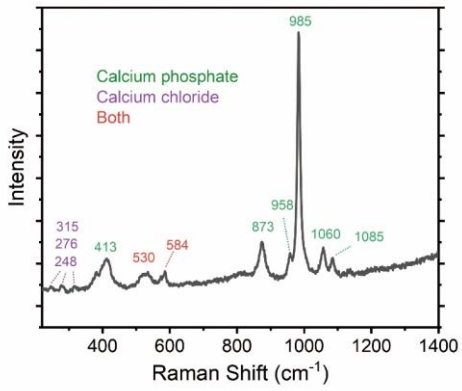

Figure S19. Raman spectrum of the white substance precipitated in the mixture solution of $CaCl_2$

water and phosphate buffered saline. Literature values of characteristic Raman peaks for $Ca(OH)_2$ are reported to be found at around 260 cm^{-1}, 260 cm^{-1}, 360 cm^{-1}, 700 cm^{-1}, and 1100 cm^{-1},[S8,S9] which are not present in the spectrum obtained for the white precipitates (red). Instead, the pronounced peaks at around 400 cm^{-1} and 1000 cm^{-1} (green) suggest that the white precipitates are comprised mostly with $CaPO_x$[S10,S11], in addition to a small amount of $CaCl_2$ (purple).

Figure S20

(Added)

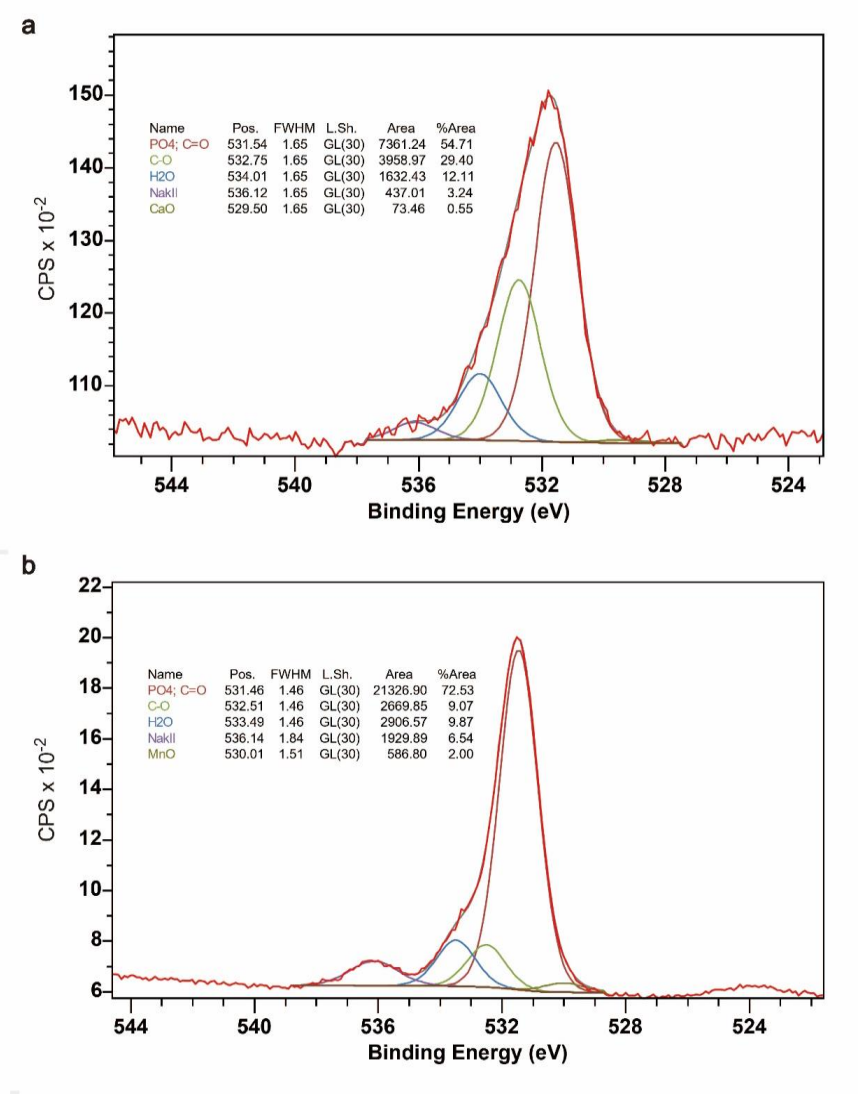

Figure S20. X-ray photoelectron spectroscopy (XPS) analysis of precipitate compounds. a-b, XPS spectra of white precipitated appeared in mixture solutions of 2 M $MnCl_2$ (a) and $CaCl_2$ (b) with phosphate buffered saline. The features at around 531 eV indicate that the precipitates are phosphate compounds.

Main text (p2 line 52 – p3 line 54)

(Added)

Ionic current (I_{ion}) was measured under transmembrane voltage (V_b) with a scan rate (r_{scan}) of 65 mV/s in phosphate buffered saline containing 1.37 M NaCl at pH 7.4 (hereafter, NaCl solution refers to the phosphate buffer unless otherwise denoted).

Main text (p5 line 110 – p6 line 128)

(Added)

In fact, white substance appeared upon mixing bulk solutions in a flask (Figure S18), which is ascribable to precipitation reactions of divalent and trivalent cations with the phosphoric acid included in the electrolyte buffer to form metal phosphates, as we confirmed by x-ray photoelectron and Raman spectroscopy analyses (Figures S19-S20).[7,33]

The role of phosphoric acid was verified by replacing the phosphate-buffered saline at the *trans* with phosphate-free NaCl water of salt concentration 1.4 M. The ionic current characteristics were revealed as featureless denoting the absence of the precipitation reactions in the range of pH from 5.5 to 11.7 (Figure S21). Consistently, no precipitates were found in the mixture solutions (Figures S22). These results unambiguously indicated the in-pore formations and dissolutions of metal phosphates via the reaction between the divalent cations and phosphoric acids as the cause of the extreme ionic current rectification behaviors, where the electromigration of Ca^{2+} at negative voltages leads to the local synthesis and growth of the phosphate layer to almost completely seal the pore, and the reverse reaction in the acidic $CaCl_2$ solution dissolve the nanoprecipitate upon ceasing the Ca^{2+} supply at $V_b > 0$. As such, solution pH plays a role in the reaction equilibrium, where the rectifying behaviors were demonstrated to disappear under acidic conditions prohibiting the in-pore precipitations of the metal phosphates (Figure S24).

Main text (p6 line 146 – 150)

(Revised)

Although the synthesis of the metal phosphates in non-alkaline media is generally complicated processes for predicting whether the reactions inside the nanopore should be endothermic or exothermic,[39,40] the overall results consistently suggest the ion transport-mediated in-pore precipitation/dissolution as a primary factor of the extreme I_{ion} rectifications.

- In Figure 6h, the white and grey lines can hardly be seen. It is also not clear to me what the blue curve is.

(Reply)

Thank you for the comment. We have changed the color and the line widths to make

the fit curves easier to see. We also added schematic images on the sides of the histograms depicting the different forms of DNA detected for each case.

Figure 6

(Revised)

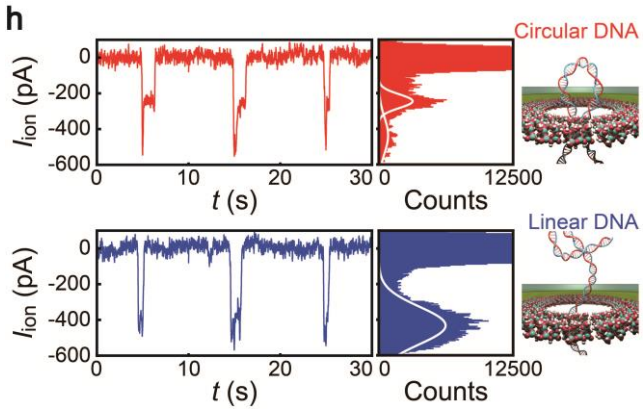

Response to the reviewers

Reviewer #3

In this manuscript, the authors have made voltage gated solid-state nanopores that act as nanofluidic diodes which are electrically tunable with much higher rectification ratios than that have been reported before for such devices. The electrical tunability comes from modulating ion flow by reversible chemical reactions that form precipitation and dissolution of metal hydroxides at opposite biases. Local heat measurements show the change in temperature during the reaction and changing the voltage scan rates show reaction mediated memory effects. The authors also show single molecule sensing of DNA using a robust aluminum hydroxide precipitated nanopore.

While the experiments are innovative and yield promising results, many sections of the manuscript lack clarity and need further elaboration and detail to adequately support the conclusions. Also, the overall text readability and figure labels can be improved and here are some comments.

(Reply)

We appreciate the positive remark on our work.

Novelty: The authors appear to be not aware of the first study that reported nanopore precipitation ["Nanoprecipitation-assisted ion current oscillations", Nature Nanotechnology, 3:51 (2008)], which introduced many of the phenomena described in the present manuscript. The authors should properly describe that work in the introduction and describe their finding in the context of that previous work.

(Reply)

Thank you for letting us know about this important article. The pioneering work demonstrated the nucleation of nanoprecipitates at the tips of micrometer-long conical nanopores for a specific arrangement of salt solutions (a $CaCl_2$/NaCl system) and pH conditions. The precipitates were observed to clog the pores. At the same time, the ionic current tended to fluctuate, which was attributed to the oscillatory mode of nanoprecipitate motions at the orifices. Compared to this previous experiment, as well as the other follow-up studies (J. Phys. Condens. Matter. 2010, 22, 454127; ACS Nano 2011, 5, 3191-319; Cryst. Growth Des. 2017, 17, 6565-6571), the present work provides an

advanced method for *in situ* control of the precipitation/dissolution reactions to fine-tune the nanopore size in real time, which enables a novel mechanism for nanofluidic memristors. More specifically, the ultra-thin silicon nitride nanopore membranes along with the type of salts, solution pH, and voltage scan rates are found as key features for the precise control of the growth/dissolution of the nanoprecipitate. It allows almost complete sealing of 300 nm-sized nanopores by the precipitate layer with leakage current around 100 pA stable for at least 100 seconds under negative transmembrane voltage (please see newly added Figure S14). On the other hand, positive voltage induces immediate dissolution of the precipitate layer under the pre-adjusted pH conditions that return the pore to fully open. Most importantly, the precipitation/dissolution reaction-mediated nanopore shrinkage/enlargement processes can be finely manipulated by the transmembrane voltage pulses in a stable manner (please see the revised Figure 5 and newly added Figures S28-S30), which was not possible in the conventional conical nanopore approach where the oscillatory motions of the nucleated nanoprecipitates bring large and non-controllable current fluctuations unsuitable for the iontronics and resistive pulse sensors applications.

Following the suggestion by the reviewer, the above information was added in the main text as follows.

Main text (p2 line 28 – 49)

(Previous) Stochastic collisions of two or more substances provide opportunities for transforming their atomic components. Principles of chemistry govern these processes, facilitating the creation of diverse compounds with desirable properties, where factors such as pH, temperature, and pressure shape the energy landscape of reaction pathways at equilibrium. In contrast to the conventional diffusion-based chemical systems, meanwhile, nanoreactors have emerged as efficient platforms capable of controlling reaction kinetics within a nanoconfined space through mass flow control.[1-3] Inspired by the concept, we herein report tunable chemical reactions by electrical manipulation of ion transport in a small hole for advanced fluidic devices. This method employs a thin dielectric membrane hosting a nanopore connecting two distinct ionic reactant solutions. By applying transmembrane voltage, we induce electromigration of ions to trigger reversible precipitation/dissolution reactions of metal hydroxides within the conduit (Figure 1a). The resulting dynamic opening and closure of the fluidic channel enable a spectrum of ion transport behaviors ranging from fluidic diodes[4] regulating ion flux with a high rectification ratio over 10^4 to ionic memristors[5-9] characterized by sub-nanowatt energy consumption. Alternatively, the in-pore reaction can be configured to synthesize insoluble precipitates through the choice of ion valency allowing enhanced sensor spatial resolution for resistive

pulse detections of biomolecules (Figure 1b).

(Revised) Stochastic collisions of two or more substances provide opportunities for transforming their atomic components. Principles of chemistry govern these processes, facilitating the creation of diverse compounds with desirable properties, where factors such as pH, temperature, and pressure shape the energy landscape of reaction pathways at equilibrium. In contrast to the conventional diffusion-based chemical systems, meanwhile, nanoreactors have emerged as efficient platforms capable of controlling reaction kinetics within a nanoconfined space through mass flow control.[1-3] In particular, solid-state nanopore technology has proven useful for *operando* observations of the chemical synthesis of an individual nanoparticle at real time (Au nanorod, nanoparticles).[4,5] Motion control of the *in situ* formed nanoprecipitates was also demonstrated with high length-to-diameter aspect ratio conical nanochannels,[6,7] which allowed novel nanofluidic diodes via the transmembrane voltage-dependent clogging of the nanoscale conduits.[6-10] Inspired by the pioneering work, we herein report tunable chemical reactions by electrical manipulation of ion transport in a small hole for advanced fluidic devices. This method employs an ultrathin dielectric membrane hosting a nanopore connecting two distinct ionic reactant solutions for precise manipulations of the ion electromigration to enable reversible precipitation/dissolution reactions of a metal compound layer (Figure 1a). The resulting dynamic opening and closure of the fluidic channel enable a spectrum of ion transport behaviors ranging from fluidic diodes[11] regulating ion flux with a high rectification ratio over 10^4 to ionic memristors[12-18] characterized by sub-nanowatt energy consumption. Alternatively, the in-pore reaction can be configured to synthesize insoluble precipitates through the choice of ion valency allowing enhanced sensor spatial resolution for resistive pulse detections of biomolecules (Figure 1b).

Figure S14
(Added)

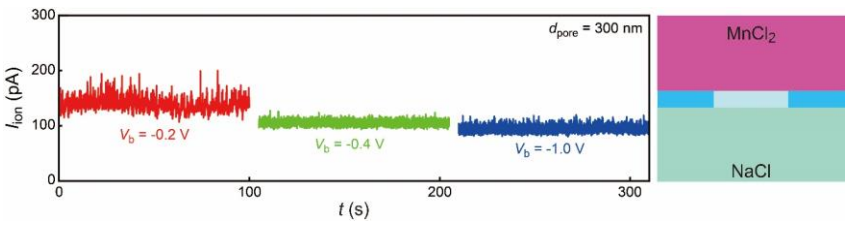

Figure S14. Ionic current flowing through a 300 nm nanopore of a $MnCl_2$/phosphate buffered saline configuration under negative transmembrane voltage recorded at 10 kHz. I_{ion} – t traces of a 300 nm nanopore sealed by the phosphate compound under the negative transmembrane voltage of -0.2 V (red), -0.4 V (green), and -1.0 V (blue). The initial conditions were set as the same by applying +1.0 V to

fully open the nanopore prior to the measurements at the negative voltages. The ionic current is stable at around 100 pA for over 100 seconds indicative of nearly complete sealing of the nanopore via the precipitated phosphate layer. The infinitesimal ionic current may be attributed to a single-digit nanopore formed in the precipitate layer, where particular ion-ion interactions[S6,S7] would take place to affect the ionic conductance.

Figure 5
(Revised)

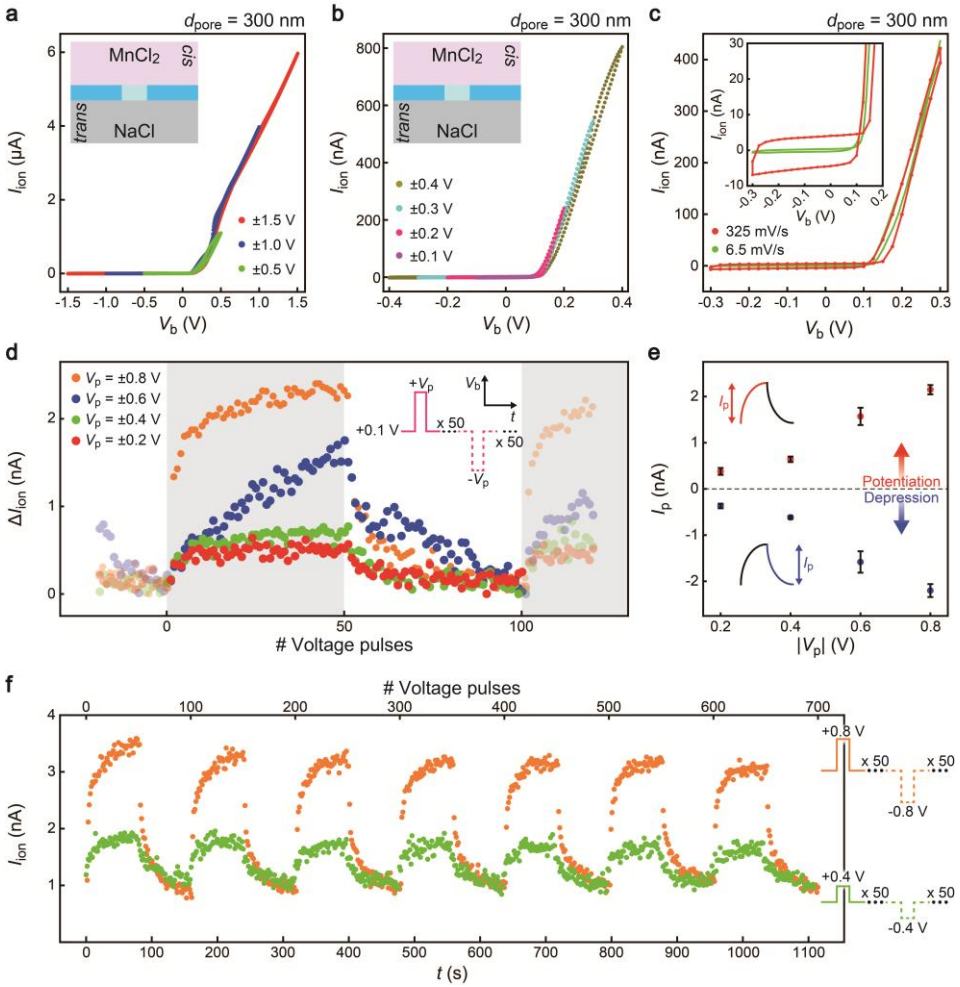

Figure 5. In-pore chemical reaction-driven nanofluidic memristor. **a-b,** I_{ion} – V_b characteristics of a 300 nm-sized nanopore with a $MnCl_2$/NaCl configuration measured under various ranges of transmembrane voltages. Note the I_{ion} remains suppressed when scanning V_b between -0.1 V and 0.1 V (b). **c,** Scan rate dependence of I_{ion} – V_b displaying pinched hysteresis loops. Inset shows a magnified view of the suppressed I_{ion} states. **d,** Memristive characteristics under the applications of 50 ms transmembrane voltage pulses of ±0.5 V amplitudes. ΔI_{ion} is the ionic current recorded at +0.1 V after each voltage pulsing (the baseline current was subtracted). The positive and negative pulses drive the potentiation (grey regions) and depression (white regions) processes of the nanopore memristor via the induced in-pore dissolution/precipitation reactions. **e,** The ionic current change I_p by the positive (red) and negative (blue) voltage pulses of amplitudes V_p. Error bars denote the standard deviations within four cycles of potentiation/depression processes. **f,** Potentiation/depression of the nanopore memristors under the voltage pulses of V_p = ±0.8 V (orange) and ±0.4 V (green). Read voltage was +0.1 V.

Figure S28

(Added)

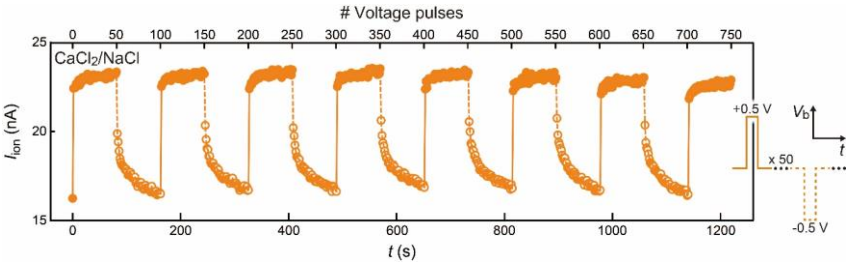

Figure S28. Stable memristive characteristics of a 300 nm-sized nanopore with a $CaCl_2$/phosphate buffered saline after training. Note the relatively high ionic current states of the $CaCl_2$ memristors ascribable to the chemical reaction equilibrium distinct to that in a $MnCl_2$/phosphate buffered saline configuration.

Figure S29

(Added)

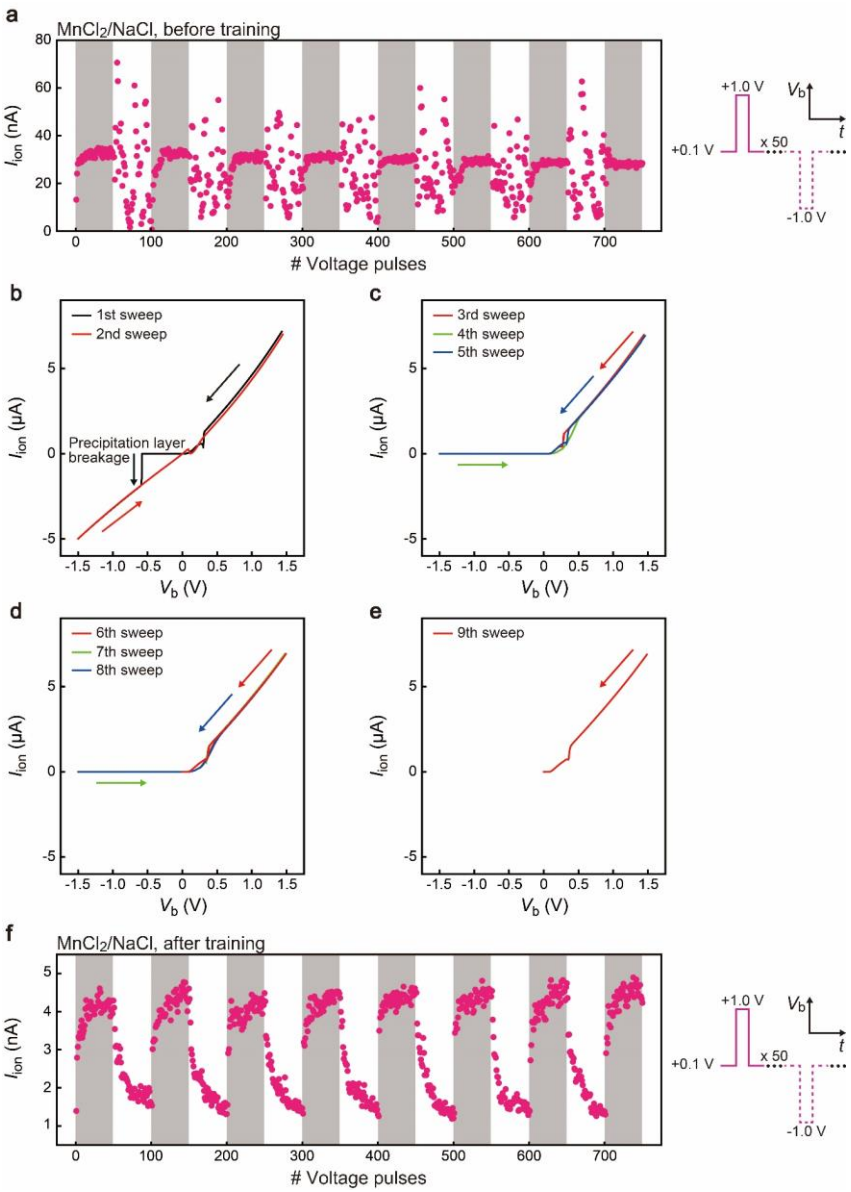

Figure S29. Training protocol for stable nanopore memristors. **a,** Memristive characteristics of a 300 nm-sized nanopore with a $MnCl_2$/phosphate buffered saline configuration without training. Applying positive and negative voltage pulses of 50 ms widths and ±0.5 V amplitudes, the ionic current tends to fluctuate upon the depression processes indicative of unstable nature of the in-pore precipitated phosphate layer under the given conditions. **b-e,** Training processes. Before driving the memristors, transmembrane voltage was scanned for 9 times between +1.5 V and -1.5 V. Initially, the precipitate layer was unstable at negative voltages (b). Repeating the voltage scanning, the I_{ion} – V_b curves become highly reversible suggesting the formation/dissolution of phosphate layers in a reproducible manner (b-d). The training ends by sweeping V_b back to 0 V (e). Subsequently, the memristors were driven by the sequence of the voltage pulses applied. **f,** An example of the memristive characteristics recorded after the training processes showing stable features in the potentiation/depression cycles.

Figure S30

(Added)

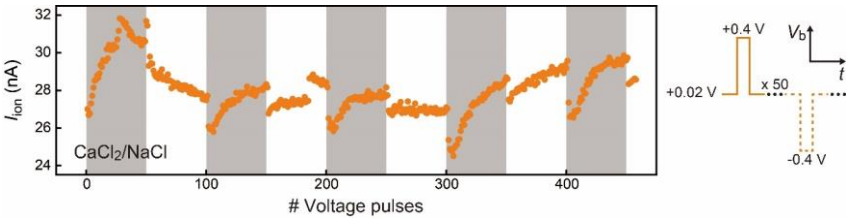

Figure S30. Unstable memristive characteristics of a 300 nm-sized nanopore with a $CaCl_2$/phosphate buffered saline without training. The ionic conductance tends to change in irregular manner against the voltage pulsing.

Clarity: The first question that a reader will have after looking at Figure 1b and 2c is whether the blockades seen at negative voltages are reversible. It is, in a way, implied as the I-V curves are measured using a voltage scan. But the authors should describe, well upfront, how the current changes as a function of time, showing multiple voltage scans and the corresponding changes in the current. Showing that the nanoprecipitation phenomena are (nearly) 100% reversible is required for the study to be of practical interest.

(Reply)

We appreciate the reviewer for giving us the opportunity to evaluate the reproducibility of the ionic current characteristics. Following the suggestions, we have newly performed repetitive I_{ion}-V_b measurements for the $MnCl_2$/NaCl and $CaCl_2$/NaCl systems over an hour at three different scan rate conditions (please see Figures S2 – S7). The low conductance states at the negative voltages were highly reproducible under the hundreds of voltage scans. In contrast, the ionic current characteristics was found to be slightly unstable in the positive voltage regime during the first several cycles of voltage scanning, suggesting a variation in the dissolution processes of the precipitated compounds under the given scan speed. After this incubation period, meanwhile, the curves become reversible giving rectification ratio up to 10^6, thereby confirming the high reproducibility of the nanoprecipitation phenomenon.

Furthermore, we leverage this finding to construct a protocol for stable operations of the nanopore memristors. It comprises multiple voltage scanning between +1.5 V and -1.5 V in prior to drive the memristor (for details, please see newly added Figures S29). This allowed to initialize the conditions of the precipitated layers inside the nanopores that led to stable conductance modulations via the voltage pulses (please see revised Figure 5). By this, we were able to identify a difference in the memristive characteristics between $MnCl_2$ and $CaCl_2$, which is attributed to their distinct reaction equilibrium (please see newly added

Figure S28).

We have added the above results in Supplementary Information as follows.

Main text (p4 line 73 – 75)

(Revised) Strikingly, the rectification ratio r_{rec} = $|I_{+1}/ I_{-1}|$ reached over 40000, where I_{+1} and I_{-1} are I_{ion} at V_b = 1 V and -1 V, respectively (Figure 2d, see also Figures S1-S7).

Main text (p7 line 169 – p8 line 183)

(Revised) Indeed, the nanopore conductance at 0.1 V could be modulated by external stimuli with sub-nanowatt power, where the potentiation and depression were implemented via positive and negative V_b pulses (Figures 5d) that induced sequential dissolution and precipitation of metal phosphates inside the nanopore for over 1000 seconds (Figure 5e). Similar characteristics were also found in $CaCl_2$/NaCl buffer systems, but at a relatively high conductance regime reflecting its reaction equilibrium distinct to that in the $MnCl_2$ solution (Figure S28). Here we add the importance of a training process to obtain the stable memristive characteristics. More specifically, V_b scans were implemented multiple times to reproducibly form a phosphate layer inside a nanopore that served to initialize the memristor state in prior to the subsequent potentiation/depression cycling (Figures S29 – S30). Without this pretreatment, the nanopore memristors tend to be non-controllable by the voltage pulses.

Figure S2

(Added)

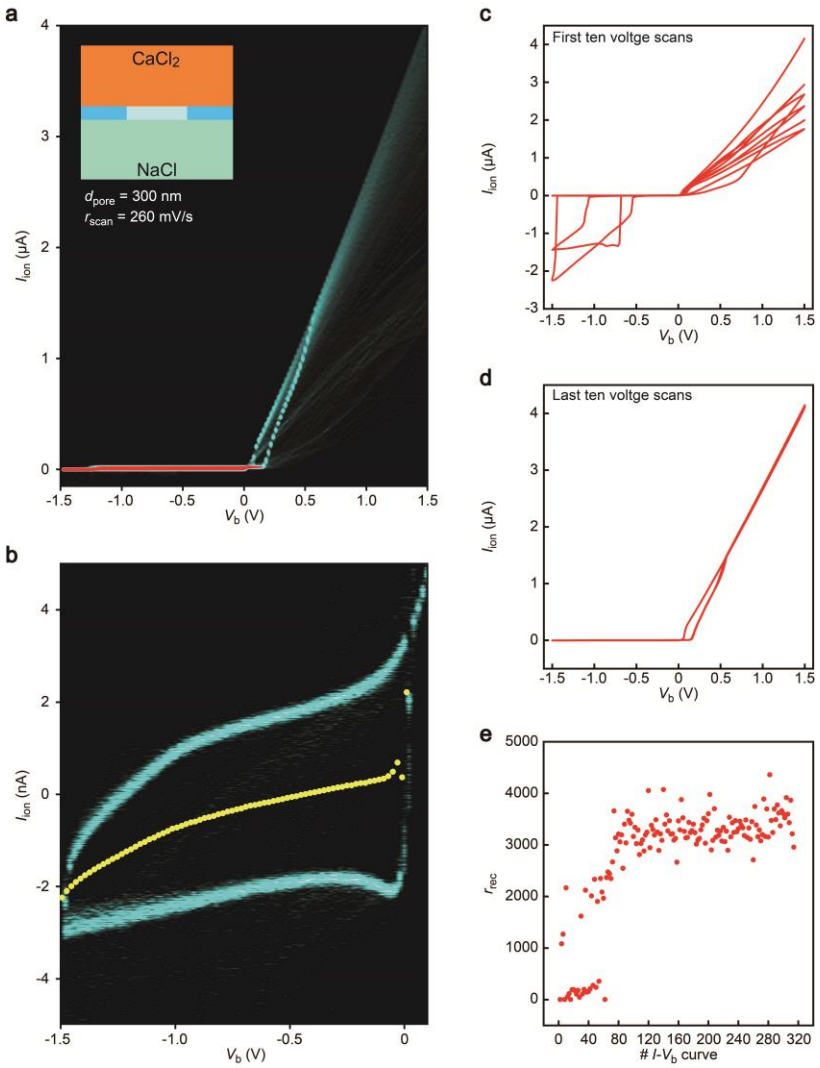

Figure S2. Reproducibility of the rectification characteristics in a 300 nm nanopore with a $CaCl_2$/phosphate buffered saline configuration under a voltage scan rate of 260 mV/s. a-b, Two dimensional histograms of 314 I_{ion} – V_b curves (a) and its close view at the negative voltage regime (b) obtained under repetitive voltage scanning from +1.5 V to -1.5 V. Yellow plots are the average of the curves acquired under the positive and negative voltage sweeps. **c,** The first ten I_{ion} – V_b curves showing relatively unstable nature of the ionic current characteristics suggestive of the fluctuating dissolution processes of the in-pore precipitated layer. **d,** In contrast, the last ten curves are highly reproducible indicating the stabilized precipitation/dissolution processes of the calcium phosphate layer formed in the nanopore. **e,** The rectification ratio r_{rec} calculated from each curve. Initially, r_{rec} tends to be low due to the inadequate time for forming nanoprecipitate seeds on the pore wall surface. After about 100 cycles of measurements, the precipitation/dissolution processes become stable giving r_{rec} around 3000.

Figure S3

(Added)

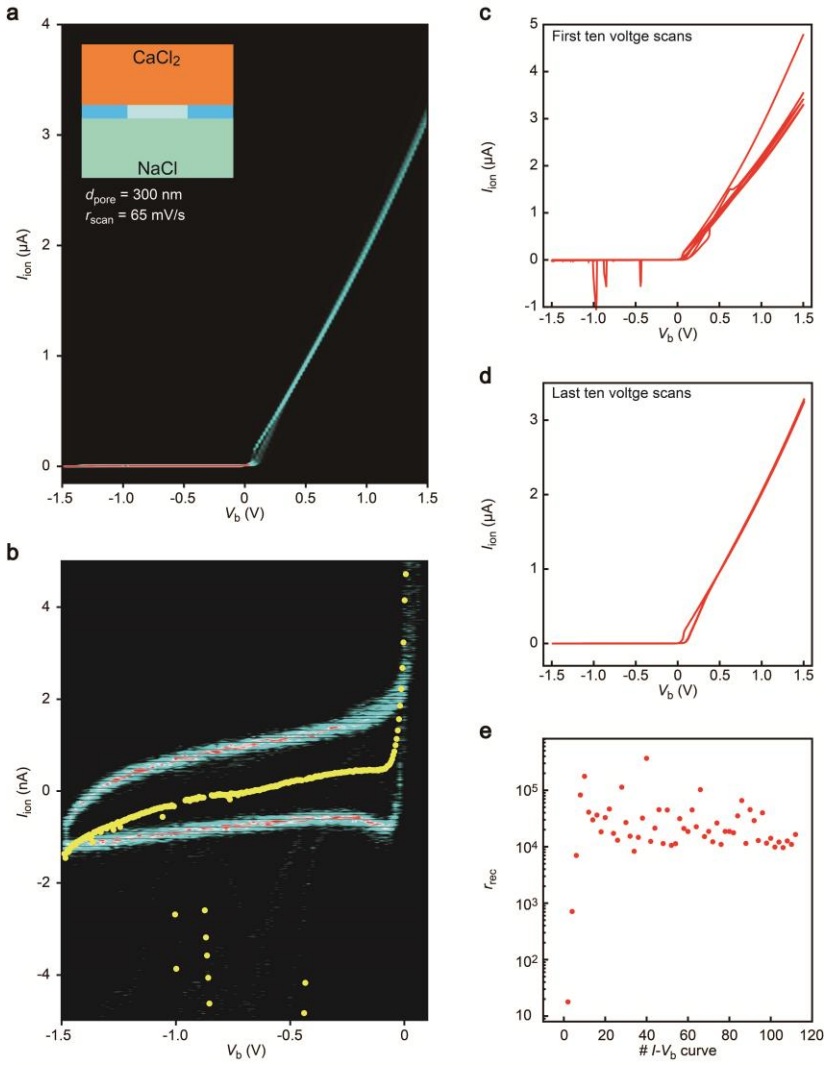

Figure S3. Reproducibility of the rectification characteristics in a 300 nm nanopore with a $CaCl_2$/phosphate buffered saline configuration under a voltage scan rate of 65 mV/s. a-b, Two dimensional histograms of 112 I_{ion} – V_b curves (a) and its close view at the negative voltage regime (b) obtained under repetitive voltage scanning from +1.5 V to -1.5 V. Yellow plots are the average of the curves acquired under the positive and negative voltage sweeps. **c,** The first ten I_{ion} – V_b curves showing relatively unstable nature of the ionic current characteristics suggestive of the fluctuating dissolution processes of the in-pore precipitated layer. **d,** In contrast, the last ten curves are highly reproducible indicating the stabilized precipitation/dissolution processes of the calcium phosphate layer formed in the nanopore. **e,** The rectification ratio r_{rec} calculated from each curve. After several cycles of measurements, r_{rec} tends to be stable at around 10^4 to 10^5.

Figure S4

(Added)

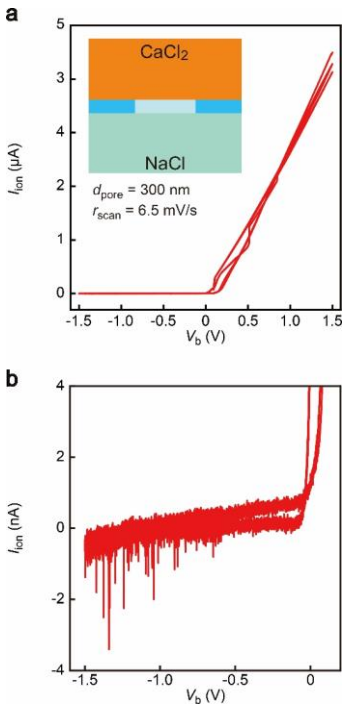

Figure S4. Reproducibility of the rectification characteristics in a 300 nm nanopore with a $CaCl_2$/phosphate buffered saline configuration under a voltage scan rate of 6.5 mV/s. a, $I_{ion} - V_b$ curves obtained under five cycles of voltage scanning from +1.5 V to -1.5 V. **b,** A close view of the suppressed ionic current at the negative V_b.

Figure S5

(Added)

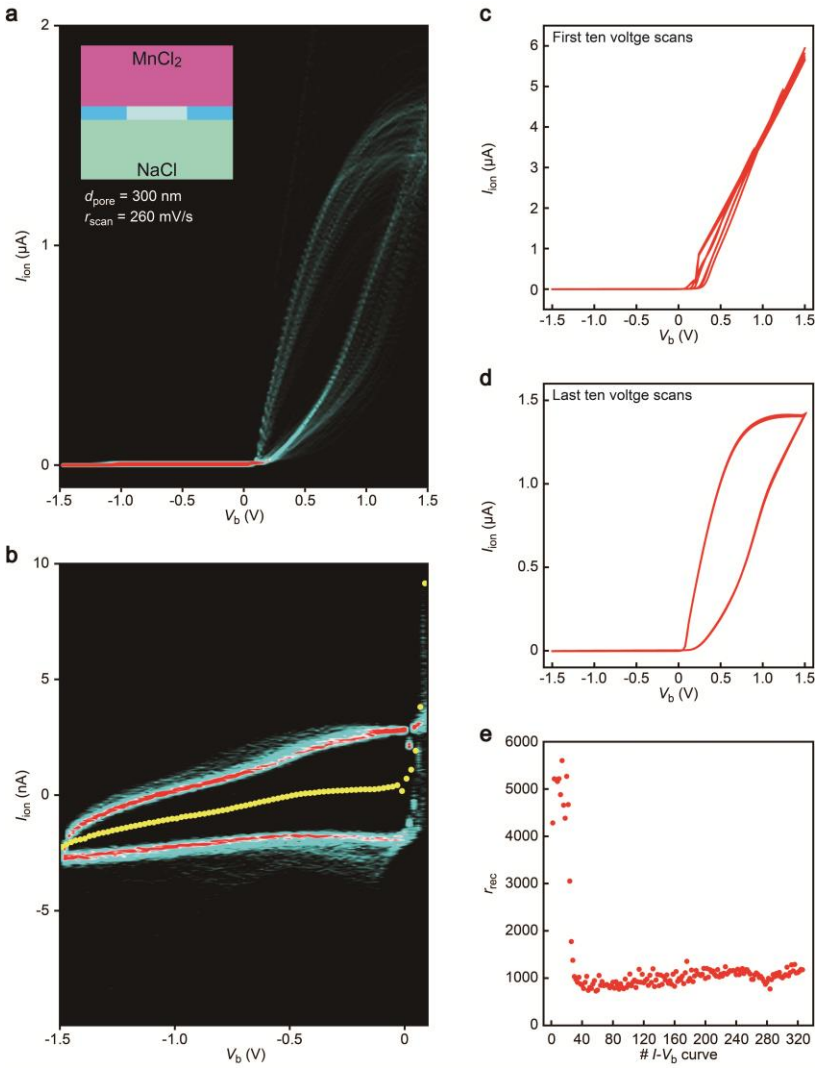

Figure S5. Reproducibility of the rectification characteristics in a 300 nm nanopore with a $MnCl_2$/phosphate buffered saline configuration under a voltage scan rate of 260 mV/s. a-b, Two dimensional histograms of 314 I_{ion} – V_b curves (a) and its close view at the negative voltage regime (b) obtained under repetitive voltage scanning from +1.5 V to -1.5 V. Yellow plots are the average of the curves acquired under the positive and negative voltage sweeps. **c,** The first ten I_{ion} – V_b curves showing relatively unstable nature of the ionic current characteristics at the positive voltages suggestive of the fluctuating dissolution processes of the in-pore precipitated layer. **d,** In contrast, the last ten curves are highly reproducible indicating the stabilized precipitation/dissolution processes of the calcium phosphate layer formed in the nanopore. **e,** The rectification ratio r_{rec} calculated from each curve. Initially, r_{rec} tends to be low due to the inadequate time for forming nanoprecipitate seeds on the pore wall surface. After tens of cycles of measurements, the precipitation/dissolution processes become stable giving r_{rec} around 1000.

Figure S6

(Added)

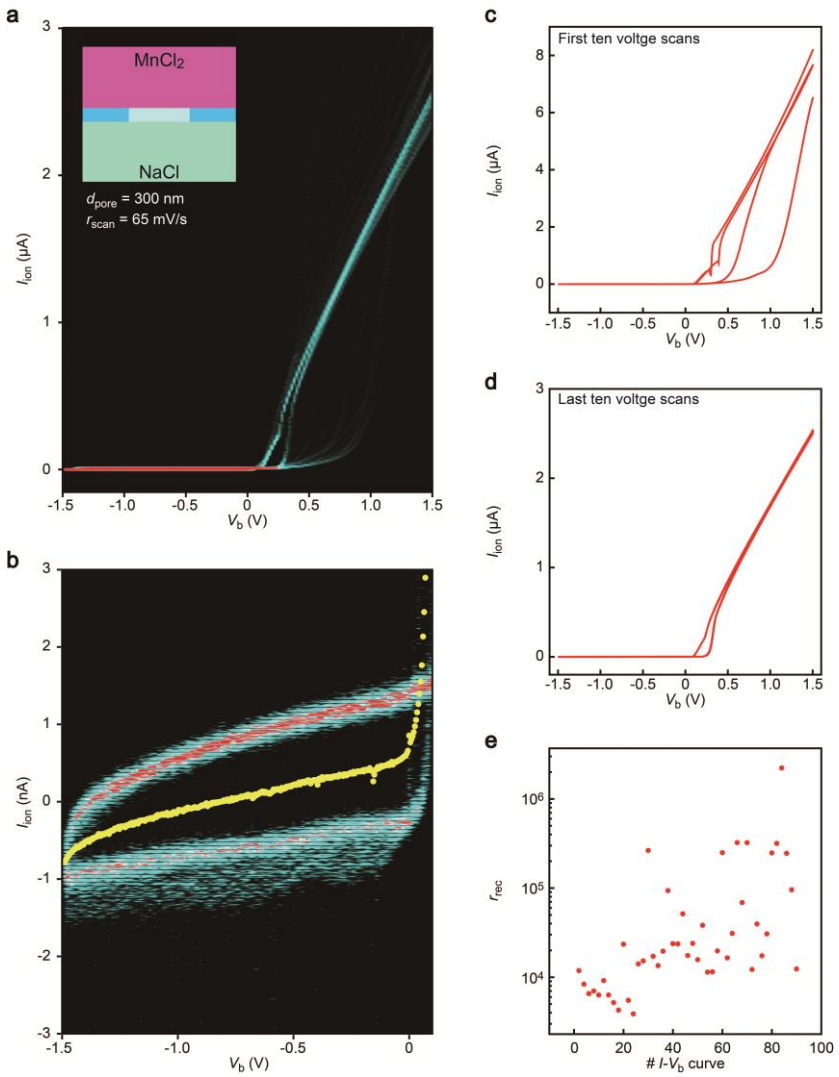

Figure S6. Reproducibility of the rectification characteristics in a 300 nm nanopore with a $MnCl_2$/phosphate buffered saline configuration under a voltage scan rate of 65 mV/s. a-b, Two dimensional histograms of 112 I_{ion} – V_b curves (a) and its close view at the negative voltage regime (b) obtained under repetitive voltage scanning from +1.5 V to -1.5 V. Yellow plots are the average of the curves acquired under the positive and negative voltage sweeps. **c,** The first ten I_{ion} – V_b curves showing relatively unstable nature of the ionic current characteristics suggestive of the fluctuating dissolution processes of the in-pore precipitated layer. **d,** In contrast, the last ten curves are highly reproducible indicating the stabilized precipitation/dissolution processes of the calcium phosphate layer formed in the nanopore. **e,** The rectification ratio r_{rec} calculated from each curve with values up to over 10^6.

Figure S7

(Added)

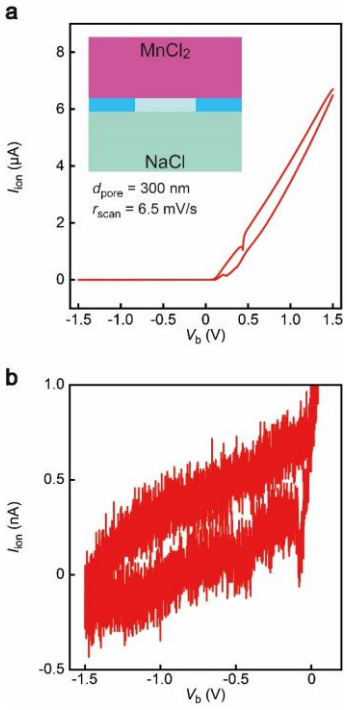

Figure S7. Reproducibility of the rectification characteristics in a 300 nm nanopore with a $MnCl_2$/phosphate buffered saline configuration under a voltage scan rate of 6.5 mV/s. **a,** $I_{ion} - V_b$ curves obtained under five cycles of voltage scanning from +1.5 V to -1.5 V. **b,** A close view of the suppressed ionic current at the negative V_b.

Figure 5
(Revised)

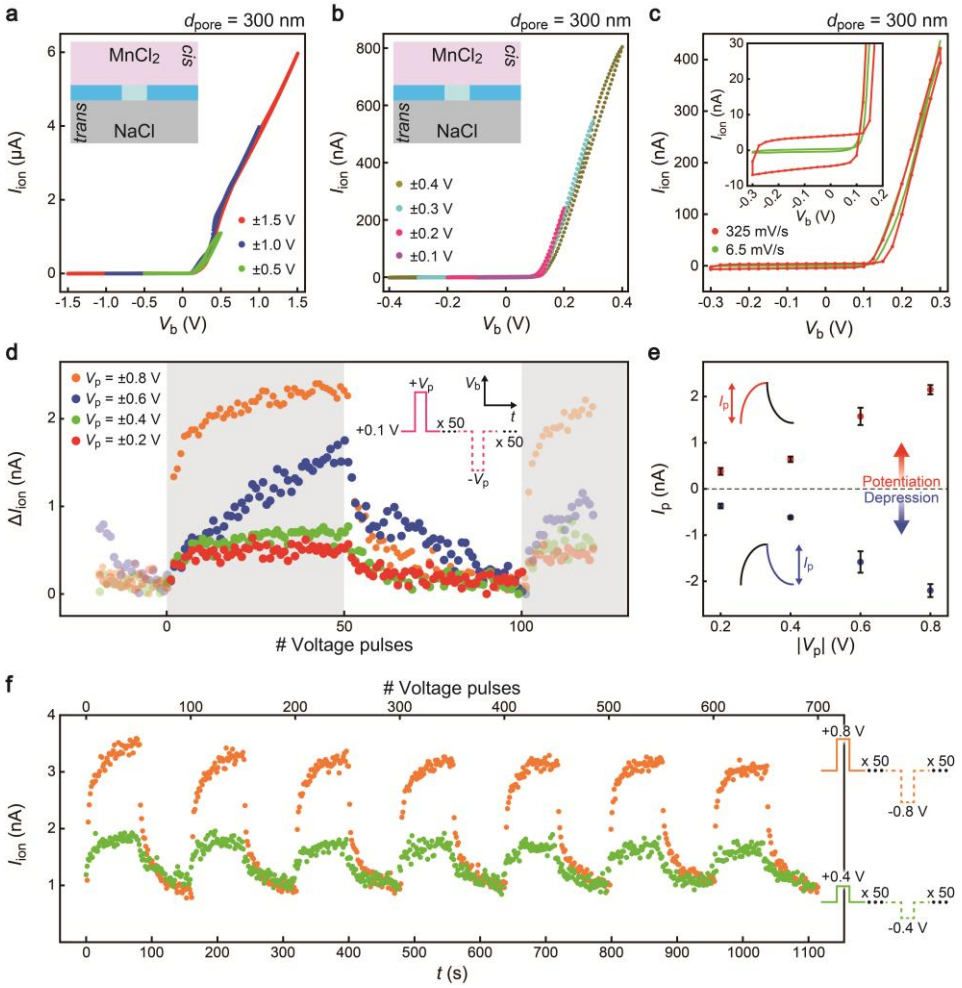

Figure 5. In-pore chemical reaction-driven nanofluidic memristor. **a-b,** I_{ion} – V_b characteristics of a 300 nm-sized nanopore with a $MnCl_2$/NaCl configuration measured under various ranges of transmembrane voltages. Note the I_{ion} remains suppressed when scanning V_b between -0.1 V and 0.1 V (b). **c,** Scan rate dependence of I_{ion} – V_b displaying pinched hysteresis loops. Inset shows a magnified view of the suppressed I_{ion} states. **d,** Memristive characteristics under the applications of 50 ms transmembrane voltage pulses of ±0.5 V amplitudes. ΔI_{ion} is the ionic current recorded at +0.1 V after each voltage pulsing (the baseline current was subtracted). The positive and negative pulses drive the potentiation (grey regions) and depression (white regions) processes of the nanopore memristor via the induced in-pore dissolution/precipitation reactions. **e,** The ionic current change I_p by the positive (red) and negative (blue) voltage pulses of amplitudes V_p. Error bars denote the standard deviations within four cycles of potentiation/depression processes. **f,** Potentiation/depression of the nanopore memristors under the voltage pulses of V_p = ±0.8 V (orange) and ±0.4 V (green). Read voltage was +0.1 V.

Figure S28

(Added)

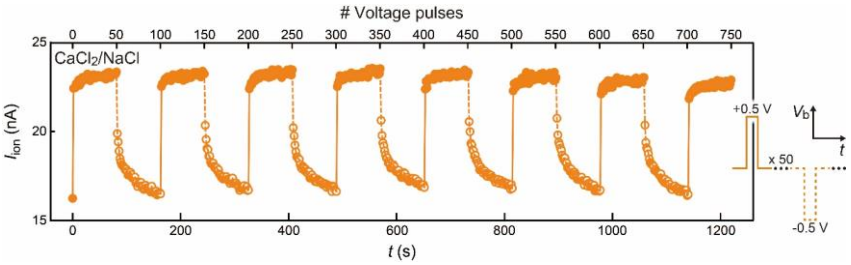

Figure S28. Stable memristive characteristics of a 300 nm-sized nanopore with a $CaCl_2$/phosphate buffered saline after training. Note the relatively high ionic current states of the $CaCl_2$ memristors ascribable to the chemical reaction equilibrium distinct to that in a $MnCl_2$/phosphate buffered saline configuration.

Figure S29

(Added)

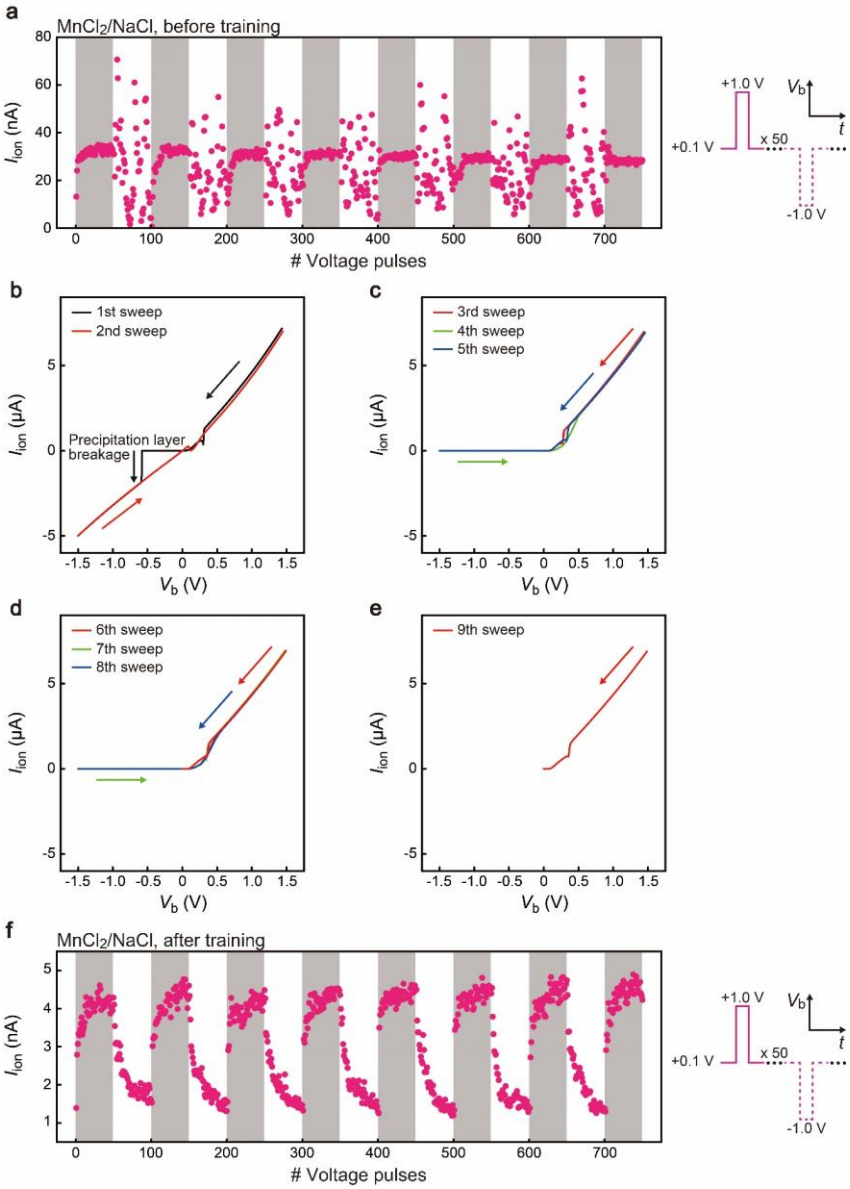

Figure S29. Training protocol for stable nanopore memristors. a, Memristive characteristics of a 300 nm-sized nanopore with a $MnCl_2$/phosphate buffered saline configuration without training. Applying positive and negative voltage pulses of 50 ms widths and ±0.5 V amplitudes, the ionic current tends to fluctuate upon the depression processes indicative of unstable nature of the in-pore precipitated phosphate layer under the given conditions. **b-e,** Training processes. Before driving the memristors, transmembrane voltage was scanned for 9 times between +1.5 V and -1.5 V. Initially, the precipitate layer was unstable at negative voltages (b). Repeating the voltage scanning, the $I_{ion} - V_b$ curves become highly reversible suggesting the formation/dissolution of phosphate layers in a reproducible manner (b-d). The training ends by sweeping V_b back to 0 V (e). Subsequently, the memristors were driven by the sequence of the voltage pulses applied. **f,** An example of the memristive characteristics recorded after the training processes showing stable features in the potentiation/depression cycles.

Figure S30

(Added)

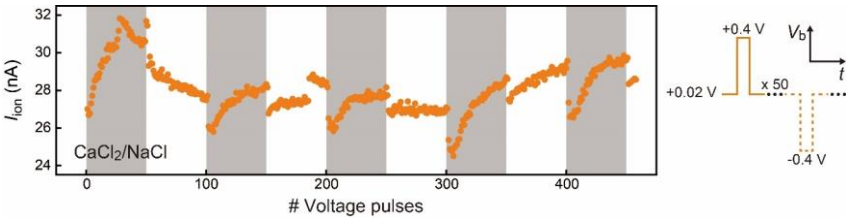

Figure S30. Unstable memristive characteristics of a 300 nm-sized nanopore with a $CaCl_2$/phosphate buffered saline without training. The ionic conductance tends to change in irregular manner against the voltage pulsing.

Presentation: Figures 1 and 4 look like proposal material. While visually impressive, they might not be the best choice to communicate a scientific result.

(Reply)

Thank you for the valuable comment. Indeed, Figure 1b may not be appropriate to appear in the biggining of the paper. The polarity of the voltage source in Figure 1a was also inconsistent with the ion flow depicted. These points were corrected in the revised Figure 1. On the other hand, we would like to keep Figure 4 as is, since we think it is a good way to represent the repetitive reaction-mediated diode-to-resistor transition processes.

Figure 1

(Revised)

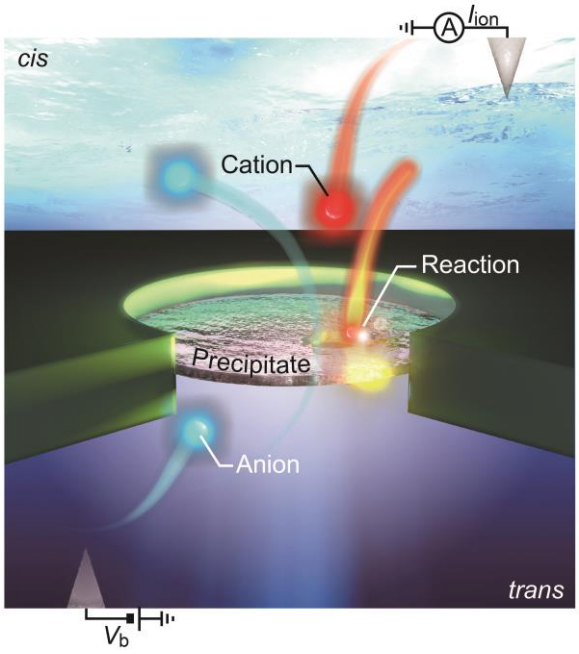

Figure 1. Transmembrane voltage-controlled precipitation reactions inside a nanopore. a, Schematic illustration depicting ion transport-triggered precipitation reaction inside a nanopore. The transmembrane voltage V_b induces electromigration of ions. The resulting cation flow causes chemical reactions to form or dissolve a metal hydroxide compound in a voltage-controllable fashion. The associated dynamic change in the effective pore size is measured by the ionic current I_{ion}.

Other major points:

1) For figure 2a-b, the authors mention that the conductance at negative voltages can be explained by the distinct mobilities of the three cations, as shown by the linear relationship under homogeneous salt solutions. However, the order for Mg (pink) and Na (black) is

opposite at negative bias between 2a and 2b as compared to the other ions. The inset of Fig. 2b showing the slope is also unclear as the ions are not labeled, with there being 3 points as compared to 4 ions shown in (a).

(Reply)

We appreciate the comment. The reason why $MgCl_2$ gives higher conductance than that for NaCl at the negative transmembrane voltage regime in Figure 2b is because of the difference in the contributions of Cl^- on the ionic current. In Figure 2a, the ionic current is given by the flow of 1.37 M Cl^- and 2M Mg^{2+} under negative voltage. On the contrary, both sides of the membrane were filled with 2 M $MgCl_2$ for the measurements in Figure 2b. In this case, the current is generated by the transport of 2 M Cl^- and 2 M $MgCl_2$. This larger contribution of Cl^- would be the cause of the slighter higher conductance of 2 M $MgCl_2$ than 1.37 M NaCl in Figure 2b.

For Figure 2b inset, we have labeled the type of salts measured as shown below.

Figure 2b

(Revised)

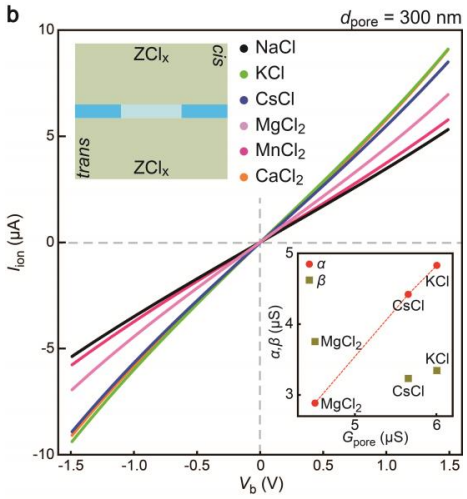

2) Another issue in Figures 2a and 2b is the I-V curve for 1.37M NaCl. As for this case, the conditions are same between 2a and 2b, the black line should be the same across the two figures. However, the slopes of the two lines seem different, the black line ranging from roughly -4.5 to 4.5 in (a) and between -8 to 7 in (b). What is the reason for this difference and if there are any conditions different in these two plots for NaCl, please specify.

(Reply)

The reviewer is correct that there is a discrepancy in the conductance between Figure 2a and 2b. To check this point, we have newly performed the measurements with the same conditions used in Figure 2b. The results showed similar conductance in 1.37 M NaCl suggesting that the previous data were taken with a slightly larger pore. Meanwhile, it is noted that the relative difference in the conductance among the salts remains the same as the previous results.

We thank the reviewer for letting us know the discrepancy between Figures 2a and 2b. We have replaced Figure 2b with the new result explained above.

Figure 2b

(Previous)

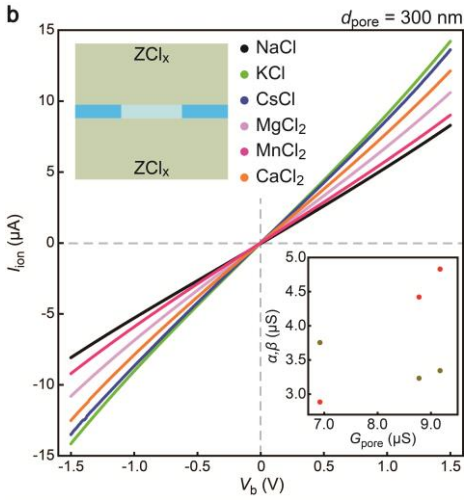

(Revised)

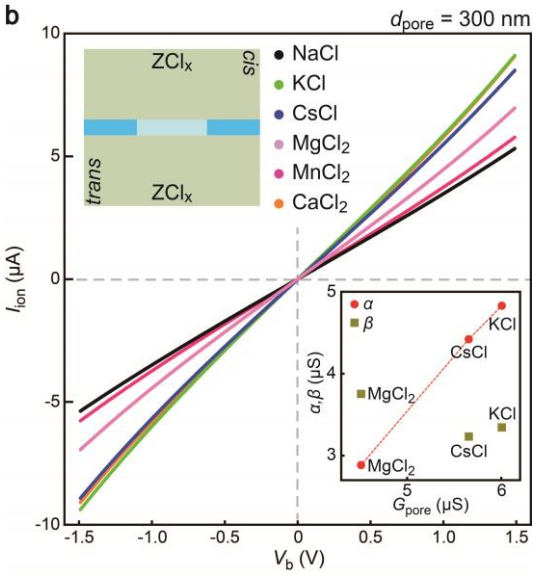

3) The rectification ratio defined in Page 3, Line 68 should have an absolute value around the division for accuracy, as all rectification numbers reported are positive. The ionic currents shown in nA in the inset of Figure 2c and used for calculating rectification are quite small. How reproducible are these numbers, as they are used throughout the paper? In the methods section (page 11, line 275), the authors mention carrying out each measurement three times to get the average ionic current. Are these three independent measurements? If so, the error bars can be plotted for the rectification values shown in Fig. 2d to provide robust statistical significance to the derived conclusions.

(Reply)

Thank you for the suggestion. We have changed the definition of the rectification ratio to $r_{rec} = |I_{+1} / I_{-1}|$. As for the small ionic current at negative voltages, we confirmed that it is highly stable and reproducible as we already explained in the previous comment (Figures S2-S7, S14). We have also added error bars in Figure 2d from the multiple $I_{ion} - V_b$ curves recorded.

Figure 2d

(Error bars added)

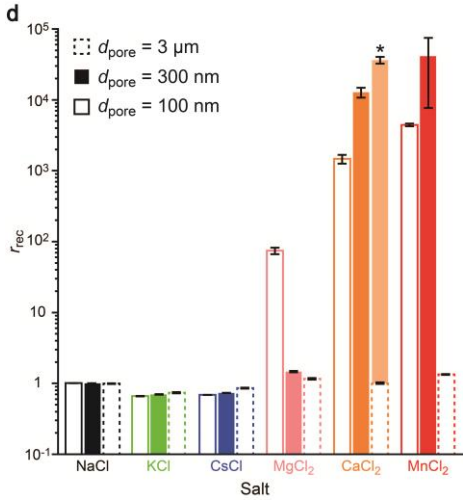

d, The rectification ratio r_{rec} at V_b = ±1 V obtained from the ionic current characteristics measured in pores of three different diameter d_{pore} and various salts at the *cis* (with the *trans* filled with 1.37 M NaCl at pH 7.4). r_{rec} tends to be close to 1 when the $I_{ion} - V_b$ characteristics show ohmic behaviors. On the other hand, r_{rec} > 1 denotes I_{ion} suppression at negative transmembrane voltage. The high r_{rec} for the 3 μm micropore with $CaCl_2$ is a result obtained at a low V_b scan rate of 6.5 mV/s (marked by an asterisk) while the other data are of 65 mV/s. Note that the rectification ratio attains over 40000 for the case of 300 nm-sized nanopore with a $MnCl_2$/NaCl configuration. Error bars denote standard deviations.

4) Also in Page 3, Line 74, the authors mention that the strong rectification behaviors were dependent on the voltage scan speed (Figures S3-S6). Firstly, the figures S3-S6 are all

reported at the same 65 mV/s scan speed. Page 4, Line 78 also cites Figure S3 with an order of magnitude lower scan speed, but that figure is labeled to be at 65 mV/s and does not contain the MnCl2 data as described in text.

(Reply)

Thank you for pointing out our mistake regarding Figure S3 (now Figure S9 the revised Supplementary Information). We have added the I_{ion} – V_b curves obtained at 6.5 mV/s with a 3 μm micropore in Figure S9d in the revised Supplementary Information.

Figure S9

(Revised)

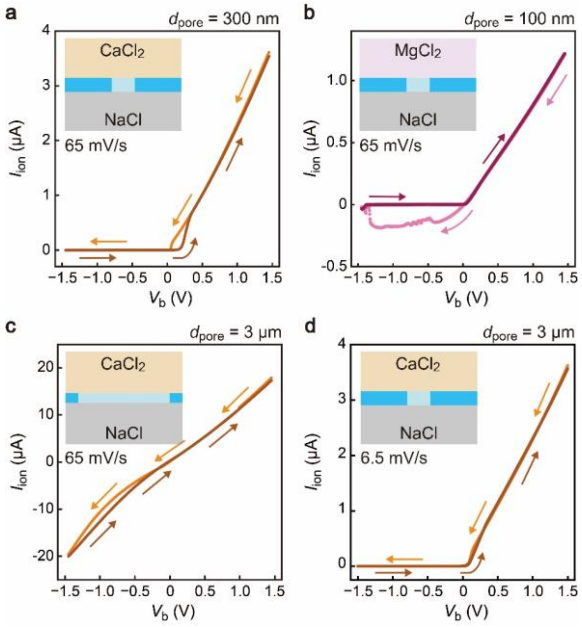

Figure S9. Pore size dependence of ionic current rectifications. **a,** $CaCl_2$/phosphate buffered saline (PBS) and $MnCl_2$/PBS configurations demonstrated extreme I_{ion} rectification for 300 nm-sized nanopores at voltage scan rate of 65 mV/s. **b,** In addition to $CaCl_2$ and $MnCl_2$, $MgCl_2$ also showed the rectifying behavior in a 100 nm-sized nanopore. **c,** On the contrary, there was no such salt dependence in the ionic current characteristics of 3 μm-sized micropores giving no rectifications nor pore shrinking with any of the salts tested including $CaCl_2$, $MnCl_2$, and $AlCl_3$. We emphasize that these properties are only for cases when the voltage scan rate is 65 mV/s. Results may vary depending on the nanopore configurations, liquid components, and voltage scan range and speed. **d,** For example, extreme ionic rectification can be found in the 3 μm micropore when lowering the scan rate to 6.5 mV/s.

But other figures in the main text show the dependence of the I-V curve on the Vb scan speed. What is the reason behind this difference? Are the measurements done at steady state conditions? Fig. 2d shows a big change in the rectification for CaCl2 at lower scan speed, which needs error bars from the replicate measurements for statistical accuracy.

(Reply)

Thank you for the comment. As we explained on page 6, we found the extreme rectifying behavior even for micropores by scanning the voltage slowly at 6.5 mV/s. Thereafter, the $I_{ion} - V_b$ curves demonstrated the rectifying characteristics at the faster scan speed of 65 mV/s (Figure 4). From these observations, we consider that nucleation of the metal compound first needs to be nucleated on the pore wall surface. However, this was not possible under the high voltage scan speed due to the inadequate time given for the precipitation on the wall, which was a case in 3 μm micropores under 650 mV/s and 65 mV/s giving rise to the ionic current characteristics with the rectification ratio close to 1. In contrast, there was enough time for the pore wall surface to be covered with the precipitate layer under 6.5 mV/s, thereby causing strong suppression of the ionic current at negative voltages.

We have added error bars in Figure 2d. We have also performed additional measurements with a 3 μm micropore under the voltage scan speed of 6.5 mV/s (please see the newly added Figure S11) that corroborated the high rectification ratio for $CaCl_2$ (please note that in the previous Figure 2d, we put the rectification ratio obtained at 65 mV/s after the measurements at 6.5 mV/s. In the revised figure, we replaced the result with the one obtained at 6.5 mV/s).

Figure 2d

(Error bars added)

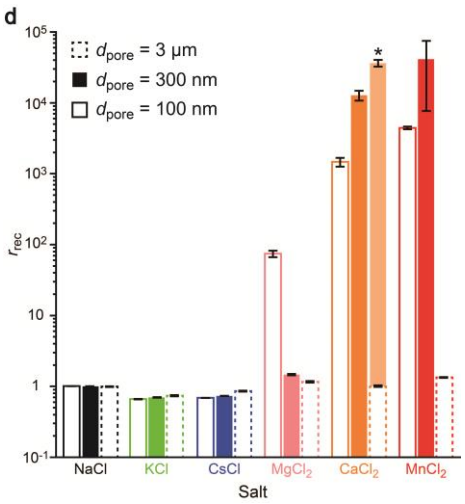

d, The rectification ratio r_{rec} at V_b = ±1 V obtained from the ionic current characteristics measured in pores of three different diameter d_{pore} and various salts at the *cis* (with the *trans* filled with 1.37 M NaCl at pH 7.4). r_{rec} tends to be close to 1 when the $I_{ion} - V_b$ characteristics show ohmic behaviors. On the other hand, r_{rec} > 1 denotes I_{ion} suppression at negative transmembrane voltage. The high r_{rec} for the 3 μm micropore with $CaCl_2$ is a result obtained at a low V_b scan rate of 6.5 mV/s (marked by an asterisk) while the other data are of 65 mV/s. Note that the rectification ratio attains over 40000 for the case of 300 nm-sized nanopore with a $MnCl_2$/NaCl configuration. Error bars denote standard deviations.

Figure S11

(Added)

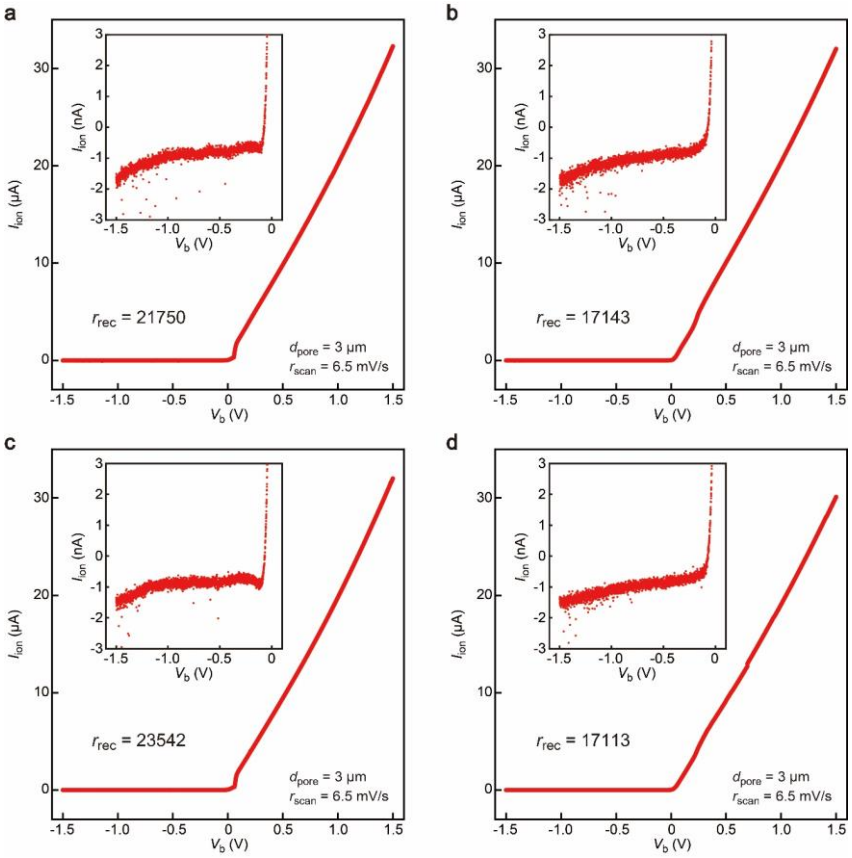

Figure S11. Extreme ionic current rectifications observed in a 3 μm micropore for the $CaCl_2$/phosphate buffered saline arrangement under a voltage scan rate of 6.5 mV/s. a-d, $I_{ion} - V_b$ characteristics showing rectifying behaviors with the rectification ratio (r_{rec}) around 20000 in the four independent measurements. Different nanopore chip was used to verify the reproducibility of the result in Figure Each curve is the average of the data recorded under positive and negative voltage scans. Insets are the close-up views of the suppressed ionic current at the negative voltage regimes.

5) For the heat dissipation measurements shown in Fig. 3d-f, the voltage scan speed is 1 mV/s. What are the rectification values for the pore at that scan speed? Is it representative of the measurement at 65 mV/ns? It is hard to gauge from the I-V curve shown. Also, it is not clear in Fig. 3e if there is a difference between the positive and negative Vb scans as all points seem the same color and not clearly distinct as Fig. 3d. Can the authors describe how the reaction enthalpy is calculated for Fig 3d at these experimental conditions?

(Reply)

Thank you for your comment. The rectification ratios calculated from the I_{ion}-V_b curves in Figure 3f are 406 for the $CaCl_2$/NaCl system and 157 for the $MgCl_2$/NaCl system (please refer to the newly added Figure S25). These values are lower than those observed in

larger pores because, while the ionic current was suppressed to a level similar to that in larger nanopores, the conductance in the positive voltage regime was significantly lower due to the smaller pore diameter. This result is consistent with the relatively low rectification ratio of the 100 nm nanopores compared to the 300 nm ones shown in Figure 2d.

For Figure 3d (now Figure 3b in the revised manuscript), we have plotted the data obtained under positive voltage scans in a different color.

Regarding the reaction enthalpy, we first would like to explain that the precipitated compound was found as not hydroxides but metal phosphates. After studying the previous literature (*Nat. Nanotechnol.* **3**, 51 (2008)), we realized the lack of evidence in the previous manuscript to rule out the influence of the trace amount of phosphoric acid included in the phosphate buffer used. More precisely, while we performed the pH and salt dependence on the rectification behaviors, we did not try the measurements under phosphate-free NaCl solution at neutral pH. To see this, we prepared phosphate-free salt water by mixing NaCl with ultrapure water. We also adjusted the pH to be between 5.5 to 11.7 with NaOH. These salt solutions gave no rectification characteristics for $CaCl_2$, $MnCl_2$, and $MgCl_2$ in a 300 nm-sized nanopore (please see newly added Figures S21-S22). On the other hand, we found the extreme rectification when exhibiting the measurements with the phosphate-buffered saline on the same nanopore. More directly, XPS and Raman spectroscopy analyses suggested the compounds contain calcium phosphates (please see newly added Figures S19-S20). These results unambiguously suggested the important role of the phosphoric acid in the electrolyte buffer on the rectification and memristive characteristics observed, that caused the metal phosphate precipitation/dissolution reactions inside the nanopores (We also confirmed that the reactions are controllable by the solution pH as we showed in the newly added Figure S24). Now, as for the reaction enthalpy, it has been widely known that the precipitation/dissolution reactions of metal phosphates are highly complicated and difficult to predict whether the processes would be endothermic or exothermic (Chem. Rev. 108, 4628-4669 (2018); Minerals 8, 281 (2018)). We noted this in the revised main text as written below. Meanwhile, we would like to emphasize that the above change does not affect the main conclusions of the present work regarding the mechanisms of the extreme ionic current rectifications and memristive characteristics,

Figure S25

(Added)

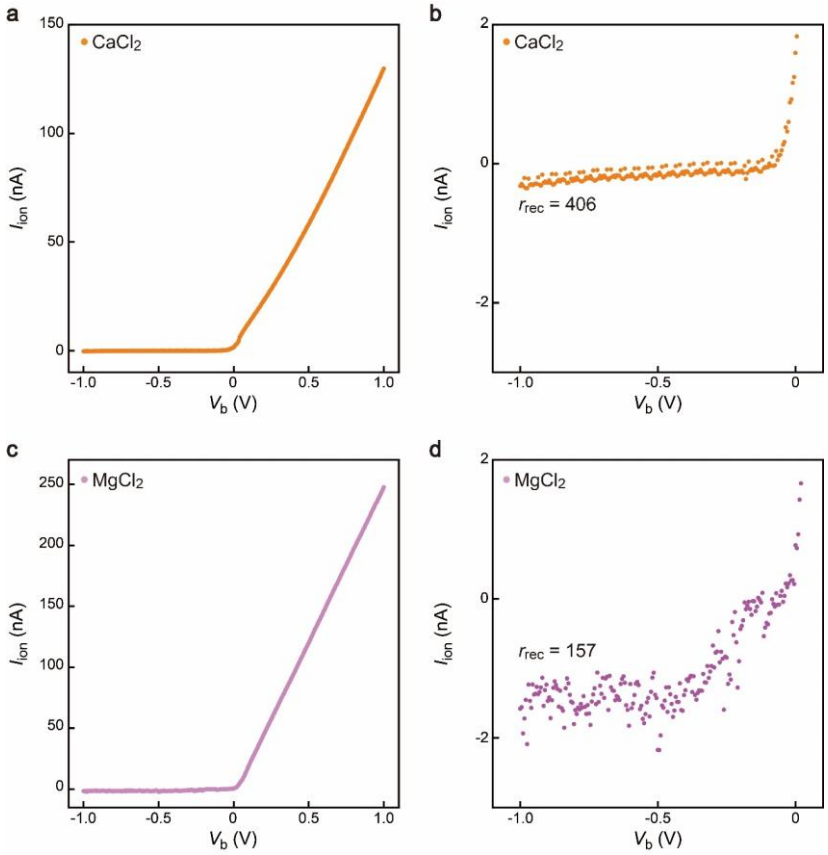

Figure S25. Ionic current characteristics measured simultaneously with the nanopore temperature using a 60 nm-sized thermocouple-embedded nanopore under the voltage scan rate of 1 mV/s. a-b, Averaged I_{ion} – V_b curves in Figure 3a. The small bumping feature in (b) is the external noise. The rectification ratio r_{rec} at V_b = ± 1 V is 406. **c-d,** The same sets of results for $MgCl_2$.

Figure 3b

(Revised)

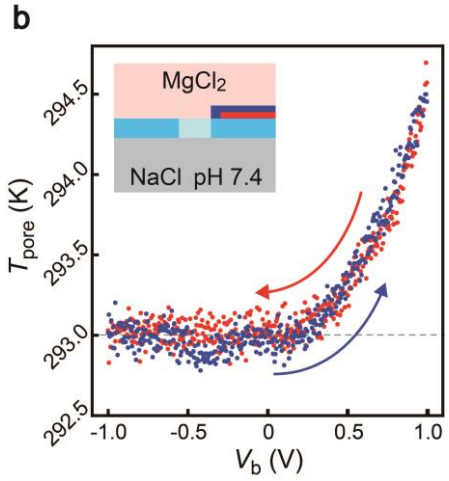

b, T_{pore}–V_b characteristics acquired for a $MgCl_2$/NaCl system. Arrows denote the voltage scan directions.

Figure S19
(Added)

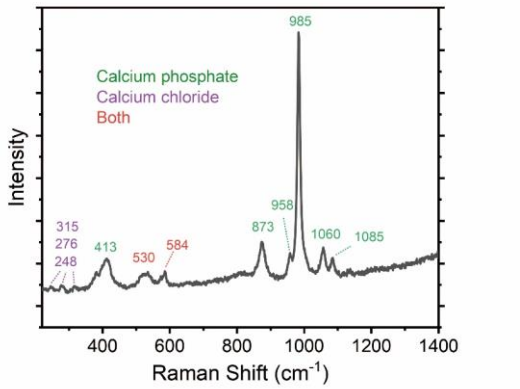

Figure S19. Raman spectrum of the white substance precipitated in the mixture solution of $CaCl_2$ water and phosphate buffered saline. Literature values of characteristic Raman peaks for $Ca(OH)_2$ are reported to be found at around 260 cm^{-1}, 260 cm^{-1}, 360 cm^{-1}, 700 cm^{-1}, and 1100 cm^{-1},[S8,S9] which are not present in the spectrum obtained for the white precipitates (red). Instead, the pronounced peaks at around 400 cm^{-1} and 1000 cm^{-1} (green) suggest that the white precipitates are comprised mostly with $CaPO_x$[S10,S11], in addition to a small amount of $CaCl_2$ (purple).

Figure S20

(Added)

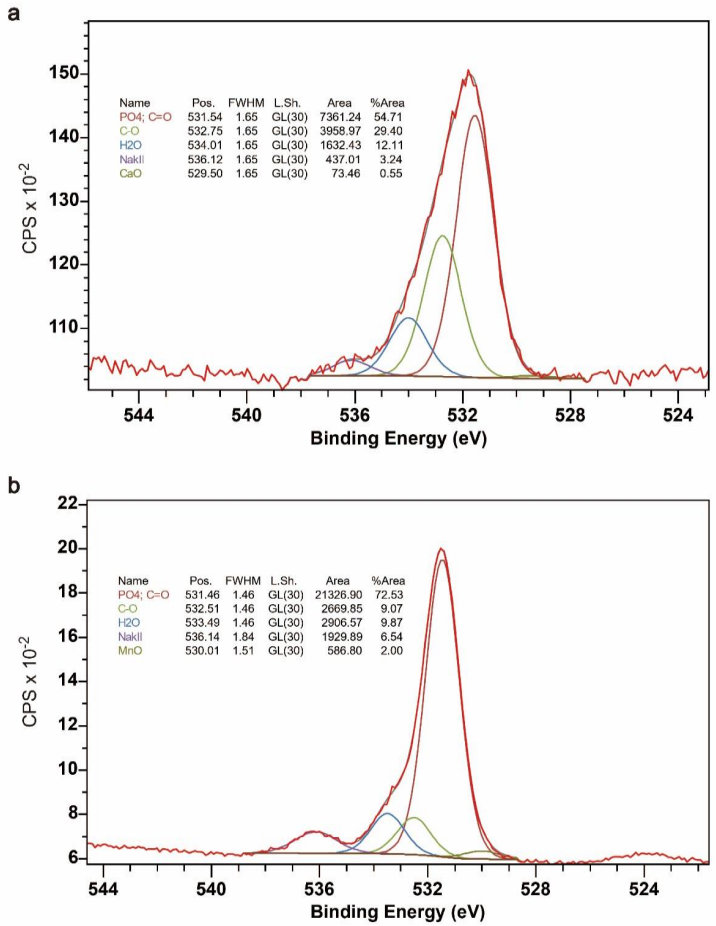

Figure S20. X-ray photoelectron spectroscopy (XPS) analysis of precipitate compounds. **a-b,** XPS spectra of white precipitated appeared in mixture solutions of 2 M $MnCl_2$ (a) and $CaCl_2$ (b) with phosphate buffered saline. The features at around 531 eV indicate that the precipitates are phosphate compounds.

Figure S21

(Added)

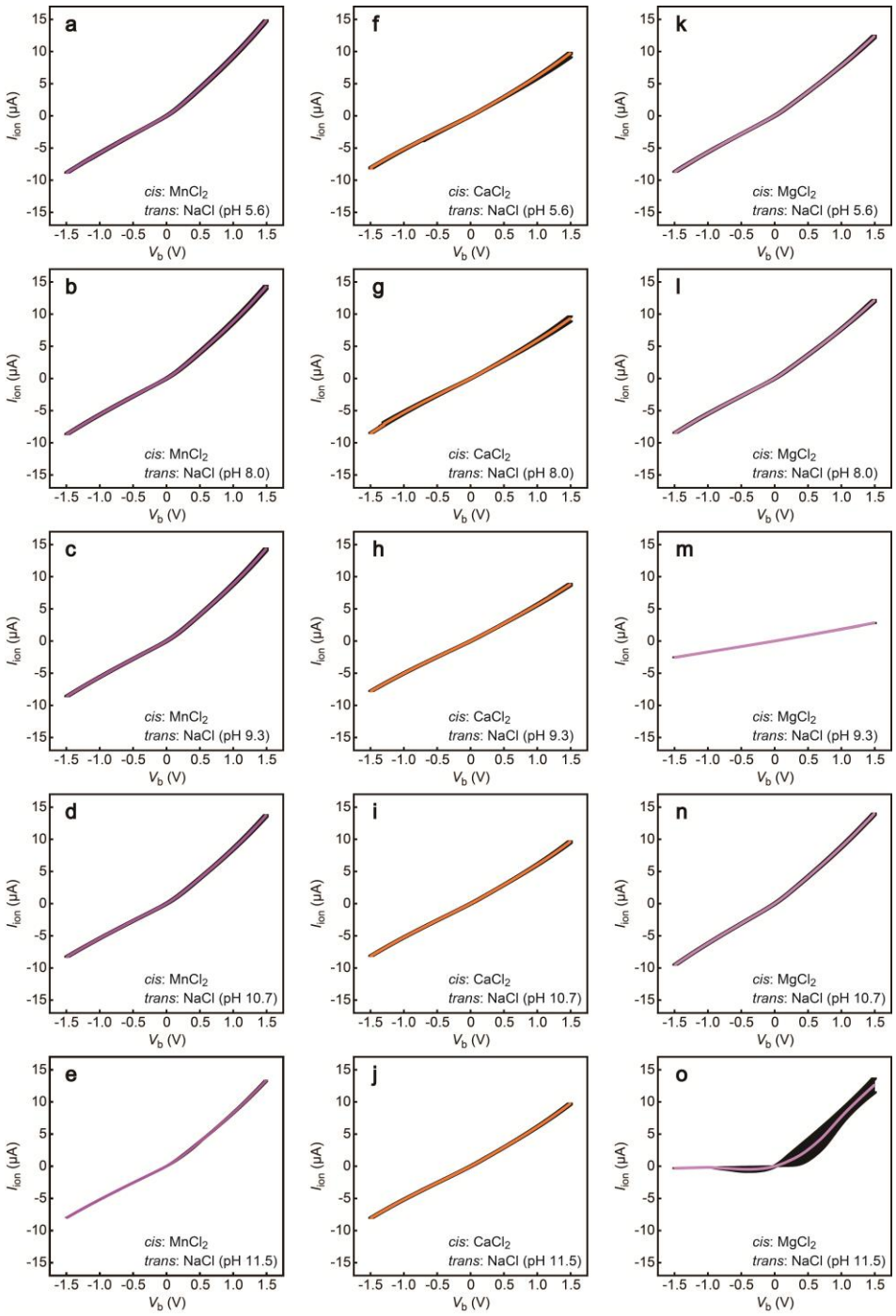

Figure S21. Ionic current characteristics in phosphate-free NaCl water (1.4 M) of various pH. a-e, I_{ion} – V_b curves recorded for a 300 nm nanopore with a $MnCl_2$/phosphate-free NaCl water configuration (r_{scan} = 65 mV/s). The pH of the NaCl water was adjusted to 5.6 (a), 8.0 (b), 9.3 (c), 10.7 (d), and 11.5 (c) using NaOH and HCl. Error bars are the standard deviations calculated from the three ionic current curves recorded. **f-o,** The same sets of data obtained for $CaCl_2$ (f-j) and $MgCl_2$ solutions (k-o). No signs of in-pore precipitation were found at moderate pH manifesting the role of the phosphoric acid in the

phosphate buffered saline on the extreme rectifications observed at pH 7.6. Meanwhile, $MgCl_2$ demonstrated a rectifying behavior (o) ascribed to precipitation/dissolution reactions of $Mg(OH)_x$ at the highly alkaline pH.

Figure S22

(Added)

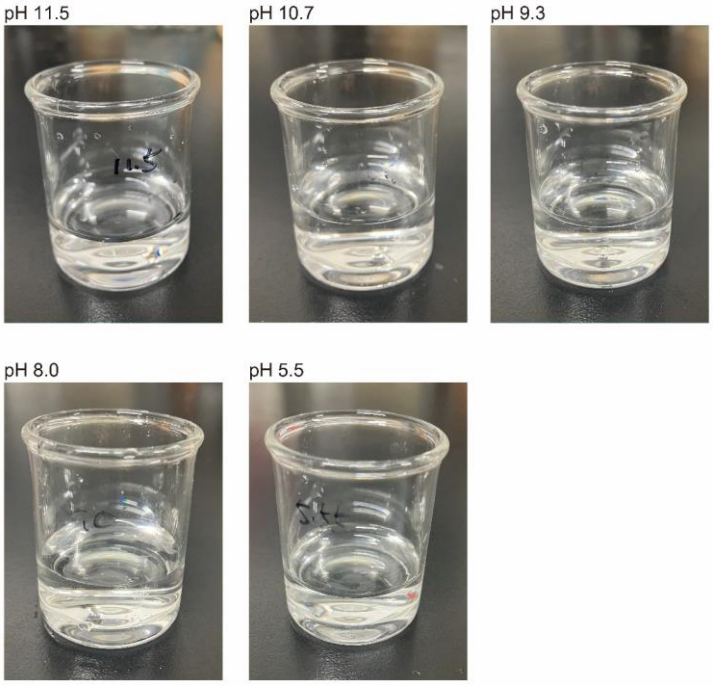

Figure S22. Reaction in phosphate-free NaCl solutions. Photographs taken after adding 100 µl of 2 M $CaCl_2$ into the 10 ml phosphate free NaCl water (1.4 M) in a beaker. No notable change in the appearance of the liquid was observed indicating the absence of any precipitation reaction. We note that this is a case only when the NaCl concentration is over 1 M. Under lower salinity conditions, precipitates were found to be generated upon mixing the $CaCl_2$ solutions with alkaline water attributed to the precipitation of calcium hydroxides.

Figure S24

(Added)

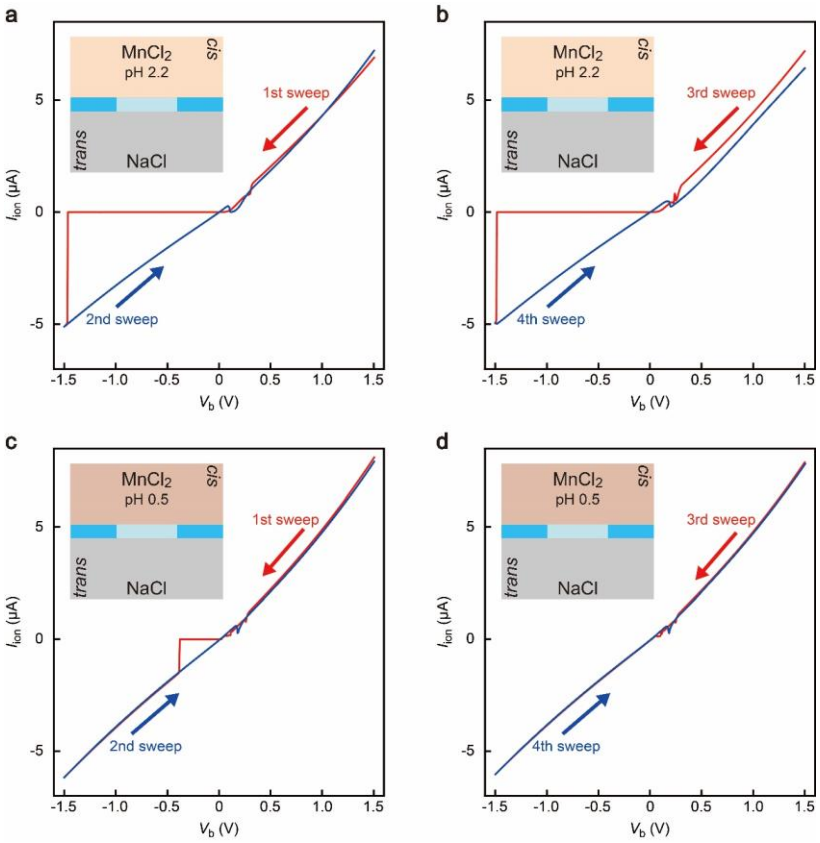

Figure S24. pH dependence of in-pore precipitation/dissolution reactions. a-d, I_{ion} – V_b curves recorded for a 300 nm nanopore of a $MnCl_2$/phosphate buffered saline configuration with the $MnCl_2$ solution pH adjusted to 2.2 (a-b) and 0.5 (c-d) with HCl (r_{scan} = 65 mV/s). The precipitated layer tends to become unstable at pH 2.2 due to the promoted dissolution reaction when the cation supply stopped at negative voltages that tends to open the pore at around -1.5 V (a-b). The lower pH condition almost completely prohibits the formations of the nanoprecipitate layer giving no rectification behaviors under the conditions tested.

Main text (p6 line 146 – 150)

(Added) Although the synthesis of the metal phosphates in non-alkaline media is generally complicated processes for predicting whether the reactions inside the nanopore should be endothermic or exothermic,[39,40] the overall results consistently suggest the ion transport-mediated in-pore precipitation/dissolution as a primary factor of the extreme I_{ion} rectifications.

6) For the memory effect results in Figure 4, have the authors calculated rectification ratio from the I-V curves for the scans shown? Are the rectification values cycled back upon changing the voltage sweep rate and does the clogging and de-clogging cycles affect the rectification properties of the diode?

(Reply)

Thank you for your comment. We have calculated the rectification ratio from the I_{ion} – V_b curves in Figure 4. After the repetitive voltage scanning, the ratio did not returned to the original value, which is ascribable to the precipitates formed on the *trans* side of the membrane surface that cannot be removed by the V_b scans alone.

We have added the rectification ratio in Figure 4e and also revised the main text to explain the above point as follows.

Main text (p7 line 156 – 162)

(Added) Whereas this transformed the microfluidic channel to a diode, it could also be returned to a resistor by eliminating the precipitates on the channel wall through the repetitive voltage scans at a faster rate (650 mV/s), though not fully reversible in terms of r_{rec} presumably due to the non-dissolvable phosphates formed at the *trans* side of the membrane surface during the repetitive voltage scans (Figure 4e). The in-pore reaction mechanism thus allows a memory effect on the ionic conductance.

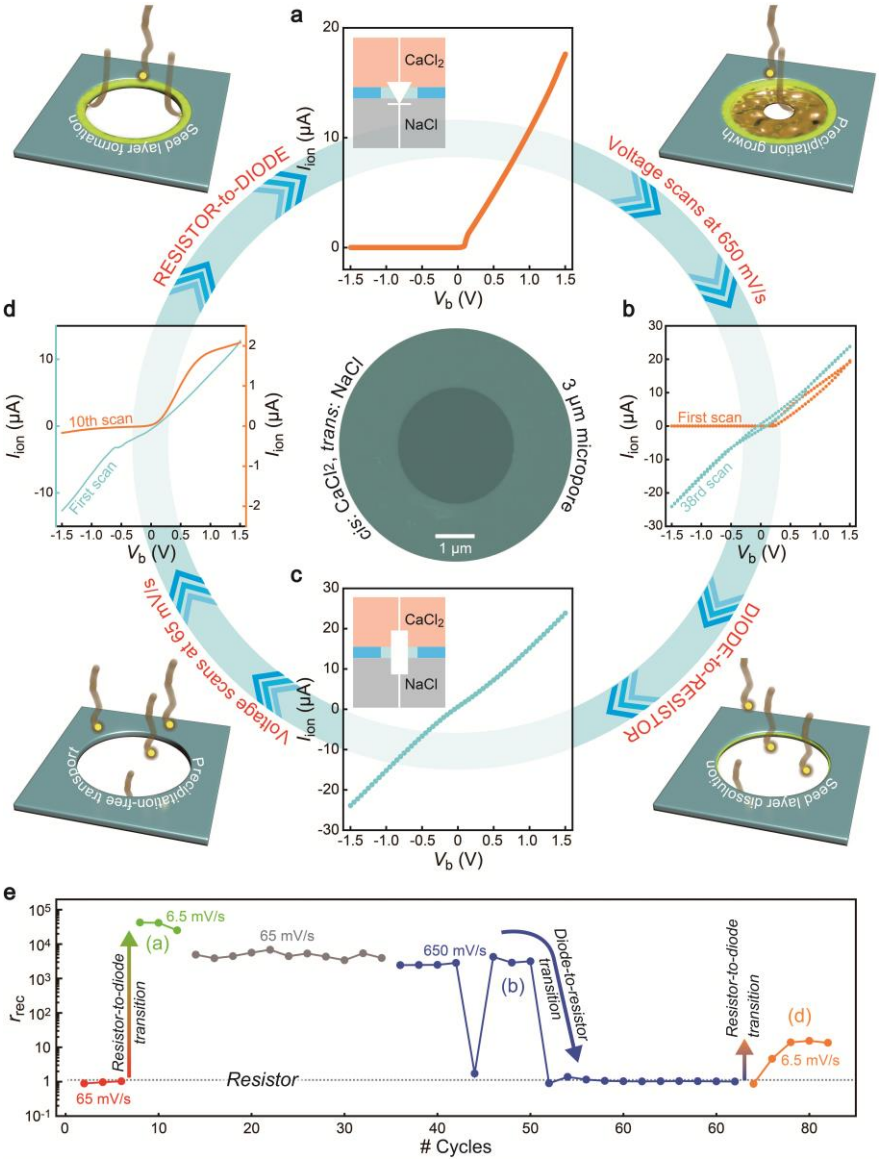

Figure 4. In-pore reaction-mediated memory effect in micropore ionic conductance. **a,** Originally, a 3 μm micropore with a $CaCl_2$/NaCl arrangement behaved as an ohmic resistor at voltage scan rate higher than 65 mV/s. However, the lower scan rate of 6.5 mV/s led to emergence of extreme rectification suggestive of precipitation/dissolution reactions of calcium phosphates in the pore. **b-c,** Meanwhile, repetitively scanning V_b at a faster rate (650 mV/s), the micropore gradually returned to exhibit a resistor-like behavior. **d,** Subsequent scanning at 65 mV/s can further make the micropore a diode. The image at the center is a scanning electron micrograph of the micropore of 3 μm diameter. **e,** Changes of the rectification behaviors upon the repetitive voltage scanning. Dotted line denotes r_{rec} = 1.

7) The trivalent Al3+ ions are shown to form robust precipitates in Fig. 6. However, the current shown in Fig. 6c at negative bias seems to be an order of magnitude higher than the other ions in Fig 2c inset. What is the reason behind this change of magnitude? Also, during subsequent scans shown in Fig. S9, the current at negative bias increases after the 8th sweep. What is the reason behind the increase, as described the current decreases at

positive bias confirming the presence of the robust precipitation layer?

(Reply)

Thank you for the comment. As the reviewer points out, the ionic conductance was larger after blocking the pore by the precipitates. The results suggest that the precipitate layer becomes stable with a nanopore of around 10 nm diameter for the case of aluminum phosphates due to the reaction equilibrium different from those in the $MnCl_2$ and $CaCl_2$ under the conditions tested.

For the abrupt increase in the ionic current shown in Figure S9 (now Figure S17 in the revised Supplementary Information), it is ascribable to the inadvertent breakage of the nucleated ultra-thin precipitate layer by electroosmotic flow. This has also been observed to be a case in Figure 4e, where the rectification ratio suddenly became close to 1 during the 5th voltage scanning at 650 mV/s.

The above points were explained in the main text and Supplementary information as written below.

Main text (p9 line 209 – 211)

(Added) (the comparatively larger pore size than those formed in the $MnCl_2$ and $CaCl_2$ solutions is presumably due to the difference in the reaction equilibrium under the given conditions)

Figure S17 caption

(Added) **a,** I_{ion} – V_b characteristics obtained under 10 voltage scans on a 300 nm-sized SiN_x nanopore with the *cis* and *trans* filled with 1 mM $AlCl_3$ and 1 M $AlCl_3$, respectively. The abrupt jumps in the ionic current at V_b around +1.0 V during the third voltage scan is presumably due to the temporal precipitation of thin aluminum phosphate layer to subsequent breakdown by the electroosmotic flow.

8) For Fig. 6h, are they two separate measurements at the same timepoints? The grey and white curves are not clear in the figure. How do the authors infer the two peaks in the same blockade to arise from folded and non-folded DNA conformations? As the sample only has a small amount of linear DNA, it is not clear how 40% of the blockades are double peaked as described.

(Reply)

Thank you for the comment. Figure 6h displays characteristic resistive pulse signals of

lineshapes with a staircase-like (red) and large simple-pulse features (blue) obtained in the same measurements. For the former case, the blockade current took the two well-defined levels at *n* x 220 pA (*n* = 1 or 2) (estimated from the positions of the two peaks in the red histogram), which is widely known as a distinct feature representing the ion blockade characteristics of DNA with (*n*-1) folds. On the other hand, the latter type of signals signify the translocation of the plasmids with cyclic forms as they exclude double the amount of ions in the nanopore compared to the linear strand counterpart.

For the relatively lower capture rates of the cyclic DNA compared to the linear counterparts, it is attributable to the difference in their flexibility that impose different entropy barriers. First of all, the gyration radii of the polynucleotide chains is estimated to be 184 nm, which is an order of magnitude larger than the size of the nanopore, which anticipates non-negligible entropy barrier for the entangled strands are required to be disentangled to electrophoretically thread through the tine pore. In this regard, it is noticeable that the cyclic DNA is known to be less flexible than the linear DNA due in part to the supercoiled conformation (Langmuir 22, 10837-10843 (2006)). The resulting larger entropy barrier for the cyclic DNA hinders its translocation, thereby gave rise to its relatively low capture rates in the present study.

The above discussion is added to the main text as follows.

Main text (p9 line 237 – 243)

(Added) Here, it is noted that the gyration radius of ColE1 DNA is estimated to be 194 nm, which is much larger than d_{pore}. Therefore, the polynucleotide chains are required to be dis-entangled before the electrophoretic translocation.[50] In this context, the supercoiled conformations of the cyclic-formed plasmids anticipate larger entropy barrier compared to that for the flexible linear DNA strands of the same length.[51] This would be a reason why the linear genome was detected relatively frequently in the resistive pulse measurements.

9) For table S1 and all pH recordings measured, is the pH recorded before or after the experiment? As there are ion translocation events and the reported pH induced rectification in Fig 3, it is important to know how much the pH varies over the course of the experiment.

(Reply)

Solution pH was recorded before the measurements. We have checked that the pH varies by less than 5 % after three hours (much longer than the measurement time). We have added this information in Table S1 as shown below.

Table S1

(Revised)

Table S1. Salt solution pH.

1.37 M NaCl (Phosphate buffered saline)	2 M KCl	2 M CsCl	2 M $MgCl_2$	2 M $CaCl_2$	2 M $MnCl_2$	2 M $AlCl_3$	2 M NaCl + HCl	2 M NaCl + NaOH
pH 7.4	pH 6.1	pH 6.2	pH 5.4	pH 5.1	pH 4.2	pH 1.3	pH 1.0	pH 13.0

* pH of these solutions was checked to vary only by less than 5 % within the measurement time (shorter than 3 hours) under ambient conditions at room temperature.

Text and label suggestions:

The authors should label the cis and trans chambers in the figures for easier understanding of directionality in the figures.
Page 3, Line 58-61: Should cite Figure 2a.
Page 4, Line 95: cis or trans?
Page 22, Line 459: cations serves -> cations that serve
Figure 4b label: 38rd -> 38th

(Reply)

Thank you for your careful reading of the manuscript. We have corrected the typos.

Response to the reviewers

Reviewer #4

I co-reviewed this manuscript with one of the reviewers who provided the listed reports. This is part of the Nature Communications initiative to facilitate training in peer review and to provide appropriate recognition for Early Career Researchers who co-review manuscripts.

(Reply)

We are grateful for your co-reviewing our manuscript.

Transmembrane voltage-gated nanopores controlled by electrically tunable in-pore chemistry

Makusu Tsutsui, Wei-Lun Hsu, Chien Hsu, Denis Garoli, Shukun Weng, Hirofumi Daiguji, and Tomoji Kawai

We would like to sincerely thank the referees for taking the time to review our manuscript and for providing valuable and constructive comments, which have been extremely helpful in improving our work. Below, we provide a point-by-point response to the comments.

Response to the reviewers

Reviewer #2

Reviewers Comments:

I thank the authors for their detailed answer of my comment. I think most of my comments were considered in the revised manuscript. However, I still think that the numbers and labels for the figures can be slightly larger for readability. Regarding my questions concerning the case where the salt is similar on both sides: the authors commented on this issue in the response letter, but I do not see any comment regarding this issue in the manuscript.

I recommend publication of the manuscript after minor revision, which do not require reviewer approval. These minor revision include: improvement of the figure readability, a short comment on the situation where the salt is similar on both sides.

(Reply)

Thank you for your comment. We have changed the text in the figures according to the journal format that allows font size in a range from 5 pt to 7 pt. To make them large enough, we arranged the text to be 7 pt Arial.

For the case with the same salts on both sides, we have added a sentence explaining that such conditions result in only weak rectification behavior, as outlined below

Main text (p5 line 109 – 112)

(Added) This was also confirmed by the ionic current measurements under salinity difference of the same types of salts at the cis and trans showing only weak rectification characteristics due to the electroosmosis mechanism (Supplementary Figure 15).

Response to the reviewers

Reviewer #3

Reviewers Comments:

The authors have implemented a number of changes to the manuscript that clarified the majority of points from the previous round of review.

One remaining concern is that the rectification measurements have not been conducted in a steady state and thus are not reproducible among repeat experiments. This can be seen in the last panels of the updated Figures S2-S7 and can also appreciated from the error bars in Fig 2d. These details are now clearly described in the text along with their reasoning for why these measurements are not fully reversible. Such stochasticity, however, somewhat limits practical utility of the described phenomena.

(Reply)

Thank you for your comment. We plan to further investigate nanopore materials and designs to achieve more stable rectification characteristics for practical applications.

The authors have added error bars to Fig 2d for the rectification measurements, described as standard deviation. The caption does not specify which measurements are included for this calculation. The range of rectification values in Fig S3e and S6e seems to be bigger. Have the authors included only a part of the curve for taking the average and the standard deviation calculations?

(Reply)

Thank you for your comment. We have specified in the caption that the data in Figs. S3e and S6e are not included in the error bars in Fig. 2d.

The choice of colors in many figures is not color blind friendly, in particular, the "orange" and the "green" dots in new figure 5f. Please revise the colors throughout the manuscript.

(Reply)

Thank you for your comment. We have updated the colors and styles of the plots

in the figures to improve their readability.